FACULTY OF TECHNOLOGY

USE OF BIOCHAR AS A SLAG FOAMING AGENT IN EAF STEELMAKING

Eetu Hoikkaniemi

PROCESS ENGINEERING

Master's Thesis

May 2022

ABSTRACT

Use of Biochar as a Slag Foaming Agent in EAF Steelmaking

Eetu Hoikkaniemi

University of Oulu, Degree Programme in Process Engineering

Master's Thesis 2022, 106 pp. + 3 Appendixes

Supervisors at the University: Petri Sulasalmi, D.Sc. (Tech.), Aki Koskela, M.Sc. (Tech.)

The transition to fossil-neutral steel production involves finding a substitute for fossil-based carbonaceous materials used in the EAF process. Foaming of slag is an important part of EAF steelmaking, where usually fossil-based carbonaceous material is injected into the melt to cause the foaming of the slag. The aim of this thesis is to study the suitability of biochar as a foaming agent.

In the theory part of the thesis the EAF process and the slag foaming phenomenon are reviewed at a general level. The properties of the slag and their effect on the foaming phenomenon are reviewed, and the composition limits of the slag favorable for the foaming are evaluated. In addition, biochar, its production and properties are briefly presented. The theory part also includes a literature review of previously made studies related to the use of biochar as a slag foaming agent.

In the experimental part of the thesis some laboratory-scale slag foaming experiments were performed. The slag used in the experiments was from an actual EAF process. The observation of the foaming during the experiments was performed by imaging the experiments with a CCD camera using a laser light source. By analyzing the obtained video image, the foaming behavior could be evaluated. After the experiments the cooled slag and the crucibles were analyzed with microscopical methods. Based on the results, the biochar used in the experiments acted as a foaming agent in a similar way to the coke dust. During the injection the iron oxide in the slag was reduced, creating CO bubbles that caused the foaming phenomenon and an increase in the volume of the slag.

Keywords: biochar, electric arc furnace, slag, foaming

TIIVISTELMÄ

Biohiilen käyttö kuonan kuohutuksessa valokaariuunissa

Eetu Hoikkaniemi

Oulun yliopisto, Prosessitekniikan tutkinto-ohjelma

Diplomityö 2022, 106 s. + 3 liitettä

Työn ohjaajat yliopistolla: TkT Petri Sulasalmi, DI Aki Koskela

Siirryttäessä fossiilineutraaliin terästuotantoon täytyy valokaariuuniprosessissa käytettäville fossiilisille hiilimateriaaleille löytää korvaaja. Kuonan kuohutus on valokaariuuniprosessin tärkeä vaihe, jossa käytetään tavallisesti fossiilista, injektoitavaa hiilimateriaalia kuohun aikaansaamiseksi. Tämän diplomityön tavoitteena on selvittää biohiilen soveltuvuutta kuohutusagentiksi.

Työn teoriaosassa on esitetty yleisesti valokaariuuniprosessi sekä kuonan kuohuminen ilmiönä. Kuonan ominaisuuksia ja niiden vaikutusta kuohumiseen käydään läpi, ja kuohumisilmiön kannalta suotuisia kuonan koostumusrajoja pyritään arvioimaan. Lisäksi biohiili, sen valmistus ja ominaisuudet esitellään lyhyesti. Teoriaosaan on sisällytetty myös kirjallisuusselvitys aiemmin suoritetusta tutkimuksesta biohiilen käyttöön kuohutusagenttina liittyen.

Työn kokeellisessa osiossa suoritettiin laboratoriotason kuonankuohutuskokeita. Kuonana kokeissa käytettiin todellisesta valokaariuuniprosessista saatua kuonaa. Kuohumisen havainnointi kokeiden aikana suoritettiin kuvaamalla CCD-kameralla laservalonlähdettä apuna käyttäen. Saatua videokuvaa analysoimalla kuohumiskäyttäytymistä voitiin arvioida. Kokeiden jälkeen jäähtynyttä kuonaa ja upokkaita analysoitiin mikroskooppisilla menetelmillä. Tulosten perusteella kokeissa käytetty biohiili toimi kuohutusagenttina hyvin samankaltaisesti kuin koksipöly. Injektoinnin aikana kuonan sisältämä rautaoksidi pelkistyi muodostaen kuohumisreaktion aiheuttavia CO-kuplia, ja kuonan tilavuus kasvoi.

Asiasanat: biohiili, valokaariuuni, kuona, kuohuminen

PREFACE

This thesis was done for the Process Metallurgy Research Unit at the University of Oulu during 1.12.2021–31.5.2022. The topic of the thesis was part of the FFS project, and the thesis was commissioned by SSAB Europe Oy.

I would like to thank Prof. Timo Fabritius for providing the opportunity to work at the Process Metallurgy Research Unit during the completion of this thesis. I would also like to thank the supervisors of this thesis at the University of Oulu: Dr. Petri Sulasalmi and Mr. Aki Koskela, who provided great amount of help and guidance throughout the course of the thesis. In addition, I would like to thank the supervisors of this thesis at SSAB Europe Oy: Dr. Timo Paananen and Mr. Seppo Ollila, for all the advice and encouragement. I also thank Mr. Jarmo Lilja from SSAB Europe Oy for the efforts and interest towards my work.

All of the staff of the Process Metallurgy Research Unit are thanked for creating a warm and welcoming working environment. Particular acknowledgements I would like to express to Mr. Riku Mattila, who made the laboratory experiments related to this thesis possible.

Lastly, I would like to thank my family and friends for their help and support during my studies. This has been a challenging but rewarding journey.

Oulu, 31.5.2022

Eetu Hoikkaniemi
Eetu Hoikkaniemi

TABLE OF CONTENTS

NOMENCLATURE

Abbreviations

BF	blast furnace
BOF	basic oxygen furnace
CCD	charge-coupled device
daf	dry ash-free basis
db	dry basis
DR	direct reduction
DRI	direct reduced iron
EAF	electric arc furnace
EBT	eccentric bottom tapping
EDS	energy dispersive spectroscopy
FC	fixed carbon
FESEM	field emission scanning electron microscopy
fps	frames per second
GDOES	glow discharge optical emission spectroscopy
H-DR	hydrogen direct reduction
os	related to original substance
VM	volatile matter
wb	wet basis
XRF	X-ray fluorescence

Symbols

A	cross-sectional area [m^2]
A_A	pre-exponential frequency factor
B	basicity
D_b	bubble diameter [m]
E_A	activation energy [J/mol]
h	height [m]
M_i	molar mass of component *i* [kg/mol]
Q	gas flow rate [m^3/s]

R	gas constant [J/(K·mol)]
t	time [min]
T	temperature [K]
V	volume [m^3]
V_g^s	superficial gas velocity [m/s]
V_m	molar volume [m^3/mol]
W	weight [kg]
X_i	mole fraction of component *i*
Δh	change in the height [m]
ΔV	change in the volume [m^3]
η	dynamic viscosity [Pa·s]
η_c	effective dynamic viscosity [Pa·s]
Θ	fraction of precipitated solid phases in slag
σ	surface tension [N/m]
σ_i	surface tension factor of component *i*
ρ	density [kg/m^3]
ϕ	void fraction
Σ	foaming index

Brackets

( )	species in slag phase
[ ]	species in metal phase
⟨ ⟩	species in solid phase
{ }	species in gas phase

1 INTRODUCTION

Slag is a by-product of steelmaking. In electric arc furnace (EAF) steelmaking, approximately 120–170 kg of slag is produced per one tonne of steel. The slag consists mainly of different silicates and oxides, and the composition and properties of the slag depend highly on the ratio of materials, such as scrap steel and direct reduced iron (DRI) fed to the EAF. (Skaf et al. 2017, p. 177)

The foaming of slag plays an important role in modern EAF steelmaking. It enhances the service life of refractory, saves energy, inhibits steel re-oxidation and reduces noise pollution when making steel with EAF. (Luz et al. 2011, p. 91; Zhu et al. 2012, p. 751) The foaming phenomenon is usually created by feeding fossil carbon, e.g. pulverized coke, into EAF. However, in order to move to fossil-free steel production, alternatives to fossil foaming agent carbon sources must be found. Biomass and biochar are considered to be a potential way to replace the fossil foaming agents. (Bianco et al. 2013, p. 18)

The aim of this thesis is to investigate the use of biochar as a slag foaming agent in EAF steelmaking. The first section of the thesis is a literature review that includes general information about EAF, slag foaming phenomenon and biochar, and previous research related to the topic of the thesis. The second section of the thesis is based on laboratory-scale research, where the potential of biochar as a foaming agent is studied with laboratory-scale slag foaming experiments.

2 EAF PROCESS

Most of the global steelmaking is carried out through blast furnace-basic oxygen furnace route (BF-BOF) or through EAF-based route. Of these, the BF-BOF route is a more common method. It is based on the use of fossil coal and iron ore, so the carbon dioxide emissions of the BF-BOF steelmaking are at a high level. The scrap steel and electricity-based EAF route produces less carbon dioxide emissions, which makes it environmentally friendlier steelmaking route in comparison to BF-BOF route. (He et al. 2017, p. 29) The BF-BOF route produces approximately 90% of the total carbon dioxide emissions of steelmaking. One option to reduce emissions in steelmaking is to switch from the BF-BOF-based steelmaking to EAF-based, using scrap steel and climate-friendly direct reduced iron as a raw material. (Wang et al. 2021, p. 1–2)

The history of EAF steelmaking began in the late 1800s, but to a greater extent the method was introduced in the first half of the 20th century as the price and availability of electric power improved. Until the 1960s the capacity of the furnaces was only some tens of thousands of tonnes, and the tap-to-tap time was relatively long, typically even 3–4 h. The development of the process has been rapid over the last fifty years. The invention of oxygen blowing, Ultra High Power (UHP) transformers, and introduction of the slag foaming practice have reduced the tap-to-tap time to less than an hour. The electricity consumption of furnaces has fallen from 630 kWh/t (the 1960s) to almost 300 kWh/t, and the electrode material consumption per tonne of steel produced is nowadays significantly lower than it was fifty years ago. (Madias 2014, p. 271–273; Hannula et al. 2020, p. 22–23)

2.1 Raw materials

2.1.1 Scrap

Scrap steel is the main raw material for the EAF process. The scrap being used as raw material can be divided into three different classes. Obsolete scrap means all of the scrap steel that comes from consumers, such as cars and household appliances, machinery from industry, etc. Industrial scrap means the scrap that comes from the processing of steel slabs and rolled steel, so it is a circulating material of steel industry. Internal scrap means the scrap that comes internally from the steel mill, e.g. tundish bottoms and steel that has

been recovered from the slag. (Madias 2014, p. 275) Before the scrap can be fed to the furnace, it must be sorted and divided into different fractions. If the scrap was fed unsorted to the process, it would affect the quality of the steel produced and the running of the furnace negatively. The separating and grading of scrap is done at the scrap yard. The obsolete scrap can be prepared for the process with different kinds of methods, e.g. with a shredder, by pressing the scrap to bales, or by cutting it into smaller fractions with oxygen. When the scrap is being prepared, the scrap yard operator fills scrap buckets according to the recipe of desired steel. The density and size of the scrap is being considered when filling the buckets so that the distribution of scrap in the furnace would be favorable for the process. (Wang 2016, p. 24; Madias 2014, p. 275)

2.1.2 DRI and pig iron

Direct reduced iron (sometimes *sponge iron*) is iron produced by the direct reduction, a solid-state process, where coal, natural gas, or some other element like hydrogen is used to remove the oxygen from the iron oxide. The iron oxide used in the direct reduction (DR) process is usually in a form of pellet, lump or as fines. Since there is no melting in the process, the external shape of the raw material remains nearly the same during the whole process. The weight of the material can be reduced up to 30% due to the reduction of oxygen, so DRI is very porous material. Because of that DRI is often compacted for sales or storage purposes. (Dutta & Sah 2016, p. 1083; Vogl et al. 2018, p. 736)

DRI is not always used in EAF steelmaking, even though almost 90% of DRI produced in the world goes to electric arc steelmaking. In many steel mills only scrap steel is used as a source of iron for the EAF process. In developing countries DRI can be added to the EAF charge because of the low price compared to scrap steel. DRI has also been used among scrap in Europe and North America to lower the content of metallic residuals and nitrogen when producing high-grade steel products. (Batle et al. 2014, p. 143, 156)

Normally DRI is used among the scrap, as a mixture in the scrap buckets. The normal feed rate is 40% or less DRI and at least 60% of scrap in one bucket. Other ways to charge DRI into EAF are injection from the storage silos and hot charging directly from the DR plant. (Batle et al. 2014, p. 146–149) A future plan for the steel industry is to use hydrogen-based direct reduced (H-DR) iron in large volumes in the EAF steelmaking process. (Vogl et al. 2018, p. 736)

Also hot metal or pig iron can be used in the EAF process. In Brazil, using cheap pig iron produced at charcoal-based blast furnaces is a common way to lower the production costs. In China, replacing scrap steel with hot metal is often done due to a shortage of scrap material. (Madias 2014, p. 278)

2.1.3 Fluxes

Fluxes such as quicklime or dolomite are used as additives in furnaces to generate the slag. The lime can be added to the furnace together with the scrap at the buckets, or separately during the melting process, e.g. by injection or by charging the flux to the furnace from additional hoppers. (Wang 2016, p. 26; Morales et al. 1995, p. 1054)

2.1.4 Carbon

Carbon can be used in the EAF process in two ways: either by charging it to the furnace in larger particles together with the scrap steel, or in a finer particle size by injection. Anthracite, petroleum coke, coke breeze, graphite and/or iron carbide are usual carbon sources used in EAF. The main function of carbon in EAF is to act as a slag foaming agent and to control the FeO content. Depending on the grade of steel and the power of the furnace, approximately 2–10 kg of carbon per one tonne of steel is usually being used for slag foaming. (Luz et al. 2018, p. 8728; Madias 2014, p. 282; Jones et al. 1998, p. 597)

2.1.5 Oxygen and other gases

Chemical energy is brought to the EAF process by injecting oxygen or natural gas, either with lance manipulators from the slag door or with oxy-fuel or natural gas burners attached to the side walls of the furnace. The purpose of injecting these gases is to assist in the melting of scrap and to increase the productivity of the furnace. In addition, adding oxygen to the process plays a key role in oxidizing the present impurities. It is also necessary for the slag foaming phenomenon. Also, inert gases like argon or nitrogen can be injected into the steel from the bottom of the EAF to enhance the melting process by stirring. (Madias 2014, p. 282; Jones et al. 1998, p. 598–599; Hannula et al. 2020, p. 23)

2.2 Basic principle of the process

Most of the EAFs use alternate current (AC) mechanism for the electrodes. Furnaces using direct current (DC) are also in use. (Madias 2014, p. 273) The EAF acts as a melting unit, in which the decarburization and removal of harmful components for the steel, such as phosphorus, occurs during the melting (Hannula et al. 2020, p. 23). It produces batches of molten steel based on the desired chemical composition. The operations of EAF can be divided into following steps: 1) Furnace charging 2) Melting 3) Refining 4) De-slagging 5) Tapping 6) Furnace turn-around. (Singh 2020, p. 35)

The scrap and in some cases the additives or DRI mixed with the scrap are being fed to the furnace by pouring from the buckets. The roof of the furnace is opened, and the electrodes are moved aside during the charging. The usual number of electrodes is three in AC furnace, but other amounts are also possible. The charging of scrap is usually done by a crane that lifts the scrap bucket over the furnace. Usually, the bottom of the bucket is openable. The crane operator drives the bucket on top of the furnace, opens the bottom of the bucket, and the scrap and other possible charge materials are being loaded inside the furnace. The roof of the furnace and electrodes are then moved back to the top of the furnace, and the melting phase begins. The electrodes are lowered near the surface of the pile of scrap in the furnace, and an electric current is passed through the electrodes which form an arc on the scrap. The temperature of the arc can be up to 6000 °C. The heat that melts the scrap is generated by the arc and the resistance of metal to the flow of electricity. As the scrap melts, the surface of the material in the furnace lowers due to the porosity of the scrap. Also, the electrodes are being lowered. Their distance to the scrap must be correct all the time for the process to work optimally. Oxygen or natural gas can also be injected to adjust the melting of the scrap. Fluxes are added either with the scrap charge or separately. (Wang 2016, p. 26; Teräskirja 2014, p. 37)

At a point where the process gets quite stable and a large portion of the steel has melted, the steel refining starts. Oxygen is injected into the steel via oxygen lance and/or oxy-burners which causes the oxidation of iron and impurities such as silicon, phosphorus, aluminum and manganese. Together with lime those oxidized impurities form the slag layer on top of the steel. Also, carbon is being injected during the refining stage so that the CO and CO_2 gases can be formed, which leads to the wanted slag foaming phenomenon. When the composition and quality of the molten steel is at the desired level,

the slag is poured and the steel is tapped out of the furnace. Usually, these are done from opposite sides of the furnace by tilting it. The slag is poured from the slag door either to slag pots or to the ground where it is removed by an earthmoving machine. The temperature of slag when poured is approximately 1600 °C. For tapping of steel the furnace is tilted in the other direction. Usually, the molten steel is tapped to a steel ladle through a submerged taphole. The tapping temperature ranges between 1550 °C and 1750 °C depending on the need for further processing of steel and other process requirements. After tapping, the steel is transported to the next process step, such as ladle treatments. (Wang 2016, p. 26; Hosseini et al. 2016, p. 1, 4; Pfeifer et al. 2002, p. 10)

The whole melting process cycle lasts usually about 60 minutes, and with some double-shell furnaces the tap-to-tap time can be only 30 minutes. Producing of one tonne of steel in EAF requires around 0.4 MWh of electrical energy. To improve the energy efficiency, a hot-heel practice can be employed in which a portion of the molten steel is left on the bottom of the furnace for the next melting. Scrap steel can also be preheated before charging. (Singh 2020, p. 35; Jones et al. 1998, p. 551; Hannula et al. 2020, p. 23)

2.3 Layout and components

EAF consists of numerous components such as structures for containment of raw materials and molten steel, power supply components, components that move different mobile parts of the furnace, and auxiliary process equipment like injection systems (Jones et al. 1998, p. 526). This section of the thesis reviews the most common and the most relevant components for the topic of the thesis.

2.3.1 General structure

The usual shape of EAF is cylindrical. The bottom shape of the furnace is spherical, and the roof is usually flattened sphere-like. The shell between the bottom and the roof is cylindrical. Usually, the main shelling of EAF is divided into two detachable parts, which makes the maintenance and change of the shell practical. (Jones et al. 1998, p. 526)

The roof and the center of EAF contain water-cooled panels which are placed on a supporting water-cooled cage. In addition, the off-gas duct can be water-cooled. The water cooling allows the use of large heat inputs without damaging the structure of the furnace. Moreover, water cooling reduces the need to use refractory. The panels are

usually made of steel or copper, which is used in areas where high heat levels are applied. (Jones et al. 1998, p. 526–529; Madias 2014, p. 280–281)

The bottom of the EAF is made of a spherical plate section and refractory materials on top of it, and it contains the tapping mechanism and sometimes gas stirring elements. The type and material of refractory used in the bottom depends on the type of the furnace. In bottom tapping furnaces (EBT) the main refractory material that is being used is magnesite or magnesite carbon. The refractory lining consists of safety lining and working lining and the typical thickness of refractory is 500–700 mm. Bottom tapping is the most common method to get the molten steel out of the furnace. The tap hole is typically filled with sand after the tapping, and the hole is being shut with a valve or a slide gate. When the melting process has come to the tapping phase, the hole is being opened and the steel is being poured in a ladle which is typically being moved under the furnace on rails. Another common way to tap the steel out of the furnace is through a tapping spout. (Jones et al. 1998, p. 530–531, 545; Madias 2014, p. 280–281)

Besides the tap hole, the lower shell of the furnace has usually another opening, the slag door. Its function is to act as an opening for the removal of slag from the furnace. In addition, injection lances are pushed into the furnace via slag door. Other openings in the furnace cell are the openings from which the electrodes are being penetrated into the furnace, a roof hole for the furnace fume outlet, and possible additional holes, e.g. for raw material feed or injection equipment. (Jones et al. 1998, p. 537) The main structure and equipment of EAF is presented in Figure 1.

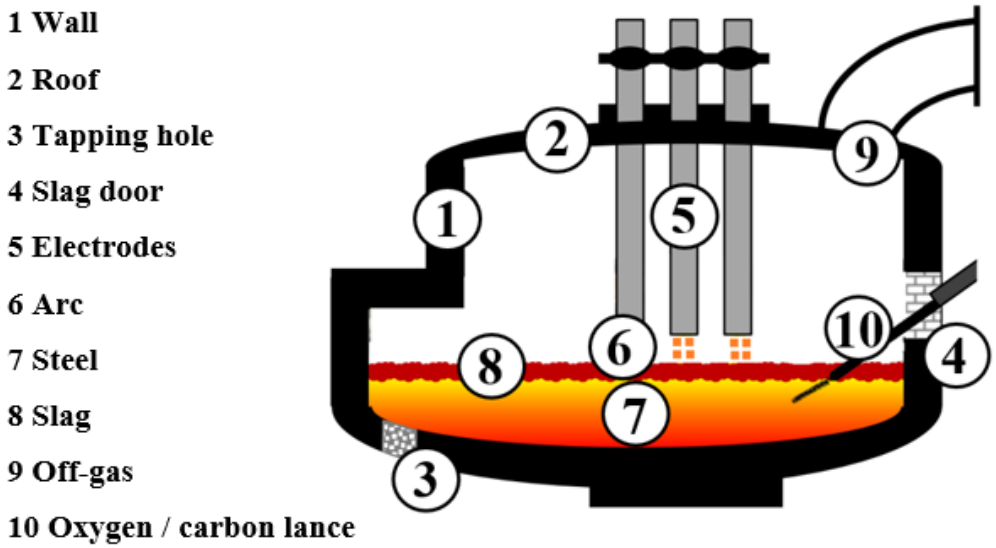

Figure 1. Main structure and equipment of EAF (modified from Meier et al. 2017).

2.3.2 Electrodes

The electrodes used in the EAF operations are artificially made graphite electrodes. Raw materials such as petroleum coke and coal tar pitch are used at the electrodes, and they are manufactured at high temperatures. The diameter of the electrodes can vary between 45 cm and 70 cm. The electrodes tend to wear during the EAF process, and by controlling and minimizing the wear of the electrodes significant savings of money, raw materials and energy can be achieved. The wear can be continuous, such as tip wearing or side wall oxidation, or discontinuous such as tip spalling, butt losses and electrode breakage. The electrode lifting device consists of columns and electrode arms that are usually current conductive. The lifting and swinging movements are typically done hydraulically. (Madias 2014, p. 281; Rafiei et al. 2018, p. 465; Jones et al. 1998, p. 533–534, 564–565)

2.3.3 Injection and burner systems

Injection of different kinds of solids and gases to the furnace is done by lances and burners. Oxygen is mainly supplied to the steel through the slag door by lances, which can be consumable pipe lances or non-consumable water-cooled lances. The consumable lances can penetrate the slag-metal interface in the furnace, which causes melting and wearing of the lance over time. Thus the lance must be periodically replaced. As the tip of the lance melts the lance is being driven forward to keep the injection operation optimal. Non-consumable lances do not wear significantly. They use high pressure injection and an appropriate angle so that the oxygen can penetrate the slag-metal interface without the need for a contact of the lance with molten metal. The lances are mainly made of either high alloy or stainless steel. The slag door lances can be so-called multi-use lances which can be used either in an oxy-fuel burner or oxygen lance mode. Sometimes carbon and fluxes can be injected with the oxygen lances. The general way is to use two lances at the slag door, one for injecting oxygen and the other for injecting carbon. The slag door lances are usually operated with a manipulator, which can be partly or fully automated. The injection firing rate can be adjusted, and the minimum flow rate is being used to prevent clogging caused by the splashing of slag. Injection through the slag door increases harmful air infiltration into the furnace, so alternative configurations such as injecting through the side wall of the furnace have been introduced in some steel melting shops. (Jones et al. 1998, p. 538–539, 601)

Oxy-fuel or natural gas burners are used to improve the smelting of steel in so-called cold spots which are located for example between the electrodes and at the nose section of the furnace. The burners can be located to the side walls, to the roof of the furnace, or to the slag door. (Jones et al. 1998, p. 537–538)

Carbon and flux injection can also be done via separate injectors located in different places around the furnace shell. Injection of carbon from several different places improves the slag foaming process and makes the foam layer more uniform. Injectors may be located around the furnace at the same vertical level or at different vertical levels so that the upper injectors can be used when the slag bath rises due to foaming. Usually, the injected carbon is in a powder form, and it is being injected by using air as a carrier gas. (Rodriquez et al. 2001, p. 298; Jones et al. 1998, p. 540) An example of EAF with different kinds of injectors and lances is presented in Figure 2.

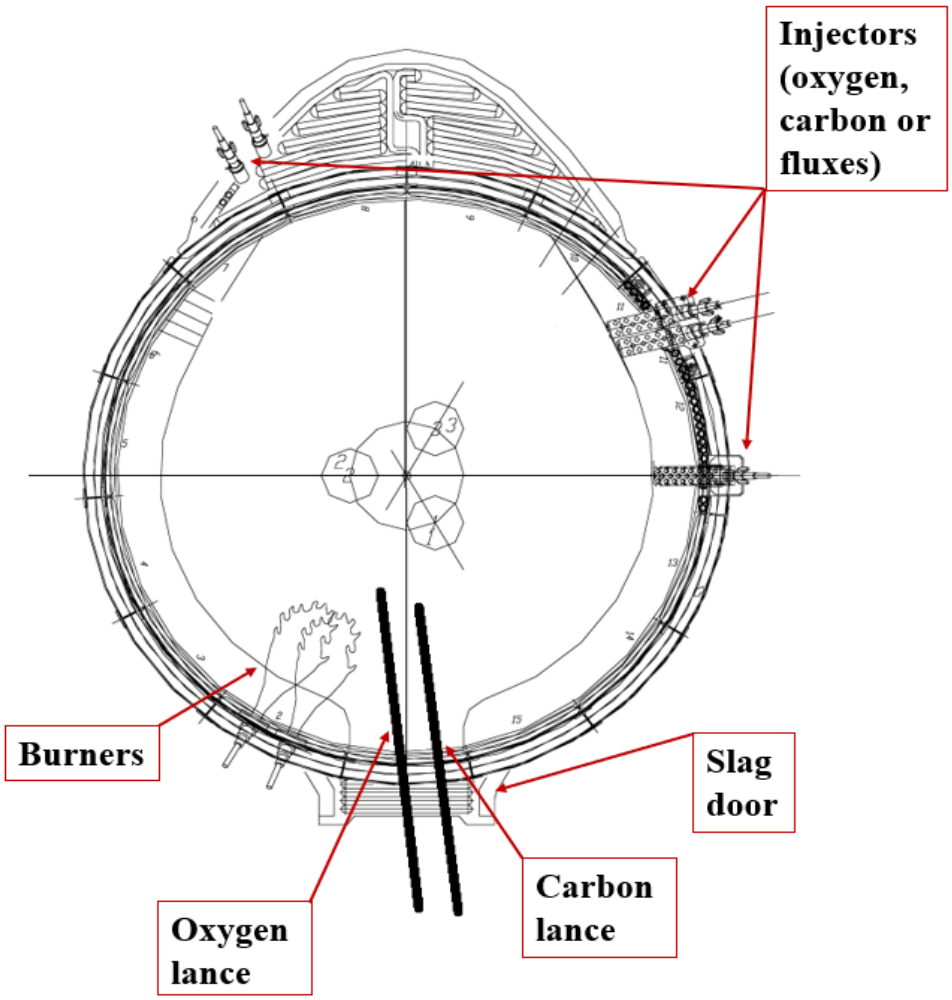

Figure 2. An example of EAF layout with additional injection and burner systems (modified from Memoli et al. 2004).

3 FOAMING OF SLAG

The foaming of slag in steelmaking has been investigated extensively in recent decades, but the phenomenon can still be sometimes unpredictable and cause problems in the steelmaking process. The foaming of slag occurs in a number of different steelmaking processes, such as EAF and BOF. The foaming is being caused by bubbles which are formed by chemical reactions, and it can be observed as lifting of the slag layer on top of the molten steel. The size of bubbles in the foam can vary a lot, and the foam can behave in different ways depending on the physical and chemical conditions in the steel-slag system. (Zhu et al. 2012, p. 751; Sahajwalla et al. 2006, p. 639; Liukkonen et al. 2021, p. 11)

3.1 EAF slag

Slag is a by-product of steelmaking process. Often slag is described as a harmful waste, but in fact it has several important functions in steelmaking. It absorbs deoxidation products and impurities from steel, prevents steel reoxidation, protects electrodes and refractories from thermal radiation and acts as a thermal insulator between the metal and air. (Luz et al. 2011, p. 91; Te et al. 2020, p. 5)

In metallurgy, slags are formed when a flux material reacts with unwanted materials or products of oxidation of solute elements which are not suitable for the process or the final product. The slag usually forms a distinct layer which is unmixable with the metal, enabling the slag and metal to be separated with relative ease. (Gaskell 2007, p. 442)

The color of EAF slag is typically black or grey, and the main chemical components are CaO, SiO_2, FeO and Al_2O_3. In addition, EAF slag usually contains minor elements, like MnO and MgO, which may have been dissolved from the furnace refractory materials into the slag. (Teo et al. 2020, p. 5–7; Luz et al. 2011, p. 92)

3.1.1 Basicity of slag

Basicity is an indicator of the structure of slag, and it affects the behavior and properties of slag. A common way to describe the basicity is to divide different components of slag into network formers and network breakers. SiO_2, which is a base component of slag,

forms a tetrahedral SiO_4^- structure, a so-called base network of slag, in which the Si^{4+} cations are surrounded by four O^{2-} anions. Depending on the amount of SiO_2 in the slag a varying amount of slag can be in this tetrahedral network form, where O^{2-} anions are shared with tetrahedrons next to each other. The amount of such a network structure in slag reflects its basicity. Other oxidic components can either break those oxygen bridges between tetrahedrons or create new bridges. The oxidic components which break the oxygen bridges between tetrahedrons when being dissolved into the slag are called basic components. Similarly, oxides that create new oxygen bridges between tetrahedrons when being dissolved into the slag are called acidic slag components. In addition, some components are called amphoteric, which means that they can act either basic or acidic, depending on the composition of the slag. An example of this kind of component is Al_2O_3. Amphoteric components act as basic components if the slag already contains a lot of acidic components in it and vice versa. (Slag Atlas 1995, p. 10; Husslage 2004, p. 43)

In practice, a numerical value for the basicity of slag is often calculated using the ratios of basic and acidic components in it. Components like CaO, MgO and FeO are described as basic, and components like SiO_2 as acidic. In metallurgical processes Al_2O_3 is also often described as an acidic component when calculating the basicity of the slag. The most common way to calculate the slag basicity B is described in Equation (1):

$$B_1 = \frac{wt\text{-}\%\ (CaO)}{wt\text{-}\%\ (SiO_2)}. \tag{1}$$

This equation does not consider other components of the slag. In EAF slag, components like MgO, Al_2O_3 and FeO can greatly affect the basicity of the slag. Basicity can be described by several other indices, as presented in Equations (2)–(4): (Slag Atlas 1995, p. 10; Pretorius & Carlisle 1998, p. 82)

$$B_2 = \frac{wt\text{-}\%\ (CaO)}{(wt\text{-}\%\ (SiO_2) + wt\text{-}\%\ (Al_2O_3))} \tag{2}$$

$$B_3 = \frac{(wt\text{-}\%\ (CaO) + wt\text{-}\%\ (MgO))}{(wt\text{-}\%\ (SiO_2) + wt\text{-}\%\ (Al_2O_3))} \tag{3}$$

$$B_4 = \frac{(wt\text{-}\%\ (CaO) + wt\text{-}\%\ (MgO))}{wt\text{-}\%\ (SiO_2)}. \tag{4}$$

3.1.2 Viscosity of slag

The viscosity of slag is an important property which affects the behavior of the slag and the whole steelmaking process a lot. A usual way to describe viscosity is the internal friction of liquid. The chemical composition of the slag greatly affects its viscosity. Basic slag components and their tendency to break the silicate network of slag causes a decrease in the viscosity of the slag. On the other hand, acidic components and their tendency to build up the silicate network causes an increase in the viscosity of the slag. The viscosity of slag containing a large amount of silica is therefore very high, and correspondingly the addition of basic components such as CaO or MgO to the slag reduces its viscosity. (Seetharaman et al. 2005, p. 267)

Another important variable affecting the viscosity of the slag is the temperature. In general, when the temperature of the slag gets higher, the viscosity of the slag decreases due to the loosening of the structure of the slag. The relationship between the temperature of slag and the viscosity is shown in the Arrhenius equation (5):

$$\eta = A_A \cdot e^{\frac{E_A}{RT}}, \tag{5}$$

where η is the dynamic viscosity of the slag, A_A is the pre-exponential frequency factor, R is the gas constant, T is the temperature of slag (K) and E_A is the activation energy for viscous flow. The SI-unit for viscosity is Pa·s. (Seetharaman et al. 2005, p. 269; Kekkonen et al. 2012, p. 7, 9)

Effective viscosity is a way to express the effect of solid particles on the viscosity of the slag. In certain phenomena, solid particles have a great effect on the viscous behavior of the slag. The effective viscosity can be calculated for example by Equation (6):

$$\eta_c = \eta(1 - 1.35\Theta)^{-5/2}, \tag{6}$$

where η_c is the effective dynamic viscosity of the slag and Θ is the fraction of precipitated solid phases in the slag. (de Almeida et al. 2017, p. 475)

3.1.3 Surface tension of slag

The surface tension of slag is a property of the interface between the slag and air. The surface of the bulk affects the surface tension more than the bulk itself. Surfactants with

low surface tension tend to occupy the surface layer of slag. The surface tension of slag can be calculated with the following Equation (7):

$$\sigma = \Sigma_i \sigma_i \cdot X_{i,} \quad (7)$$

where σ is the surface tension of slag, σ_i is the surface tension factor of a certain component in slag and X_i is the molar fraction of a certain component in slag. The surface tension factors have been determined with different kinds of surface tension measurement methods in different temperatures. In general, the surface tension factor for SiO_2 is the smallest one of the most common slag components. In 1673 K the surface tension factor for SiO_2 is 0.29, for MgO 0.51, for FeO 0.57, for CaO 0.60 and for Al_2O_3 0.64. Normally the higher the temperature of slag the lower the surface tension. An exception is slags with high content of SiO_2, which have the opposite effect to the surface tension. However, it should be noted that the effect of temperature on the surface tension of slags is relatively low compared to the effect of chemical composition. Normally the surface tension of slag is 0.2–0.7 N/m, which is lower than the surface tension of metals. (Nakashima & Mori 1992, p. 13; Mills et al. 2011, p. 656–657)

3.1.4 Slag-metal interfacial tension

The interface between the slag and the metal phase is one of the key elements in steelmaking. The interface and its properties are greatly affected by the composition of both the metal and the slag. Measuring the interfacial tension between slag and metal is difficult due to the reactions happening between the phases. The compositions at the interface vary greatly during steelmaking processes. Also, the electrochemical characteristics between the slag and steel phases affects the interfacial phenomenon. (Nakashima & Mori 1992, p. 15)

For the composition of metal, oxygen and sulfur are the most common surfactant elements thus having a great effect on the interfacial tension. From compounds, SiO_2, P_2O_5, Cr_2O_3, CaS, V_2O_5 and CaF_2 are examples of surfactants. Even small amounts of surfactants adsorbed to the metal side of the interface can decrease the interface tension at the slag-metal interface largely. (Nakashima & Mori 1992, p. 15; Hara & Ogino 1992, p. 83; Lahiri & Pal 2004, p. 474)

3.1.5 Density of slag

The density of slag is lower than the density of steel, resulting a typical phenomenon of steelmaking where the molten slag layer floats on top of the steel layer (Hosseini et al. 2016, p. 1). The density of slag can be calculated with the following Equation (8):

$$\rho = \frac{\Sigma_i X_i \cdot M_i}{Vm}, \tag{8}$$

where ρ is the density of the slag, X_i is the mole fraction of component i in the slag, M_i is the molar mass of component i in the slag and V_m is the molar volume of the slag. V_m can be calculated from the molar fractions and molar volumes of components in the slag. (Xin et al. 2017, p. 1340; Shu & Chou 2013, p. 572) The density of SiO_2 is lower than the density of the other common slag components, and thus the amount of SiO_2 in the slag affects the total density of the slag a lot. Also, the temperature of the slag affects the density, usually the lower the temperature of the slag the higher the density. However, this effect is small in comparison to the effect of the chemical composition of the slag and therefore it is not considered in Equation (8). (Turkdogan 1996, p. 170–171; Lee et al. 2012, p. 2145)

3.2 Foaming practice in EAF

In EAF steelmaking slag foaming is usually promoted by injecting oxygen and pulverized carbon into the steel. The source of carbon varies, but it is mainly fossil type: anthracite, or metallurgical coke. (Fidalgo et al. 2015, p. 274) Optimizing the foaming of slag is very important for the efficiency and productivity of the EAF process. In successful slag foaming practice, the foam covers the electrodes appropriately and prevents the refractory materials from harmful shocks of the arc. This enables higher power supply and efficient energy transfer and prevents heat losses. Foaming can also be too intense, which can lead to process disturbance and equipment breakdowns. Thus, the appropriate foaming reaction is neither too strong nor too weak. By looking at the foaming practice from the perspective of different chemical and physical phenomena, favorable conditions for the foaming can be achieved. Also, the properties of the materials that affect the foaming process must be considered. (Son et al. 2021, p. 556)

3.2.1 Gas generation

The foaming of the slag is associated with several reactions that result in the generation of gaseous components. The oxygen injected into the metal reacts with the iron in the liquid metal, and iron oxide is formed. The reaction is described in Equation (9):

$$[Fe] + ½\{O_2\} = (FeO). \quad (9)$$

The amount of formed iron oxide varies depending on the chemical composition of the metal and the amount of oxygen injected, but in general, it can be said that the percentage of iron oxide in the slag is normally at least 20 wt-%. The iron oxide reacts with the injected solid carbon and the carbon in the liquid steel, thus forming liquid iron and gaseous carbon monoxide (Equations (10)–(11)):

$$(FeO) + \langle C\rangle = [Fe] + \{CO\} \quad (10)$$

$$(FeO) + [C] = [Fe] + \{CO\}. \quad (11)$$

Equation (12) shows another reaction in which carbon monoxide is formed:

$$[C] + ½\{O_2\} = \{CO\}, \quad (12)$$

where the carbon from the liquid steel reacts with the oxygen and forms gaseous carbon monoxide. Another gaseous component being formed is carbon dioxide. Its formation is affected by Equation (13):

$$(FeO) + \{CO\} = [Fe] + \{CO_2\}, \quad (13)$$

where iron oxide reacts with carbon monoxide and forms iron and carbon dioxide. Part of the carbon dioxide then reacts with injected carbon, and forms carbon monoxide as Equation (14) shows:

$$\{CO_2\} + \langle C\rangle = 2\{CO\}. \quad (14)$$

The round brackets, square brackets, angle brackets and curly brackets used in the equations denote a species in slag phase, metal phase, solid phase and gas phase, respectively. All of the reactions (10)–(14) form carbon monoxide or carbon dioxide, of which carbon monoxide, in particular, is important for the foaming of the slag. The equations show that both the oxygen injected into the metal and the iron oxide generated

in the slag play a major role in foaming. Reactions (9) and (12) take place in the metal-gas interface, reactions (10) and (14) at the carbon-slag interface, reaction (11) at the metal-slag interface and reaction (13) at the slag-gas interface. (Luz et al. 2011, p. 91; Morales et al. 1995, p. 1058)

3.2.2 The structure and characteristics of foam

The chemical reactions at the slag-metal interface are important for the slag foaming. Two principal factors can be pointed out about the foaming phenomenon: 1) The gas evolution rate by chemical reactions and the consequent rate of bubble generation and 2) Foam stability in the melt. If the gas evolution rate at the slag-metal interface is vigorous, it facilitates the creation of a foamy slag which composition is based on bubbles. In practice, an accurate examination of the internal structure of slag is not possible. However, some generalizations can be made. Two clearly separable layers in the melt associated with foaming are the foam layer itself and a denser layer of the slag below the foam layer that has a much lower void fraction. In Figure 3, the general structure of a foaming liquid can be seen. The upper foamy layer (void fraction over 0.74) consists of likely metastable bubbles which form a lamellae-kind of structure to the foam where the bubbles are in the shape of quasiregular polyhedron and well-drained. The bubbles at the lower part (void fraction between 0.52 and 0.74) are more transient and they tend to form an assembly of thick-filmed spheres. Although the behavior of bubbles in real situation cannot be accurately characterized, this kind of angle of view to the foaming phenomenon has been presented in many studies. (Nexhip et al. 2004, p. 287; Hara & Ogino 1992, p. 81)

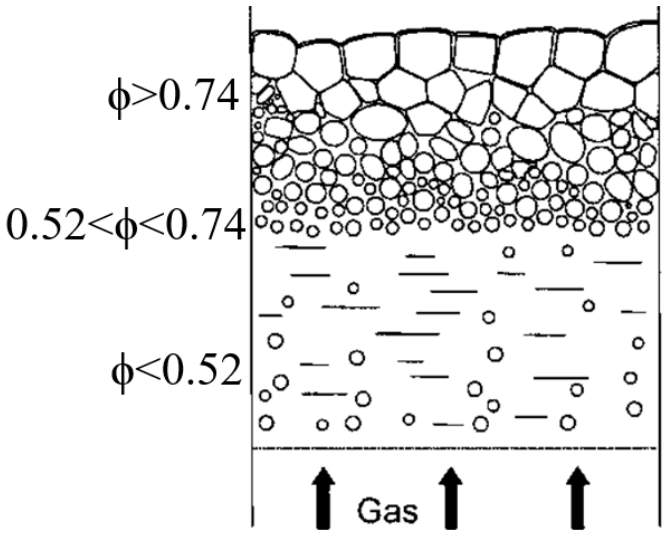

Figure 3. The structure of a foaming liquid (ϕ = void fraction of gas within bubbles) (modified from Nexhip et al. 2004).

The bubbles in the foam are separated by very thin liquid films. At the angles of the polyhedral bubbles and at the liquid between spherical bubbles are connecting points of films called Plateau borders where three adjacent films meet each other. This junction occurs in all foams and it interconnects the cell lamellae in a triangular connecting point. Between the borders are planar films, which are longer and have a relatively large part of common surface area with the bubbles. The bubble structure is illustrated in Figure 4.

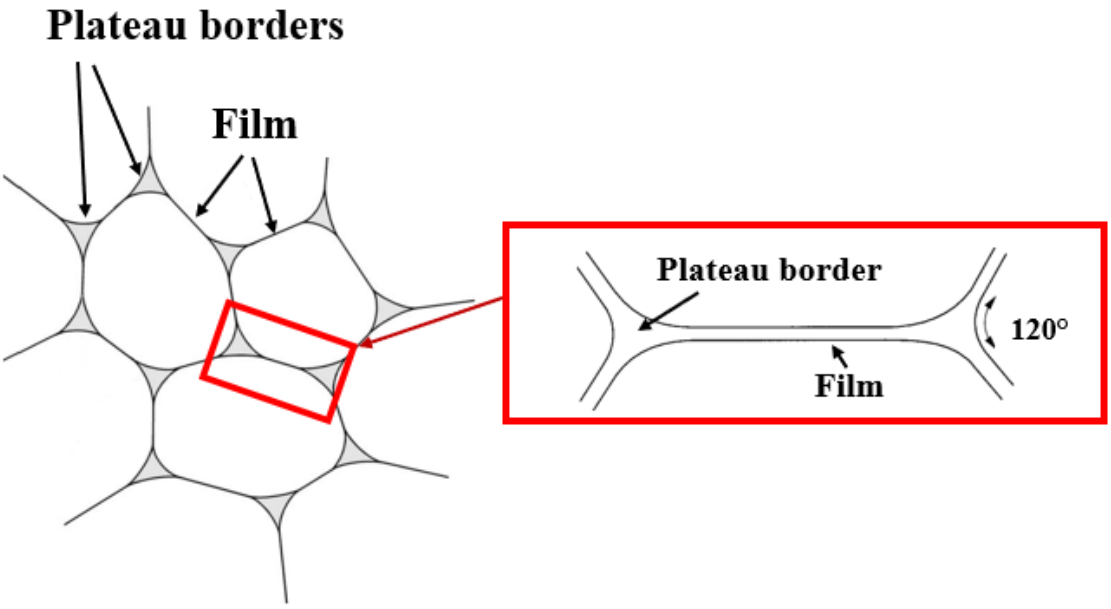

Figure 4. Schematic of bubble films and Plateau borders in foam (modified from Nexhip et al. 2004 & Ireland 2008).

When new layers of bubbles are formed into the foam, the bubbles move under the influence of surface tension and capillary forces to new places, and their relative order may change. Momentarily more than three planar films can join on the borders, but to achieve mechanical equilibrium and stable geometry of packing, junctures of four films will instantaneously disproportionate into two junctures by the generation of a new film. This will happen until only three films meet at the borders again. In an ideal situation the films always radiate 120° outward from the Plateau borders. (Nexhip et al. 2004, p. 288; Lahiri & Pal 2004, p. 474)

The Plateau borders play a critical role in the lifetime of bubbles. Between the borders and the film is a suction produced by a pressure difference. The pressure at the border region is lower than at the region where films of two bubbles are facing each other, and this pressure difference creates a suction that drives the liquid from the film to the Plateau

borders. The liquid flows downwards in the foam along the border channels under the influence of gravity. This causes the drainage of liquid out of the film, which leads to thinner films. When the thinness of film reaches a critical point, the film ruptures due to mechanical or thermal fluctuation, and the bubble collapses. (Nexhip et al. 2004, p. 288; Lahiri & Pal 2004, p. 474)

The force resisting the gravity at the films between the bubbles is called Marangoni force. When the bubbles rise towards the surface of the foam and the film gets thinner, slow-moving surfactants may be distributed vertically unevenly at the film. If no adsorption of the surfactants occurs at the top of the bubbles and no desorption occurs at the bottom of the bubbles, a surface tension gradient is being formed due to the uneven distribution of the surfactants. The surface tension gradient tends to lift the liquid upwards in the border channels between the bubbles, preventing the gravity-based fast draining of liquid from the film. In well-drained films, the collapsing of the bubbles may be prevented if the stabilizing effect is powerful enough to counterbalance the existing forces. This may lead to a greater number of bubbles generated in the upper layer of the slag foam. (Lahiri & Pal 2004, p. 474)

The structure of the foam in metallurgical processes varies greatly depending on the superficial gas velocity. At high velocities, the foam can behave quite differently compared to a case of slower velocities. Many studies related to foaming have focused only on gas velocities of 0.1 m/s or less. In the EAF process the gas velocities can vary from 0.1 to 0.7 m/s, so the information based on most of the laboratory-scale studies on foaming must be considered with caution. Zhu et al. (2012) brought together some differences between foaming reactions with low (up to 0.1 m/s) gas velocities and high (>1 m/s) velocities. Actually, the slags where high superficial gas velocities are involved can be called expanded slags instead of foaming slags because their structure is not likely for foaming liquids. The thin-walled, cellular structure of bubbles is missing, and the structure is more like a fluidized, foamy gas-slag mixture. This kind of expanded slag collapses immediately when the flow of gas to the slag is being stopped. The entire volume of the slag is expanded uniformly, in a raging, turbulent way, and the slag is composed only of one visible layer. With low gas velocities, one denser layer with a much lower void fraction can be seen separately under another layer of beer or soap kind of foam with cellular structure, as described earlier in this section. In Table 1 the differences between slag with low and high gas velocities are being compared.

Table 1. Comparison between the foaming and expanded slag (modified from Zhu et al. 2012).

Characteristics	**Foaming slag**	**Expanded slag**
Picture	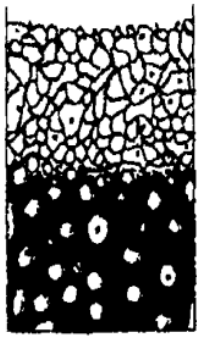	
Appearance	Like beer or soap foam	Turbulent
Uniformity	Two layers	One uniform layer
Gas velocity	0.01 to 0.10 m/s	>1 m/s
Void fraction	0.8 to 0.9	Varies with velocity
Foam height	Independent of tot. liquid vol.	Dependent on the tot. liquid vol.
Stability	Takes time to collapse	Collapses immediately

3.2.3 Foaming index

Various methods and models have been developed to estimate the intensity of foaming. One of those is the foaming index. It is in its simplest form defined as the ratio of the foam height in the vessel to the superficial gas velocity (Equation (15)):

$$\Sigma = \frac{\Delta h}{V_g^s}, \tag{15}$$

where Σ is the foaming index, Δh is the change in slag height and V_g^s is the superficial gas velocity, which can be calculated with Equation (16):

$$V_g^s = \frac{Q}{A}, \tag{16}$$

where Q is the gas flow rate through the slag and A is the cross-sectional area of the vessel. (Zhu et al. 2012, p. 571) In physical terms, the foaming index is the average traveling time of the gas in the foam. This kind of foaming index gives a straightforward way to observe the foaming phenomenon in any kind of process where foaming takes place, but its use for the foaming in metallurgical processes is questionable as many important factors occurring in the processes have not been taken into account. The

foaming index described in Equation (15) only considers the behavior of liquid, but not the interaction between molten liquid and the refractory materials or the chemical interaction between the slag and metal, although these interactions are present in foaming in metallurgical processes. In addition, the linear relationship between the height of the slag layer and the superficial gas velocity only takes place at temperatures above 1500 °C. For these reasons, alternative foaming indices have been developed in several different studies that also consider other aspects related to the foaming phenomenon. (Luz et al. 2011, p. 91–93)

In more developed models used for evaluation of foaming of metallurgical slags the viscosity, surface tension and density of slag are considered. Ito & Fruehan (1989a) derived the following Equation (17) for slag system containing CaO, SiO_2, FeO and Al_2O_3:

$$\Sigma = 5.7 \cdot 10^2 \frac{\eta}{\sqrt{\sigma\rho}}. \tag{17}$$

Equation (17) does not take into account the present solid particles in the liquid or the bubble size in the foam, and it overemphasizes the effect of viscosity. Later, Jiang & Fruehan (1991) adjusted the equation. They studied the effect of different properties with dimensional analysis resulting in a smaller effect of viscosity to the foaming index, which can be seen in Equation (18):

$$\Sigma = 115 \frac{\eta}{\sqrt{\sigma\rho}}. \tag{18}$$

Also some other similar equations where the value of the coefficient is different have been obtained. The value and the effect of different parameters in the equations are strongly related to the composition of the slag and other materials and other differences between the studies. In 1995 Zhang & Fruehan added the effect of bubble size to the equation. They studied the effect of different kinds of bubbles in a laboratory-scale by injecting argon gas with a special nozzle into liquid $CaO{\cdot}SiO_2{\cdot}FeO{\cdot}Al_2O_3$ slag mixed with carbon saturated iron. The study resulted in Equation (19):

$$\Sigma = 115 \frac{\eta^{1.2}}{\sqrt{\sigma^{0.2}\rho {D_b}^{0.9}}}, \tag{19}$$

where D_b is the average bubble size in the slag. Zhang & Fruehan found out in their studies that adjusting bubble size created significant differences to the foaming phenomenon. This index increases with the viscosity and decreases with the bubble diameter and density, and it is quite independent of the surface tension. It should be noted that the effect of additional carbon injected into the melt is not being considered in the indices above. The values that can be obtained for the foaming index vary greatly depending on the equation used, but they still provide a basis for examining the foaming phenomenon.

3.3 Suitable slag properties for optimal foaming

Several different properties of slag affect the characteristics of the foaming phenomenon. Research has been focused on the subject, and it has been found that the properties of slag and the foam itself may limit or improve the generation and lifetime of foam. Many of the properties also have an effect on each other, not only on the foaming.

3.3.1 Effect of basicity

When the basicity of the slag increases, the surface tension of the slag increases and the viscosity of the slag decreases. E.g. CaO, which is a basic slag component, tends to break the silicate network structure and therefore decreases the viscosity of the slag. The surface tension factor of CaO is high, so its effect on the surface tension is increasing. On the other hand, components like SiO_2 work the opposite way. Studies on the effect of the basicity to slag foaming often use a simple way to describe the basicity of the slag as the ratio of CaO/SiO_2 in the slag (Equation (1)). The effect of basicity on the foaming is related to the viscosity and surface tension in the previous studies, such as Jung & Fruehan (2000) and Ito & Fruehan (1989a). Figure 5 shows two diagrams obtained from the studies related to the basicity of slag and foaming. On the left side of the figure the foaming index for $CaO{\cdot}SiO_2{\cdot}FeO$ slag with around 3–5 wt-% of Al_2O_3 dissolved from the refractories is shown as a function of basicity calculated with Equation (2). It also describes the effect of two different contents of FeO in the slag (60 wt-% and 30 wt-%), and 1 wt-% of P_2O_5 in two scores. On the right side of the Figure 5 a calculated foaming index as a function of basicity of $CaO{\cdot}SiO_2{\cdot}FeO$ slag with 20 wt-% of FeO is being shown. (Ito & Fruehan 1989a, p. 513; Ito & Fruehan 1989b, p. 518)

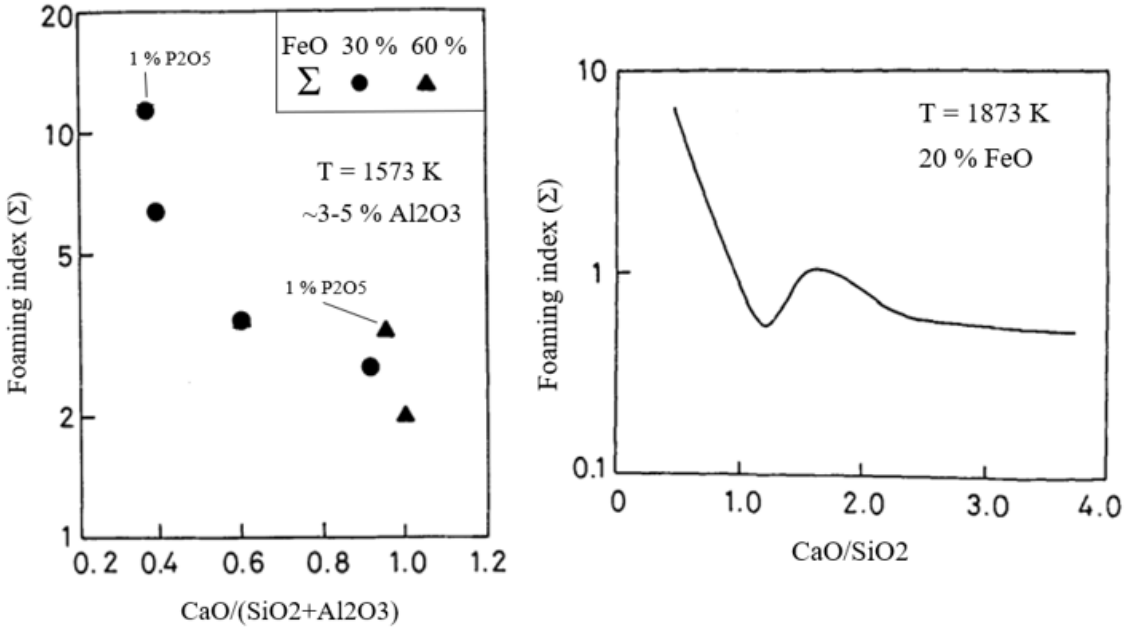

Figure 5. The change of foaming index Σ with basicity of slag (modified from Ito & Fruehan 1989a & 1989b).

Both of the graphs illustrate that as the basicity of slag increases the foaming index decreases, especially at low values of basicity. On the graph at the right side the index gets higher at the basicity values 1.2–1.8. This is being explained by the effect of second-phase particles at higher concentrations of $2CaO \cdot SiO_2$ increasing the bulk viscosity of the slag. (Ito & Fruehan 1989b, p. 517) The effect of these second-phase particles will be discussed in detail in Section 3.3.6.

3.3.2 Effect of viscosity

The effect of the viscosities of the slag and the foam on the foaming phenomenon has been studied a lot, but all of the results are not consistent. Some of the results obtained in recent studies indicate a favorable effect of increasing viscosity, and in some of the results the effect has been described as limited. The viscosity clearly has an important effect on the structure and the lifetime of the foam. (Zhang et al. 2021, p. 1348)

In the studies of Ito & Fruehan (1989a; 1989b), Jiang & Fruehan (1991) and Zhang & Fruehan (1995) the effect of viscosity to the foaming has been examined with laboratory-scale experiments. In these experiments, argon was injected into different synthetically made slags. The viscosity of these slags were modified by changing the chemical composition of the slags. The results emphasize that increasing the viscosity

also increases the foaming index and the foaming height in steady-state. This is explained by the increase of solid particles in the slag.

Barella et al. (2012) used oils and compressed air in the experimental trials considering foaming. According to them, increasing the viscosity to some extent increases the height of the foam, but the effect is not linear and it is associated with the drainage of the liquid film between the bubbles. High enough viscosity prevents this drainage effect.

Wu et al. (2010) studied the effect of viscosity by simulating the slag foaming with silicone oil and compressed air as an injection gas. In the results, the foam height only increased with viscosity to a certain point. After the critical level of the viscosity was obtained, the foam height started to come down. They concluded that an increase in the viscosity of slag does not linearly improve the foaming effect.

In the studies of Zhang et al. (2021), glycerol solution was used to simulate the physical properties of metallurgical slag. Compressed air was injected into the glycerol with different superficial gas velocities to form the foam, and glycerol with different values of viscosities was tested. The results showed that under low superficial gas velocities (<0.60 mm/s) different values of viscosity had no obvious change to the height of the foam. With higher velocities the foaming rates even decreased when the viscosity was increased.

As a summary of the results obtained from various studies, it can be said that the viscosity of the slag cannot be too low or too high. When the viscosity is low, the bubble structure is not durable and the foam may be suppressed. When the viscosity is too high, it prevents the formation of the bubbles. (Luz et al. 2011, p. 94)

3.3.3 Effect of surface tension and slag-metal interface tension

In general, a decrease in surface tension has been studied to improve the foaming of the slag. This is being considered to correlate with a decrease in the basicity and an increase in the viscosity of the slag. (Skupien & Gaskell 2000, p. 921) This principle has also been used in various foaming index formulas, such as Equations (17)–(19). When the surface tension of the foaming slag increases, the film between the bubbles at the foam gets thinner which causes rupture of the bubbles. (Luz et al. 2011, p. 94)

The amount of the surfactants in the slag has a greater effect on the foaming than the surface tension itself. The Marangoni-effect caused by a local difference in concentration of surfactants (see Section 3.2.2) affects the slag foaming (Hara & Ogino 1992, p. 84). This effect prevents the drainage of the liquid from the bubble film, and therefore the role of the surfactants is important for a stable foaming. The surfactants also lower the interfacial tension at the slag-metal interface, which leads to a low equilibrium contact angle and smaller bubble size. (Lahiri et al. 2003, p. 346–348)

3.3.4 Effect of bubble size

The stability of the foam layer is depending on the stability of the bubble layer, so the bubbles, their size and shape and their survival time in the foam play an important role in the foaming phenomenon and stability of the foam. The size of the bubbles in the foam is generally divided into two categories: large and small bubbles. The large bubbles are generated mostly by the gas injected, and the majority of the small bubbles is being formed by the reactions occurring at the slag-metal interface. Small bubbles are often described as more stable than the larger ones, and they are the ones that mostly cause the slag foaming in pyrometallurgical processes. (Hara & Ogino 1992, p. 81, 85)

The smaller the bubbles in the foam are the thicker the film between the bubbles is, as the void fraction in the foam scales with the size of the bubbles. Therefore, smaller size of the bubbles reduces the bubble-breaking drainage effect. (Luz et al. 2011, p. 94)

3.3.5 Effect of temperature

The effect of temperature on foaming is related to the viscosity. As the temperature of the slag rises, its viscosity decreases, affecting the intensity of the foaming negatively. Ozturk & Fruehan (1995) made laboratory-scale foaming experiments with synthetic slag in different temperatures. The results clearly showed that at typical slag temperatures the higher the temperature the lower the foaming index based on the height of the slag. This can be seen from Figure 6. The increase in the temperature also reduces the number of suspended second phase particles in the slag. Consequently, the effective viscosity of the slag decreases which hinders the foaming. (Luz et al. 2011, p. 95)

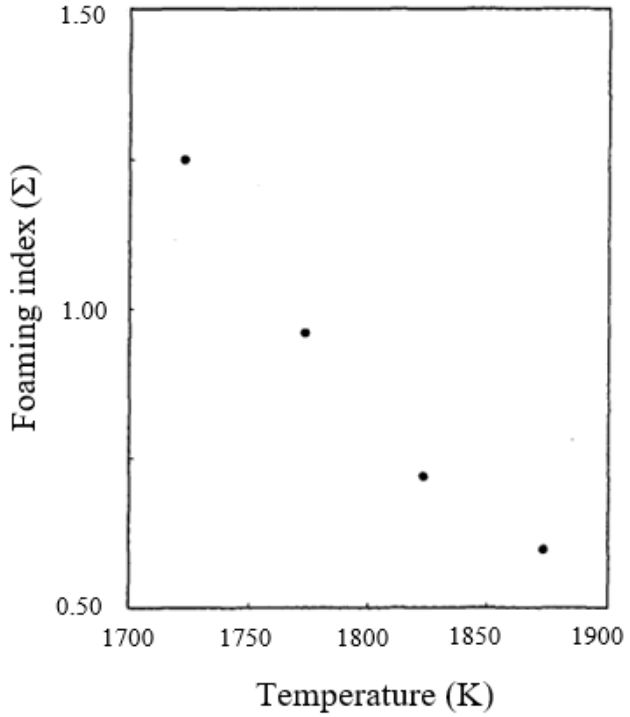

Figure 6. Effect of temperature on foaming index obtained from laboratory-scale foaming experiments (modified from Ozturk & Fruehan 1995).

3.3.6 Effect of suspended second phase particles

The suspended second phase particles in the slag have been considered to be one of the most important parameters affecting the foaming phenomenon. As already stated before, they affect the effective viscosity of the slag as shown in Equation (6). The higher the amount of suspended second phase particles the higher the effective viscosity of slag. Thus, the presence of the second phase particles is generally positive for the foaming. However, it should be noted that the number of the second phase particles in the slag cannot be too high for the foaming phenomenon to occur. In the studies of Luz et al. (2011) the coefficient Θ in Equation (6) describing the fraction of precipitated solid phases has been stated to be relevant between values from 0 to 0.74. If the amount of second phase particles and the effective viscosity of the slag gets too high, the slag gets over-saturated which negatively affects the foaming as can be seen from Figure 7. (Luz et al. 2018, p. 8735)

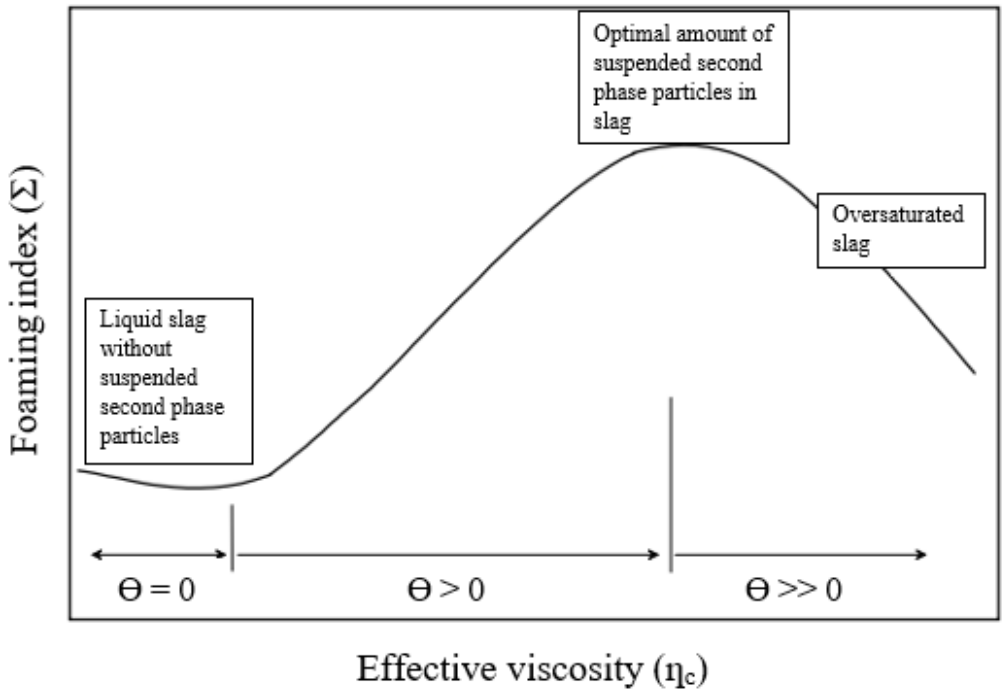

Figure 7. The effect of suspended second phase particles to foaming (modified from Pretorius & Carlisle 1998).

One example of the solid second phase particles affecting the foaming is dicalcium silicate, $2CaO \cdot SiO_2$, which is formed when the slag contains enough CaO. This also explains the effect which can be seen in Figure 5, where the foaming index is being shown as the function of basicity. When the content of CaO and the basicity of the slag gets to a high enough level, dicalcium silicate particles are being formed and the foaming index increases, although in general the increase in the basicity reduces the foaming index due to increasing viscosity and decreasing surface tension. Another important second phase particle is magnesiowüstite, MgO·FeO. In addition to the increase of effective viscosity, these particles also have another positive effect to the slag in terms of foaming. They act as gas nucleation sites for the formation of small bubbles in the gas, which are important for suitable foaming. (Kim et al. 2001, p. 321; Pretorius & Carlisle 1998, p. 80)

3.4 Relationship between the chemical composition of slag and foaming

The chemical composition of the EAF slag is a key element for the foaming. The proportions of different compounds affect the physical properties of the slag, and therefore the chemical composition of the slag should be able to be controlled in a way that the slag is favorable for the foaming.

The five main components of the EAF slag are CaO, SiO_2, FeO, Al_2O_3 and MgO. In addition, at some furnaces the average amount of MnO can be high. The EAF slag also contains a small number of other elements, like phosphorus and sulfur. (Teo et al. 2020, p. 7) The average composition of the slag can vary a lot depending on the raw materials, the wanted steel products, and other variables, which can be seen from Table 2. The average composition of the EAF slag has been listed based on a comprehensive literature review.

Table 2. Chemical composition of EAF slag averaged by literature review considering slags from different parts of world (modified from Vaiana et al. 2019).

Chemical composition	Average range (wt-%)
CaO	15–54
SiO_2	5–40
FeO	1.2–50
Al_2O_3	1–15
MgO	1–21.4
Others	0.05–5

Some authors prefer to divide these general slag components into two categories: refractory oxides (CaO and MgO) and fluxing oxides (SiO_2, FeO and Al_2O_3). The saturation of refractory oxides affects the amount of the solid second phase particles in the slag and the effective viscosity, thus being important components for stable foaming. The refractory materials of the EAF walls are usually MgO-based, which means that using a considerable amount of MgO in the slag prevents the refractories from chemical attack and wear. (Pretorius & Carlisle 1998, p. 81)

The basicity of slag can be calculated with Equations (1)–(4), depending on the situation. It has been considered to be one of the key elements of a foamable slag, and therefore especially the amounts of the most common slag components CaO and SiO_2 in slag must be determined with care. A higher basicity results in higher surface tension and lower viscosity, which is not favorable for stable foaming of the slag due to the increasing liquid drainage rate. (Zhu et al. 2012, p. 751) On the other hand, the saturation of basic components is important because of the suspended second phase particles. These factors have to be taken into account when balancing the slag basicity.

Al_2O_3 has also been considered to be an effective component for slag foaming. When SiO_2 in the slag is being replaced with Al_2O_3, it results a decrease in the solubility of MgO

and an increase in the solubility of CaO. This also has an effect on the amount of the second phase particles in the slag. This effect naturally depends on the relative amounts of MgO and CaO in the slag. In addition, an increase in Al_2O_3 content of the slag has been studied to create more aluminate tetrahedra [AlO_4^{5-}] structures to the slag with Ca^{2+} cations, which increases the viscosity of the slag. (Kim et al. 2001, p. 319)

3.4.1 Effect of FeO content

The FeO in the slag affects the CO generation, as can be seen from Equations (10)–(11). The reaction is overall important for the foaming phenomenon, so there must be some FeO in the slag to generate enough bubbles for the foam. However, the proportion of FeO cannot be too large, because increasing the amount of FeO in the slag decreases its viscosity, which affects the foaming negatively. (Chang et al. 2021, p. 1, 9) On the other hand, increasing the FeO content decreases the solubility of MgO to the slag, which means an increase in the amount of the solid second phase particles in the liquid slag (Pretorius & Carlisle 1998, p. 81). The suggested proper amount of FeO in the slag in terms of foaming is something between high (~40–50 wt-%) and low (~0–5 wt-%).

Attempts for determining suitable FeO content in the slag have been done in several studies. Bhoi et al. (2006) tested the foaming behavior of $CaO{\cdot}SiO_2{\cdot}FeO$ slag with FeO contents of 20–40 wt-%. They observed that the higher the amount of FeO, the higher the foam layer on the top of the slag. On the other hand, they also mentioned that increasing the amount of FeO decreases the viscosity, thus affecting the foaming index negatively. Corbari et al. (2009) studied the rate of the reaction of FeO in the slag with different kinds of carbon sources in a laboratory-scale. They concluded that the rate of CO generation by the reaction between FeO and carbon increases with the FeO content in the slag from 15 to 45 wt-%. They measured the foam height and observed that the height increased with FeO content from 15 to 25 wt-% and then decreased at higher contents of FeO. The higher gas generation rate at the slags with more than 25 wt-% of FeO had less effect on the foaming than the decrease in the viscosity, and therefore they suggested that 25 wt-% of FeO in the slag is the most suitable amount for proper foaming.

3.4.2 Composition ranges for suitable foaming defined in literature

It is not possible to determine one right composition for the EAF slag in terms of foaming, but some generalizations and composition ranges for suitable foaming have been defined

in research related to the topic. Morales et al. (1995) provided a foaming map that is shown in Figure 8. The map has been divided into three areas based on the calculated foaming behavior of the slag in different compositions. The foaming index and effective viscosity of the slag (Equation (6)) have been used as a basis for the calculations. Based on the map, some generalizations can be stated. Acid slags with low contents of FeO have the highest foaming index, and therefore they cause homogenous foaming according to this map. Slags with medium FeO contents and high basicity also cause foaming, which is being called heterogenous because the presence of the solid particles affect the stability of the foam formation at this composition range. At extremely high FeO contents there is no foaming at all. This is the only region where foaming will not happen. In other regions, also outside the marked "Homogenous foaming" and "Heterogenous foaming" regions, foaming might occur with varying degrees. The effect of solid particles suspended in the slag is marked on the map with a dotted line. This area has a high content of FeO and basic components.

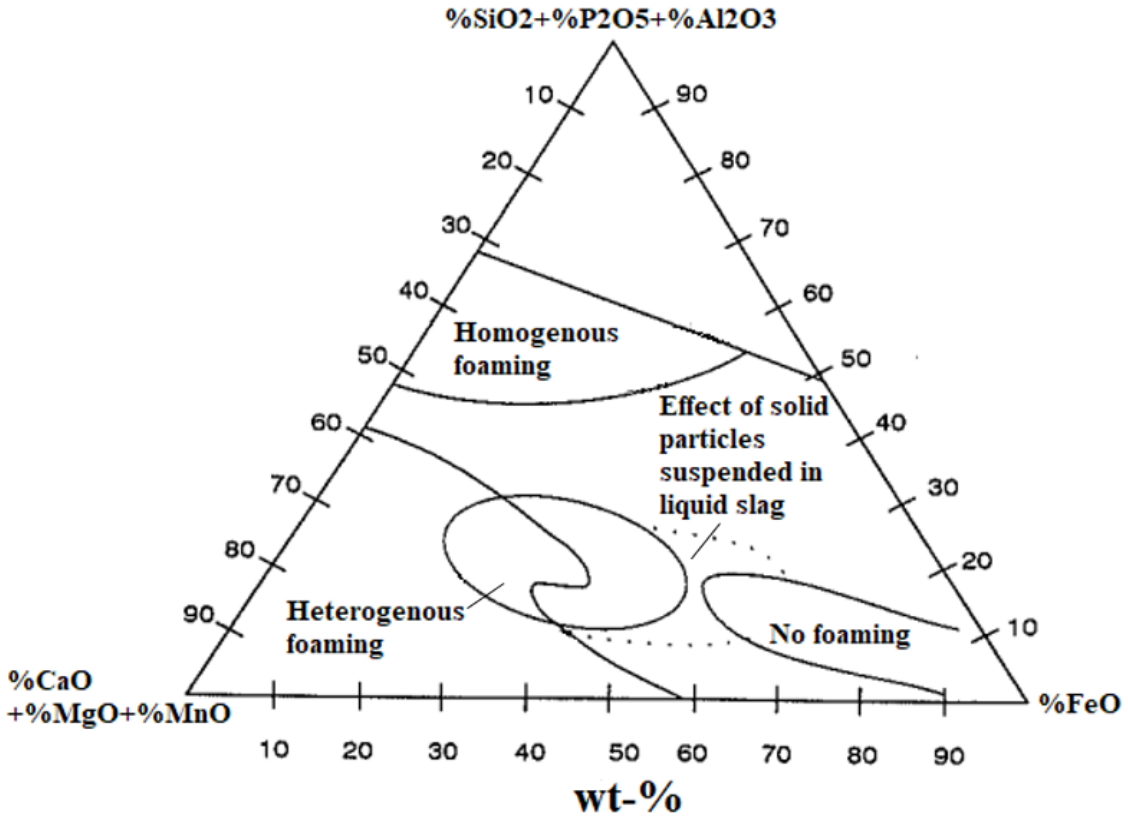

Figure 8. One example of the evaluation of suitable slag compositions in terms of foaming sketched on ternary phase diagram (modified from Morales et al. 1995).

The effect of MgO and FeO contents of the slag on its foamability has been studied by Pretorius & Carlisle (1998). They derived so-called Isothermal Solubility Diagrams for slags with different values of basicity, one of which can be seen in Figure 9 (for basicity of 2). In the diagram L means liquid, MW means magnesiowüstite and C_2S means dicalcium silicate. The region rounding the liquidus region is an inferred composition range with peak foaming characteristics, where the effect of the solid phase particles in the liquid slag is optimal. In Figure 10, the effective foaminess of slags with basicity of 1.5, 2.0 and 2.5 and suitable MgO contents is presented as a function of FeO content.

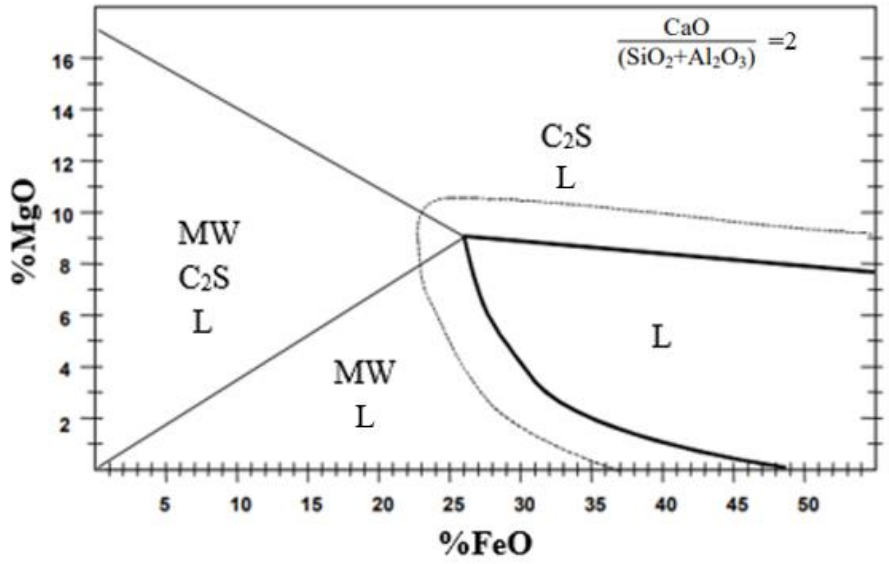

Figure 9. Isothermal Solubility Diagram considering FeO and MgO contents of slag for basicity of 2 (modified from Pretorius & Carlisle 1995).

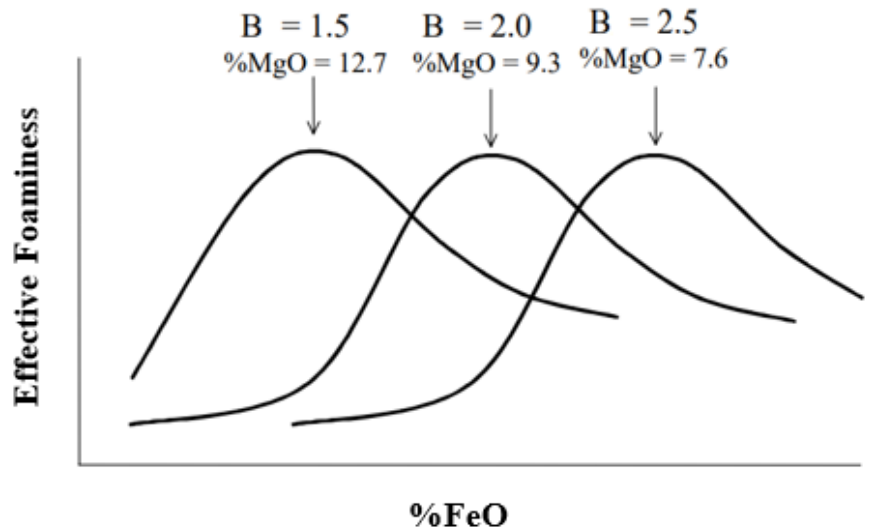

Figure 10. Effective foaminess of slags with different basicity and MgO contents as a function of FeO content (modified from Pretorius & Carlisle 1995).

With this kind of figures, possible composition ranges for slag can be estimated. However, it must be noted that these are just one kinds of suggestions. In real situations in the industry, good slag foaming behavior has been achieved with basicity less than 1.5 to more than 3.0 with FeO levels from 10 to 50% (Pretorious & Carlisle 1998, p. 94). In previous studies, the foaming index is often used as a measure of good foaming, and the assumptions are usually not being based on practical foaming observations. In the real EAF process slags with different compositions than the ones suggested above can cause optimal foaming of the slag.

4 BIOCHAR

Biochar is an organic material converted from biomass, which can be for example different parts of trees or crops. The production of biochar is done by thermal conversion of biomass under an oxygen-limited environment. Different biochar production processes are hydrothermal conversion, gasification, torrefaction and pyrolysis, which can be fast or slow. Charcoal is the name for biochar that is produced from woody biomass. (Lehmann & Joseph 2009, p. 1, 342; Ye et al. 2019, p. 3931; Weber & Quicker 2018, p. 241)

4.1 Raw materials

Biomass is the raw material of biochar. The main sources of biomass are plants and different parts of trees, but also waste from the food industry and manure of animals are categorized as biomass. In Finland, particularly different kinds of forest biomasses are available to be used as a raw material for biochar production. Forest chips from early thinnings, logging residues and stumps, forest industry residues like bark, sawdust and industrial wood chips, and recycled wood from the wood product market are potential and already used biomasses in Finland. Generally, biomass can be defined as hydrocarbon material that consists mainly of carbon, hydrogen, oxygen, and nitrogen. In addition, biomass contains smaller amounts of other components, such as sulfur. Some types of biomasses also contain significant amounts of inorganic species. The major organic components in woody and plant-based biomasses are cellulose, hemicellulose, and lignin. Cellulose is a polysaccharide that is insoluble to water. It acts as the major structure supporter in biomass cells. Cotton fibers, for example, are almost entirely pure cellulose, while in the cellular structure of trees the proportion of cellulose is roughly 50%, and the rest of the structure consists of hemicellulose and lignin. Hemicelluloses are soluble to dilute alkali, and they are in association with cellulose in the cell wall. The structures of hemicelluloses are branched, and they usually carry 50–200 monomeric units and a few sugar units like xylan. The proportion of hemicellulose in woody biomass is usually 10–30%, and the rest 20–40% consists of lignin, which is a highly branched mononuclear aromatic polymer. Lignins often bind to adjacent cellulosic fibers, and together they form a lignocellulosic complex. (Suopajärvi & Fabritius 2013, p. 1192; Yaman 2004, p. 651, 653)

4.2 Production

Biochar can be produced in different ways of thermal conversion. Pyrolysis is the most common method, and it happens under oxygen-free conditions. In pyrolysis, three different products are formed: solid biochar, liquid bio-oil, and pyrolysis gas which contains carbon monoxide, carbon dioxide, hydrogen, methane and higher hydrocarbons. The temperatures used in pyrolysis vary roughly between 300 °C and 900 °C. Other parameters varying are the heating rate and the residence time. With different parameters, different proportions of products can be achieved. The pyrolysis which happens in higher temperatures, with faster heating rates and shorter residence times is called fast pyrolysis. The pyrolysis which typically happens in lower temperatures, with slower heating rates and longer residence times is called slow pyrolysis, which is a more common method for production of biochar. The temperature of fast pyrolysis is usually at least 400 °C and the process lasts only a few seconds. It is mainly used as a way of producing bio-oil. An important part of the process is also rapid cooling of the gases generated in the process so that the maximum amount of oil can be recovered. Slow pyrolysis usually happens in temperatures lower than 500 °C, but products with high carbon contents are being achieved with higher temperatures. The residence times of slow pyrolysis are long, the process can take from half an hour up to several days or even months. Torrefaction is an incomplete form of slow pyrolysis. The temperatures are lower than 300 °C, and the process lasts usually less than 2 hours. The thermochemical conversion and evaporation happen only partially compared to slow pyrolysis. The main goal of the process is to improve the mechanical properties such as grindability of biomass and to retain most of the energy content of solid. (Weber & Quicker 2018, p. 241; Lehmann & Joseph 2009, p. 342)

Hydrothermal conversion and gasification are other processes for manufacturing biochar. In hydrothermal conversion, the raw material is being immersed in water. The heating temperatures are typically between 180 °C and 250 °C, and the residence time is usually from a couple of hours to a day. The processing atmosphere is autogenous pressure between 0.5 MPa and 1 MPa. In gasification, the main goal of the process is to obtain gas in temperatures higher than 750 °C. These processes are not so common methods for producing biochar as a main product. (Lehmann & Joseph 2009, p. 36, 132)

The changes that happen in the chemical structure of biomass during the process of making biochar are highly dependent on the temperature. The first important change that happens when the temperature increases is the change of mass due to evaporating of water at approximately 100 °C. The change in the mass happens at 160 °C when the bound water is removed from the structure of biomass. The cellulose, hemicellulose and lignin polymers start to break down at 180 °C. Between 180 °C and 270 °C the reactions are endothermic, but in temperatures higher than 280 °C some exothermic reactions may occur due to decomposition of vapors to secondary vapors. At 400 °C and above, the less volatile components are gradually driven off from the lignin-derived residual material, so these temperatures determine the final ratio of volatile matter and fixed carbon in the biochar. As the temperature rises above 600 °C the condensable components in the gas phase undergo cracking and polymerization reactions, which affect the yield of bio-oil negatively. The main phenomenon happening in certain temperatures are usually somewhat same for all kind of biomass, but naturally, there are also lots of differences between the behavior of different materials. The processing temperatures and other parameters greatly affect the quantity and quality of the biochar and other products of the process. (Nachenius et al. 2013, p. 80–81)

There are several types of reactors that are being used in biochar production. Before the raw material enters the reactor, it is usually pre-processed. Biomass can be fed into the furnace in different particle sizes and forms. The raw material can be chipped, ground or pelletized before feeding to the reactor, or it can be fed in the form of logs that are even tens of centimeters long. Biomass can also be dried before the hydrothermal conversion. Usually, the whole production process is divided into three sections or unit processes: pre-drying of the raw material, thermal decomposition, and cooling of the product. The heat used in the process is formed either by combustion of the raw material or it can be brought from outside into the process. The gases being formed can be recycled in the process to improve energy efficiency. Kilns are the most primitive forms of reactors that have been used in the biochar production. The heat required in the pyrolysis reaction is generated by burning part of the biomass that is fed into the kiln. These reactors are batch-type, and the combustion of biomass is often incomplete. In addition, the recovery of the by-products is difficult, and therefore kiln-type reactors are usually not being used in the biochar industry. More popular reactor types are reactors that use heat generated outside the vessel. E.g. retorts, screw reactors, drum reactors or moving bed reactors are being used widely in the production of biochar. Retorts are different kinds of pyrolysis vessels

where the heat is being brought to the process either by injection or by transferring across the reactor walls. Screw reactors are continuous reactors that are based on rotating screw conveyor which continuously feeds biomass to a heated sell. In drum reactors, the pyrolysis happens inside a drum which usually rotates. Moving bed reactors are reactors where the biomass is being fed to the process continuously from the top of the furnace. The raw material bed descends in the vessel during the process, and the ready product exits the oven from the bottom part. Several other types of reactors are also used in the production of biochar. The type of reactor suitable for the process depends on the properties of the raw materials and desired products. (Nachenius et al. 2013, p. 115–131, 133–134; Suopajärvi 2013, p. 28–35)

4.3 Properties of biochar

The three most important properties of biochar are generally considered to be ash, volatile matter (VM) and fixed carbon content (FC). These chemical properties are usually measured by a test called proximate analysis, and the method is also used with fossil carbon sources. (Lehmann & Joseph 2009, p. 109–110) The moisture content of biochar can also be determined with the proximate analysis. These properties are good to be used when comparing biochar to fossil-based carbonaceous material such as coke. The values of different properties are usually given on different basis, such as wet basis (wb), dry basis (db) or dry ash-free basis (daf). In addition, several physical properties, such as density, porosity, surface area, mechanical stability and grindability are often considered in relation to biochar. Also, the energy content of biochar is an important value and it is often reported among other properties. (Weber & Quicker 2018, p. 251–254)

4.3.1 Ash

The ash content of biochar is important information when determining the suitability of biochar for metallurgical processes. It means the residue in biochar after oxidation of mineral matter and combustion of organic matter. Ash of biochar includes different kinds of inorganic compounds, from which the most usual ones are SiO_2, CaO, K_2O, Al_2O_3, MgO and P_2O_5. The ash content is greatly dependent on the biomass source, and it is not directly proportional to the processing temperature as can be seen from Figure 11, although, in general, with higher temperatures the ash content of biochar usually also rises (Weber & Quicker 2018, p. 249).

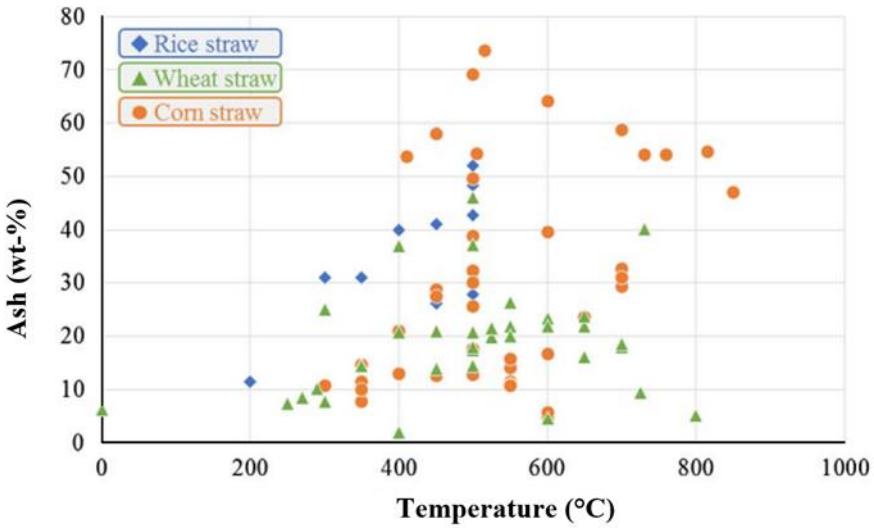

Figure 11. Ash content of biochar made from different straws, carbonized at different temperatures (dry basis) (modified from Weber & Quicker 2018).

4.3.2 Volatile matter

Volatile matter means all of the nonwatery gases formed from the biomass during heating. In standardized proximate analysis methods the heating temperature is usually 950 °C, so the volatile matter is calculated as the loss in mass during the heating and holding a certain amount of time at this temperature with the exception of the loss of mass due to evaporation of water. The amount of volatile matter reduces when the processing temperature increases, as can be seen from Figure 12. (Weber & Quicker 2018, p. 247; Miller 2013, p. 160)

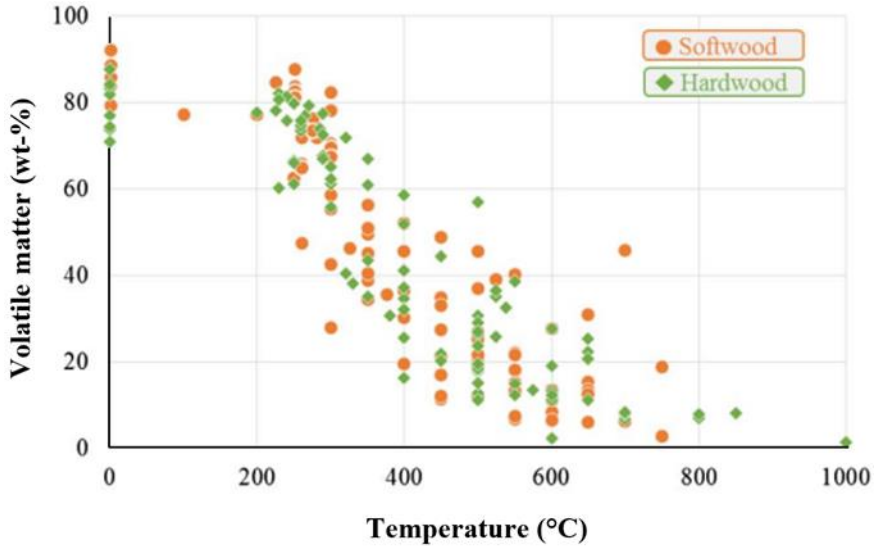

Figure 12. Volatile matter content of biochar made from soft and hardwood, carbonized at different temperatures (ash-free basis) (modified from Weber & Quicker 2018).

4.3.3 Fixed carbon

The carbon that remains in the biochar after the volatile matter is being driven off is called fixed carbon (FC). According to the standard of proximate analysis, fixed carbon is not measured, but calculated as the resultant of measured percentages of moisture, ash and volatile matter subtracted from 100%. The temperature of the production process highly affects the fixed carbon content of biochar, as can be seen from Figure 13. The fixed carbon content of raw biomass is roughly 10–30%, and it remains almost the same until the torrefaction temperature range is being reached. At 250–350 °C the amount of fixed carbon rises noticeably, and with temperatures above that, high amounts even close to 100% can be achieved. When fossil carbons used in metallurgical processes are being replaced by biochar, high content of fixed carbon is usually required. (Weber & Quicker 2018, p. 247; Curay et al. 2020, p. 135)

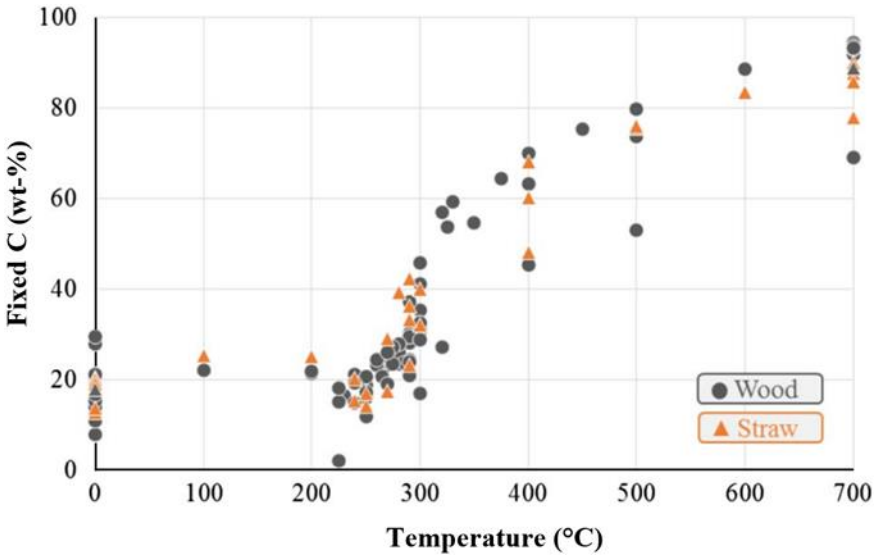

Figure 13. Fixed carbon content of biochar made from wood and straw, carbonized at different temperatures (ash-free basis) (modified from Weber & Quicker 2018).

4.3.4 Comparison between properties of biochar and fossil-based carbonaceous material

The properties of biochar and fossil-based carbonaceous material can vary a lot depending on the raw material and production method. In Table 3, properties of different kinds of biochar and coke are being compared. For wood-derived biochar, it can be generally said that the contents of moisture and volatile matter are higher than those of fossil-based carbonaceous materials, such as coke. The ash content of coke is usually higher than the

ash content of wood-derived biochar, but for biochar made from agricultural biomasses, e.g. wheat, the ash content can also be relatively high. (Ye et al. 2019, p. 3931–3932)

Table 3. Comparison between properties of biochar and coke (modified from Ye et al. 2019 & Suopajärvi et al. 2017).

Property	Biochar				Coke
	Wheat straw	Agacia	Red gum	Pine	
Chemical analysis (wt-%)					
FC	74.80	79.6	86.3	91.8	85–88
VM	4.75	15.9	12.4	6.7	1–3
Ash	20.45	4.3	1.3	1.5	>10
Moisture	7.5	9.59	8.1	–	2–4
Sulfur	0.083	0.07	0.02	–	0.7–1.2
Calorific value (kcal/kg)	6550	6635	5963	–	6500–7200
Ash composition					
SiO_2	30.09	30	42.3	12.0	40–50
CaO	4.80	46.2	23.8	44.0	2–10
Al_2O_3	1.67	7.2	10.2	4.1	30–35
Fe_2O_3	1.01	4.3	4.1	9.1	8–13
MgO	5.09	1.6	3.6	10.9	1–2
K_2O	32.60	3.6	4.3	5.7	0.6
Na_2O	13.24	0.69	1.7	24.4	0.4
Volume porosity (%)	–	54.4	43.5	–	16.6
Surface area (m^2/g)	25.1	43	28	–	4.4
Bulk density (g/cm^3)	1.68	1.79	1.53	–	2.01

The use of biochar in metallurgical processes is possible on the basis of physicochemical properties if the raw material and production method for the manufacturing of biochar are being chosen properly. Some properties of biochar, e.g. the low sulfur content, can be even advantageous for metallurgical processes. For the usage of biochar as a slag foaming agent, the density of the biochar is one thing to be considered. Usually, the density of biochar is lower than the density of fossil-based carbonaceous materials which can lead to longer blowing times and affect the penetration of the carbon into the slag. On the other hand, the lower density and higher porosity of biochar can promote the reactivity and thus the foaming phenomenon. The ash content and composition are also variables that can affect the foaming phenomenon. For coke, the composition of ash is mainly based on acidic components SiO_2 and Al_2O_3. Therefore, injection of coke affects the basicity, viscosity and surface tension of the slag. For biochar, the amount of CaO in the ash is usually high, so the effect to the basicity, viscosity and surface tension can be the opposite. (Ye et al. 2019, p. 3931–3932; Echterhof & Pfeifer 2011, p. 3–4)

5 PREVIOUS RESEARCH

The use of biochar as a slag foaming agent has been studied to some extent in recent years. Research has been done both in a laboratory-scale and in industry. In this part of the thesis these studies are being reviewed. In particular, the review focuses on studies in which the reactions between EAF slag and biochar have been studied at high temperatures: laboratory-scale sessile drop experiments and slag foaming experiments, as well as industrial scale slag foaming trials.

5.1 Sessile drop method-based studies

The sessile drop technique has been used in several studies related to slag foaming and injection of biochar into EAF slag. The method is valid for studying foaming, as the state of the interface between carbon and slag is an important factor when determining the foaming effect and suitability of carbon to act as a foaming agent. With the sessile drop method the rate of reaction and gas generation at the interface of carbonaceous material and slag can be studied closely. The method gives a possibility to detect gas bubble formation into the slag, the change in the volume of the slag, and the wettability of the slag on the biochar. The basic principle of the method is that carbon acts as a compressed platform, slag is placed on top of this carbon bed, and these samples are placed into a furnace where they are heated. The reactions between the slag and the carbon are captured with a charge-coupled device (CCD) camera and recorded. The volume of the slag and the contact angle between the carbon and the slag can be determined from the captured images. (Huang et al. 2019, p. 1387–1388; Sahajwalla et al. 2006, p. 641–642)

Sahajwalla et al. (2006) were the first ones to test the reactions between organic carbon and slag. The main focus of the study was on the fossil carbon sources, but in addition to them, they tested one bio-based char (raw material not further specified). The fixed carbon content of the char was 78.16%, and the other materials tested were coke dust, petroleum coke, natural graphite, and synthetic graphite. The fixed carbon contents of those materials were relatively higher than that of biochar, 83.5–100%. The slag employed in the experiments was real EAF slag. A horizontal tube resistance furnace was used to obtain the temperature of 1550 °C, and the samples were placed to the hot zone of the furnace only when this temperature was reached. This was performed in an inert atmosphere. The results they obtained were not so positive for the biochar. The reactivity

based on gas generation between the char and the slag was lower than with the other materials used, and the liquid slag droplet formed on top of the char bed was considered as non-wetting. The results of this study did not specifically focus on analyzing the suitability of the biochar as a foaming agent. The focus was more on the connection between already used foaming agents and the results achieved with them in the experiments.

Yunos et al. (2012) focused their study on the utilization of the palm shell char, prepared at 450 °C, as a foaming agent in the EAF. The contents of fixed carbon, ash and volatile matter for the char were 56.6%, 33.6% and 5.6%, respectively. Metallurgical coke was used as a reference material in their study. The slag they used was EAF slag with typical composition. A horizontal tube furnace with argon atmosphere and temperature of 1550 °C was used at the sessile drop experiments. The CO and CO_2 off-gases were monitored with an infrared analyzer. The samples were kept at the cold zone of the furnace until the target temperature was reached. The results of the experiments proved that the palm shell char could be a potential foaming agent. The volume of the slag droplets on top of the char was measured continuously, and with the biochar the volume change was higher than with the reference coke, which was evaluated to be due to the fact that the biochar generated more gases than the coke. The monitoring of the off-gases proved that the palm shell char released more CO gas for a longer time than the coke, which is favorable for the foaming phenomenon. The slag particles which melted in the experiments were analyzed with optical microscopy afterwards and from those analyses it was obtained that the slag used with biochar had more and smaller bubbles trapped in than the slag used with the coke. All in all the results showed that palm sell char has the potential to be a suitable foaming agent, at least in terms of gas formation.

In the study of Maayas et al. (2019) a lignin-based char was used as an organic carbon source, and metallurgical coke dust was used as reference material. EAF slag powder was placed on top of a substrate made from carbonaceous materials, and this slag-carbon system was heated in an inert atmosphere at 1600 °C in a tube furnace. The digital images that were recorded during the heating process were analyzed in a customized software and based on the analysis results, the slag foaming indices were calculated for both of the test materials as a function of heating time. Based on the foaming indices the lignin-based biochar showed good potential to perform well as a slag foaming agent. From the images recorded during the experiment, contact angles could be measured for both of the samples.

Based on the contact angle measurements, the lignin-based biochar was characterized as more slag-phobic material than the metallurgical coke, which also indicates that lignin could be suitable material for slag foaming. Slag was sampled after the experiments and analyzed with a scanning electron microscope. Two distinct phases could be observed from the images: slag and reduced iron. Both samples showed a similar distribution of iron and oxide phases, which proves that the reduction of iron oxide and gas generation worked well with both of the tested materials.

Huang et al. (2019) used the sessile drop method with two pyrolyzed materials converted from woody biomass, slow pyrolysis biochar pyrolyzed at 900 °C (FC 95.8% VM 2.4% Ash 1.7%) and fast pyrolysis biochar pyrolyzed at 400 °C (FC 40.2% VM 31.1% Ash 26.9%). They also tested the reactivity of three fossil carbonaceous materials: graphite, coke and char made from car tires. Synthetic slag based on the typical composition of EAF slag was placed in contact with the carbonaceous materials at a horizontal tube furnace. The furnace was heated first to 750 °C with a heating rate of 15 °C/min, then to 1300 °C with a heating rate of 12 °C/min, and finally to 1600 °C with a heating rate of 5 °C/min, where the temperature was held for 30 min. Based on the reaction behavior of different materials observed during the experiment and measured contact angles from the recorded images, the biochars were concluded to be the least reactive of the tested materials. Huang et al. also discussed the effect of different properties of carbon to the reactivity. Based on their results, the ash content of carbon is not a significant factor affecting the foaming behavior. Instead, they observed that the surface morphology of the carbon and wettability affect the formation of bubbles and therefore foaming: a more rough surface of carbon enhances the wetting of liquid slag, which increases the amount of gas bubbles formed and makes the foaming of slag more intense.

Huang et al. continued their study in 2021. The biochars they used in this study were fast pyrolysis biochar pyrolyzed from softwood sawdust at 400 °C (FC 40.2% VM 31.1% Ash 26.9%), slow pyrolysis biochar pyrolyzed from softwood sawdust at 475 °C (FC 95.8% VM 2.4% Ash 1.7%), slow pyrolysis biochar pyrolyzed from spruce sawdust at 475 °C (FC 79.7% VM 26.6% Ash 1.4%) and slow pyrolysis biochar pyrolyzed from pine sawdust at 475 °C (FC 87.8% VM 6.0% Ash 6.2%). In addition, they tested the effect of densifying of biochar by producing biopellets from the slow pyrolysis biochar pyrolyzed from spruce sawdust and bio-oil. They also adjusted the ash content of the fast pyrolysis biochar pyrolyzed from softwood sawdust with two different modifications, mixing 10%

of $Fe(NO_3)_3$ and 10% of slag with the biomass prior to the heating and converting the mass to biochar. Metallurgical coke produced with a pilot scale coke oven was used as a reference for these materials at the sessile drop method-based experiments. The slag that was used in the study was synthetic slag which was made based on the chemical composition of real EAF slag. The oven where the experiments were made and the heating practice were the same as with the earlier study (Huang et al. 2019). From the results it can be said that the softwood-based biochar did not show any reactivity or gas forming effect with the slag at 1600 °C. For the hardwood-based biochar, however, the results were promising, as a clear contact angle could be measured between the biochar bed and the slag droplet formed on top of it. However, the formation of gas bubbles with all of the biochar was irregular and weaker than with the reference coke. The effect of the densifying on the contact angle and wettability between the biochar and the slag was found to be positive. The authors mentioned that compaction, based on microscopic observations, increases the surface roughness of the biochar, and makes the surface morphology similar to coke. The 10% addition of $Fe(NO_3)_3$ or slag to the biomass before pyrolysis, on the other hand, did not improve the interaction between biochar and slag based on the results obtained by Huang et al.

5.2 Laboratory-scale slag foaming experiments

In previous studies, the laboratory-scale foaming experiments based on using biochar as a foaming agent have been done in a simple manner with the carbon placed directly on top of the slag at a crucible and by visually evaluating the foaming effectiveness. No injection of char has been used in the experiments found in the literature review.

Echterhof & Pfeifer (2011) tested the foaming of authentic EAF slag at 1600 °C in a furnace equipped with a natural gas/oxygen burner. Two kinds of biochar were used in the experiments, a char produced from agricultural waste from wine production (FC 81.1% VM 7.7% Ash 9.1%) and a char produced from woody biomass as a by-product of gasification (FC 64.7% VM 9.8% Ash 29.6%). Fossil carbon was used as reference material. An alumina crucible was filled with a mixture of slag and carbon and charged inside the furnace. The change in height of the slag was assessed visually after the tests on the basis of the marks left by frozen slag on the walls of the crucible. The increase in the slag height was considerably greater with both of the biochar than with the reference carbon. The biochar generally reacted much more intensively and faster than the fossil

carbon. Especially the char with the higher FC content seemed to be extremely reactive with the slag. These results were promising in the sense that a clear tendency to gas-forming between the biochar and the slag was observed, but the very intense and fast foam can also be a problem in industrial scale.

Baracchini et al. (2018) tested the capability of forming foamy slag with five different biomasses. The purpose of this was to evaluate if the higher amount of volatile matter in the foaming agent affects the formation of the foam. They used industrial EAF slag in the experiments. The foaming experiments were performed at 1600 °C. The biomasses used were: palm kernel shells (FC 27.8% VM 63.4–72.4% Ash 1.8–4.2%), wood scrap (FC 24.5% VM 85.9%), walnut shells (FC 50.2% VM 79.3% Ash 1.8%), green waste (FC 32.5% VM 64.1%), paper production residues (FC 1.43% VM 58.5%), olivary nuclei (FC 22.0% VM 77.8% Ash 4.5%) and olive residues (FC 20.7% VM 72.7% Ash 6.5%). The experiments were performed so that a crucible with slag was loaded to the furnace, and heated to 1600 °C. Then the carbonaceous material was placed on top of the molten slag, and the temperature was held at 1600 °C for 30 min. The foaming of the slag was evaluated after the experiments by the marks left on the crucible wall and based on those marks the change in volume of the slag was estimated. All of the tested materials caused foaming of slag. The volume increase compared to the volume increase with reference coke was the highest for wood scrap (130%) and the lowest for paper production residues (53%). The results obtained with the other materials were also in line with the prediction that more volatile matter in the foaming agent leads to a higher change in the slag volume, and thus more intense foaming.

Huang et al. (2021) performed foaming experiments with a laboratory-scale induction furnace of 100 kW. They used a steel-slag system and slow pyrolysis biochar pyrolyzed from softwood sawdust at 475 °C (FC 95.8% VM 2.4% Ash 1.7%) to evaluate the suitability of biochar to act as a foaming agent. Coke was used in the studies as reference material, and coke-biochar mixtures with ratios of 50–50, 60–40 and 70–30 were also used to find out the effect of mixing fossil-based carbonaceous material and biochar. In the experiments, 23 kg of steel from industry was placed in a crucible and melted at 1630 °C. When the steel had melted, 1.30 kg of EAF slag was placed in the crucible, and the heating temperature was raised to 1660 °C. When the whole steel-slag system was in a liquid form, 60 g of carbonaceous material, ground to 0.6 mm particle size, was dumped to the crucible and mixed quickly. The height of the slag was measured before, after and

during the experiment with 5 min intervals for 30 min, and the maximum height obtained from the measurements was recorded as the foaming height of the slag. From this height a relative increase in slag thickness was calculated. The thickness increase was 20% when pure biochar was used as a foaming agent and 369% when pure coke was used as a foaming agent. For the coke-biochar mixtures with ratios of 50–50, 60–40 and 70–30 the slag thickness increase was 88%, 47% and 50%, respectively. The authors concluded that the biochar remained floating on the slag surface, even when coke was mixed with the biochar. They presumed that this affected the results of the tests and was at least part of the reason why coke acted so much better as a slag foaming agent. The results also indicated that mixing coke with biochar only slightly improves the foaming.

5.3 Industrial scale slag foaming experiments

The foaming of slag by using biochar as a foaming agent has been tested in industry to some extent. Both injection carbon and charge carbon have been tested to be replaced by bio-based materials. Because the foaming of the slag is mainly done by injected carbon, in this thesis only the injection-based previous studies are being reviewed.

Bianco et al. (2013) reported about industrial scale foaming experiments made at three different steel factories. The capacities of the EAFs used in the tests were 140 t, 130 t and 40 t, with average coal injection amounts of 9 kg, 1.53 kg and 12 kg per tonne of liquid steel, respectively. The biochar used in the experiments was produced at 450 °C using a pilot pyrolysis plant. In one of the EAFs, the slag height during the foaming was observed continuously with a camera placed in front of the slag door. The camera was connected to a system that automatically calculates slag foaming index and adjusts the amount of injected carbon based on this index. The data reported from the trials is limited, but the authors summarized the results in a way that the foaming of the slag obtained with the injection of biochar was partially good and partially poor. They suggested that the injection technologies used in the EAFs should be developed in such a way that the penetration of char into the slag is improved.

As a part of a larger project concerning the usage of biochar in the EAF process, Baracchini et al. (2018) published a report about foaming experiments made at two steel factories with different kinds of biomasses, biochars, and biochar/fossil carbon pellets. In the first of those factories, biochar from husks as non-dried (FC 61.5%) and dried (FC

97.1%), chardust/woodchip char from husks (FC 81.1%), 6x30 mm wood char pellets (FC 82.3%), and 6x30 mm wood char/petroleum coke pellets (FC 89.6%) were tested. The injection was done by already existing stand-by equipment, "a gunning machine", with air pressure of 6 bar. With the system, the material was directed to a water-cooled lance, which injected the material into the slag. The 6x30 mm pellets were not suitable for this injection system, because it broke the pellets into smaller pieces. Therefore, the pellets had to be crushed into particle size less than 4 mm before the injection. No slag foaming was observed with the pure biochar materials, and only a little foaming was observed when the mixed materials were injected into the slag. The authors stated that a combination of two factors caused the poor foaming behavior when biochar was used as a foaming agent: the reactivity of the biochar used with FeO in the slag was lower than the reactivity of the normally used fossil carbons, and the low density of the bio-based material decreased the penetration of char to the molten slag. The other steel factory involved in the tests used crushed palm kernel shell biomass in the injection trials. The suitability of the biomass as a foaming agent was assessed by monitoring the EAF off-gas and wall panel temperatures, CO and H_2 content of the off-gas, and by visual observation. The obtained results varied. The temperature of the off-gas did not rise when biomass was used as a foaming agent, and the concentration of CO and H_2 in the off-gas was higher than with fossil carbon, which indicated that important gases for the foaming process were formed. The temperature of the wall panels of the EAF was higher than normally during the trials with biomass, which indicated that complete substitution of fossil carbon with this kind of biomass and cooling equipment is not possible. According to the authors, there was no visual difference in the foaming phenomenon compared to foamy slag generated with fossil carbon. After these injection trials, also a larger scale experiment with another biomass, olive kernel granulate was tried to be arranged at this steel factory. However, the injection was tested with only four heats before the test period needed to be canceled due to poor foaming behavior. The combustion of the material was too fast when injected into the slag, resulting to non-existent foaming of the slag.

5.4 Summary of previous research

The previous studies reviewed in this thesis are summarized in Table 4. The results of the studies vary a lot and based on these results foaming trials in the industrial scale EAF process could be challenging and unprofitable. For this reason, using biochar as a slag foaming agent in EAF needs to be further investigated in a laboratory-scale.

Table 4. A summary of previous research findings considering laboratory-scale and industrial scale experiments with biochar.

Laboratory-scale sessile drop experiments (5)	**Biochar type**	**Summary of results**
Sahajwalla et al. (2006)	Charcoal	Slag foaming was represented by the volume change of slag during the tests, and the volume changed only slightly with the charcoal
Yunos et al. (2012)	Palm cell char	The palm cell char showed tendency to act as a good foaming agent based on volume change of slag and gases evolving
Maayas et al. (2019)	Lignin-based char	The wettability of char in contact with slag was similar to metallurgical coke used as a reference material
Huang et al. (2019)	Fast and slow pyrolysis charcoal	The interaction between charcoal and slag was minimal
Huang et al. (2021)	Fast and slow pyrolysis chars from softwood and hardwood sawdust	Mainly poor wettability between biochar and slag; densification of char improved the wettability a lot
Laboratory-scale foaming experiments (biochar loaded to crucible) (3)	**Biochar type**	**Summary of results**
Echterhof & Pfeifer (2011)	Chars from agricultural residue and wood gasification plant	The biochar reacted with the slag faster and with greater intensity than the fossil-based carbonaceous materials used as a reference material
Baracchini et al. (2018)	5 different biomasses from wood scrap, residues, shell, and green waste	Varying results, each material caused an increase in the volume of the slag
Huang et al. (2021)	Slow pyrolysis char from softwood sawdust	The thickness of the slag layer increased, but the increase was higher with the fossil-based carbonaceous material used as a reference material
Industrial scale foaming experiments by injection (2)	**Biochar type**	**Summary of results**
Bianco et al. (2012)	Biochar produced at 450 °C in a pilot plant from different raw materials	Both good and bad foaming behavior of slag obtained with the biochar
Baracchini et al. (2018)	Different chars from wood, husks, and dust in fine and pelletized form; palm kern shell and olive kernel granulate biomass	Low or negative foaming, too fast combustion of injected material

6 MATERIALS AND METHODS

Based on the results and information gathered from the literature and previously made research on the topic, laboratory-scale slag foaming experiments were arranged as a part of the thesis. The purpose of the foaming experiments was to study the foaming of slag by using a method where the injection of carbonaceous material and real-time evaluation of the foaming efficiency have been included in the procedure. Both biochar and a fossil-based carbonaceous material were used in the experiments as a foaming agent. The experimental arrangement, materials, methods used, and the results of the foaming experiments are discussed in more detail in this section of the thesis.

The materials used in the foaming experiments were selected so that they reflect the foaming phenomenon happening in the real EAF process. The slag and the fossil-based carbonaceous material used as a reference material in the experiments were obtained from the steel industry (SSAB Europe Oy), and the biochar was received from a commercial provider (Carbofex Oy).

6.1 Carbonaceous materials

The biochar used in the foaming experiments was pyrolyzed from spruce-based wood chip biomass with industrial scale pyrolysis equipment at a temperature around 800 °C and with a pyrolysis time of under 10 minutes. The size of the chips varied, but in general, it can be said that at least one side of the biochar chip was more than 1 cm long.

Coke dust was used as a fossil-based carbonaceous reference material in the foaming experiments. It was sent from the SSAB Europe Oy Raahe coking plant, where it is produced as a by-product of the coking process. Coke dust is a material commonly used as a foaming agent and was therefore an optimal choice to act as reference material in the foaming experiments.

The compositions for the carbonaceous materials used in the experiments can be seen in Table 5. The composition of the ash in the table is related to the original substance (os).

Table 5. Chemical composition of coke dust and biochar used in the experiments.

Property	Coke dust	Biochar
Chemical analysis (wt-%)		
FC (db)	84.40	91.80
VM (db)	0.95	4.60
Ash (db)	14.64	2.60
Moisture	0.10	11.84
Sulfur	0.85	<0.03
Phosphorus	0.07	0.10
Ash composition (os)		
SiO_2	7.10	0.15
CaO	0.89	1.05
Al_2O_3	4.10	–
MgO	0.19	0.14
K_2O	0.22	0.17
Na_2O	0.05	0.02

6.1.1 Grinding procedure

The particle size of the biochar chips was too large for the injection, so the material was ground to a particle size corresponding to the particle size of the coke dust. A laboratory-scale centrifugal mill Retsch ZM 200 was used in the grinding. The rotor speed of 18000 rpm and a 12-tooth rotor were selected as the settings and as the grinding gear based on the grinding experiments previously made by Toloue Farrokh et al. (2018; 2020). Ring sieves with mesh sizes of 250 μm and 500 μm were both used in the grinding to find an optimal particle size for the biochar powder.

6.1.2 Moisture content, drying procedure

The moisture content of the biochar chips was high compared to coke dust (11.84 wt-%, analysis performed on a Shimadzu MOC63u moisture analyzer). The grinding of the biochar to particle sizes of <500 μm and <250 μm lowered the moisture content of the char to 10.12 wt-% and 9.86 wt-%, respectively, due to the heat generated during the grinding. For the foaming experiments, the use of dry biochar was determined to be optimal based on the flow and packing behavior of the material in preliminary injection experiments. The drying of the char was done according to standard SFS-EN ISO 18134. In drying, a thin layer of biochar (<1 g/cm^2) was placed on an aluminum pan. The pan was then placed in a drying oven at 105 °C, where it was held for 24 h. The drying was done right before the foaming experiments, to prevent the absorption of moisture from air.

6.1.3 Particle size

Samples of coke dust and biochar ground to both <250 µm and <500 µm particle sizes were submitted for a particle size analysis on a Beckman Coulter LS 13 320 particle size analyzer. Mean diameter and cumulative particle size distributions for the carbonaceous materials are shown in Table 6. Differential particle size distributions for the materials are illustrated in Figure 14.

Table 6. Mean particle size and cumulative particle size distributions of carbonaceous materials.

	Coke dust	Biochar <500 µm	Biochar <250 µm
Mean (µm)	52.6	39.4	25.5
%< d_{20}	35.7	37.9	47.6
%< d_{32}	47.6	59.1	72.2
%< d_{45}	57.1	73.4	85.8
%< d_{63}	67.7	84.9	96.0
%< d_{90}	80.3	91.1	98.6
%< d_{100}	83.5	92.0	98.6
%< d_{180}	97.4	98.4	100.0
%< d_{250}	99.2	99.2	100.0

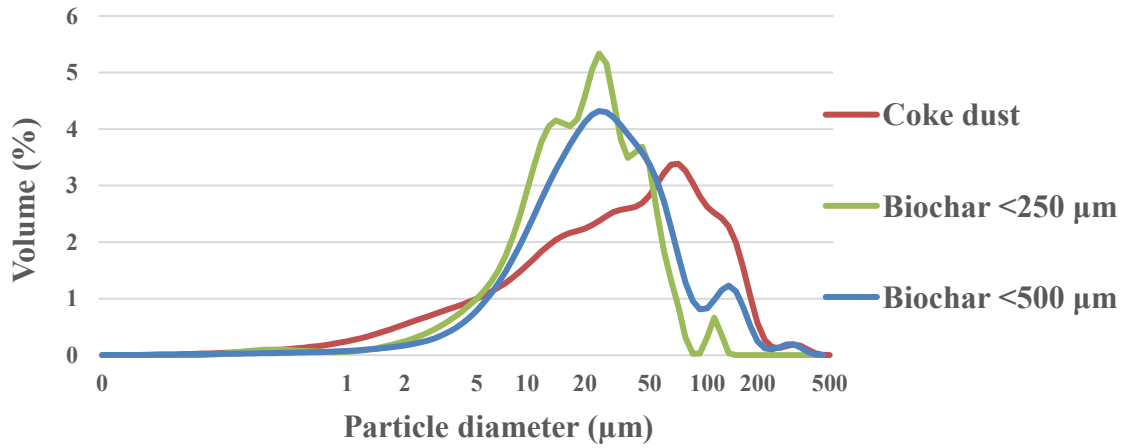

Figure 14. Differential particle size distributions of carbonaceous materials.

Based on the results, a decision was made to select the biochar ground with the 500 µm mesh size ring sieve for the foaming experiments ("Biochar <500 µm"). The particle size distributions of the biochar fractions ground with different mesh sizes were somewhat similar, so it was not considered valuable to use both of the fractions in the experiments and evaluate the effect of different particle size on that basis. The <500 µm fraction was

slightly closer to the particle size distribution of coke dust, so it was selected. For biochar, a clear peak near the particle diameter of 20 µm can be seen in the curve, whereas the distribution of coke dust is more even and the peak of the distribution is between particle diameters of 50 µm and 100 µm. An interesting observation was the second peak at the particle size distribution curves of biochar near the particle diameter of 100–150 µm. In general, the grindability of the biochar can be characterized to be good. The particle size distributions show that the grinding of biochar lead to overall fine particle size, and no large fractions were left among the fine powder. The mean sizes for both the <500 µm and <250 µm fractions are well below the mesh sizes. E.g. in the grinding of raw wood biomass, significantly larger particles than the mesh size can pass through the mesh, which is because thin and long particles that can escape through the sieve holes (Abdullah & Wu 2009, p. 4180). This kind of phenomenon did not happen in the grinding of biochar, which indicates that the pyrolysis weakens the fiber structure of the spruce in a way that the biochar is easily ground to fine powder material.

The effect of the particle size of the carbonaceous material on the foaming phenomenon has been studied previously by Wu et al. (2000). They used fossil coke with different particle sizes (3 mm, 1 mm, 110 µm and 76 µm) in their experiments. The results of their experiments can be seen in Figure 15.

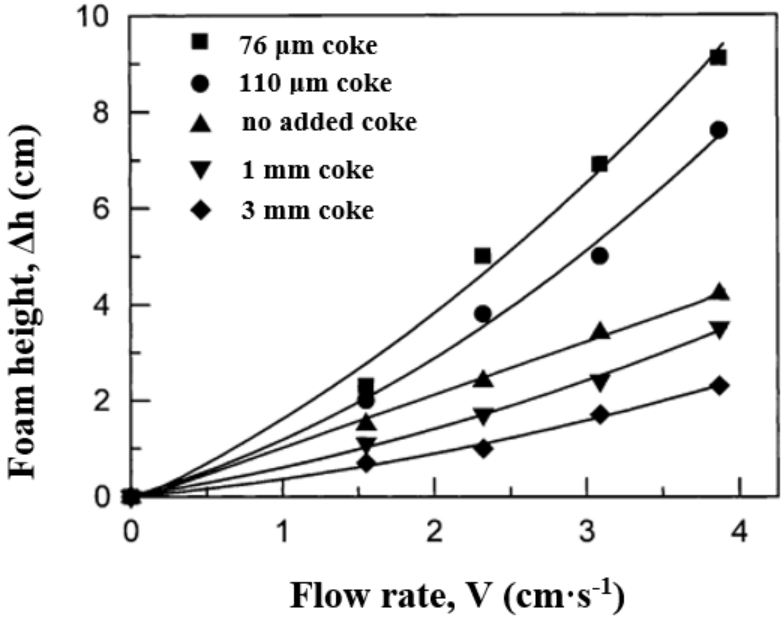

Figure 15. Effect of particle size of coke on foaming (modified from Wu et al. 2000).

Based on the results of Wu et al. (2000), it can be said that the smaller the particle size of the carbonaceous material the greater the increase in slag volume during the foaming. The foam height in the experiments conducted with particle sizes of 3 mm and 1 mm was even lower than with no additive foaming agent at all, which indicates that the particle size of the carbonaceous material needs to be well under 1 mm so that effective foaming can occur. Based on the results obtained at the studies of Wu et al. (2000) and on the particle size distributions obtained as a part of this thesis, theoretically the particle size of the "Biochar <500 µm" was suitable for the foaming experiments. Figure 16 shows the biochar used in the foaming experiments in unground and ground forms and coke dust. Visually observed the appearance of the ground biochar was near the appearance of coke dust.

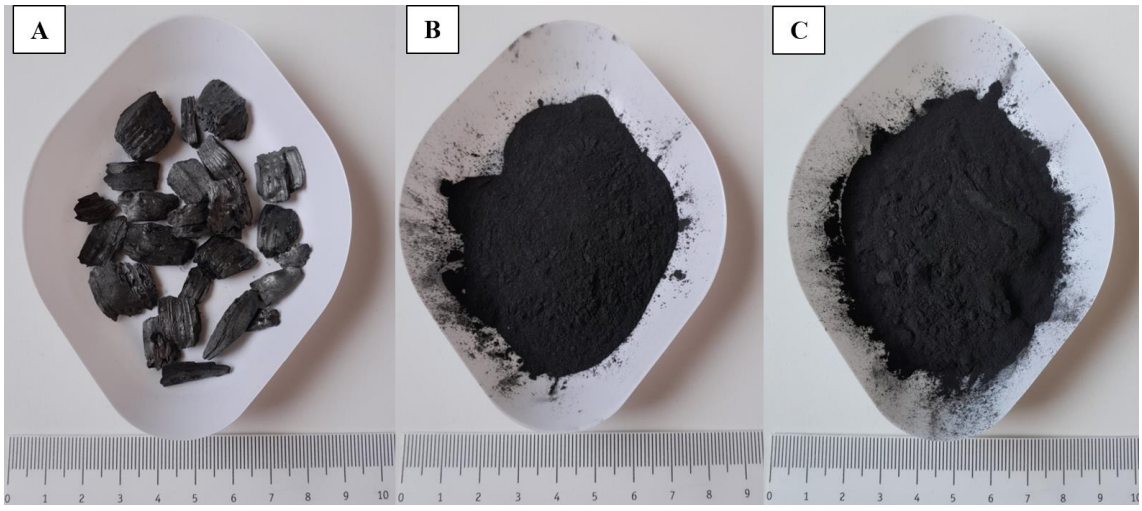

Figure 16. Biochar in (A) chip form and (B) ground to particle size of <500 µm. Coke dust (C).

6.1.4 Density

The density of the carbonaceous materials was determined in two ways. The bulk density measurements for the coke dust and for the <500 µm fraction of the biochar (both undried and dried) were performed by following the procedure described by Emrich (1985). The carbonaceous material was poured into a cylinder of known volume and stamped on a wooden board until the volume of the material remained unchanged. The bulk density was determined based on the mass and volume of the material. The measurement procedure was repeated three times for all of the tested materials. The relative standard deviation for the results was 0.64% on average. The true density of the carbonaceous materials was measured with Micromeritics AccuPyc II 1340 gas pycnometer. Gas pycnometer measures the density of material using gas displacement method, and it

excludes the effect of pores in the powder structure (Micromeritics). The true density was measured only for the dried sample of biochar, as only materials containing low percent of moisture can be fed into the pycnometer. The results for the density analysis can be seen in Table 7.

Table 7. Densities of carbonaceous materials.

	Coke dust	**Biochar <500 µm**	**Biochar <500 µm (dried)**
Bulk density (g/cm^3)	1.01	0.49	0.47
True density (g/cm^3)	2.13	–	2.56

The bulk density of ground biochar was notably lower than the bulk density of coke dust. The effect of this on both the injection and penetration behavior into slag is possible, and this was one thing to be observed in the foaming experiments. The bulk density of the dried biochar was slightly lower than the bulk density of the undried, ground biochar (10.12 wt-% moisture), which is consistent due to the removal of water. The true density of the biochar is higher than the true density of the coke dust, and the difference to bulk density measurement results were noticeable. The results were similar to those in the studies of Toloue Farrokh et al. (2018; 2020). The bulk density of fossil-based carbonaceous material is usually higher than the bulk density of biochar, but for the true density it is common that the results are the opposite. This might be due to the differences in particle shapes and the effect of void space and open pores in the structure of the ground biochar. When planning to replace fossil-based carbonaceous powders with bio-based powders, the differences in the densities of the materials must be considered. The noticeably lower bulk density of biochar can lead to storage problems, for example. A larger volume is needed to store the same amount of carbon. The differences in densities also indicate differences in flow properties.

6.2 EAF slag

The EAF slag used in the foaming experiments was obtained from SSAB Europe Oy. The slag was from a pilot plant EAF process. It was ground to <1 mm particle size for the foaming experiments. Chemical composition analysis was made to the slag with the X-ray fluorescence (XRF) technique. The original chemical composition of the slag can be seen in Table 8 in the upper row. Because the basicity of the slag (B_1, see Equation 1 and B_2, see Equation 2) was determined to be remarkably low for the foaming experiments, the

slag was modified by adding 20% of reagent grade CaO powder. The chemical composition of the slag after the modification can be seen in Table 8 in the lower row.

Table 8. Chemical composition of the EAF slag (the original one, and the one with 20% CaO addition which was in use in the foaming experiments).

$CaO_{add.}$	CaO	SiO_2	Al_2O_3	MgO	MnO	TiO_2	V_2O_5	FeO	B_1	B_2
–	20.00	19.91	8.48	9.26	1.02	1.30	1.39	34.83	1.0	0.7
20%	33.34	16.59	7.06	7.72	0.85	1.08	1.15	29.02	2.0	1.4

The slag with 20% CaO addition has proper basicity (B_1 = 2.0, B_2 = 1.4) and FeO content (29.02 wt-%) for the use in slag foaming experiments based on the information obtained from the literature review and previously made studies on this topic.

6.3 Steel

In some of the foaming experiments, a steel-slag system was used to simulate the real-life EAF process. The steel used in the experiments was low-carbon structural steel which was cut into circular discs in accordance with the shape of the crucible (⌀ = 55 mm, h = 10 mm, m = 180 g). The chemical composition of the steel was determined with XRF and glow discharge optical emission spectroscopy (GDOES) analysis. The composition of the steel can be seen in Table 9.

Table 9. Chemical composition of the steel used in the experiments.

Fe	C	Al	Mn	Si	P	S	Cr	Ni	Cu
98.00	0.18	0.03	1.24	0.31	0.02	0.04	0.05	0.02	0.02

7 EXPERIMENTAL SETUP

The configuration of the equipment was custom-made for the foaming experiments. Information gathered from previously made foaming tests was one part of the equipment design, but the final form of the equipment and the experimental arrangement was mostly unique. The main points on the basis of which the equipment was prepared were: 1) Suitable crucible and furnace settings to achieve proper kind of liquid slag and a system that can be visualized in an appropriate form 2) Workable injection of carbonaceous material into the melt 3) Functional real-time imaging of the foaming process.

7.1 Previously made laboratory-scale injection experiments

The injection of fossil-based carbonaceous foaming agents has been done previously in a laboratory-scale. The equipment used in different experiments has been somewhat similar. The measurement and visualization of foaming have been done in different ways.

Ji et al. (2003; 2005), King et al. (2009) and Zhu et al. (2012) have all used the same slag foaming equipment in their fossil carbon based foaming studies conducted at the McMaster University, Canada. The equipment includes a 75 kW induction furnace, a coal feeder and injection lance by which the carbonaceous material and nitrogen gas can be injected into melt. The authors have used MgO-crucible approximately 2 cm in diameter and 30 cm in height in their foaming studies. They have covered the crucible with a ceramic board and a steel lid during the experiments, and the injection has happened through holes in those. Kipepe & Pan (2015) have made foaming experiments in a 5 kg induction furnace. They injected both oxygen and pure carbon particles into a liquid cast iron-slag system via alumina lances. In addition, they included power consumption measurement in their experiments.

7.1.1 Measurement and visualization of foaming

Different methods have been used in several laboratory-scale studies to evaluate the efficiency of foaming of slag with fossil-based carbonaceous materials. One simple way to evaluate the height of the foam is to place a rod into the molten slag and to assess the highest point of the foam from the marks of the slag attached to the surface of the rod. Hong et al. (1998) have used a nickel rod, Kipepe & Pan (2015) have used an alumina

rod, and Ji et al. (2003; 2005), King et al. (2009), Zhu et al. (2012) and Kitamura & Okohira (1992) have used a steel rod to assess the foam height. Another simple way to try to get information about the highest point of the slag is to evaluate the marks of frozen slag at the inner wall of the crucible, as Echterhof & Pfeifer (2011) have done in their research about the usage of biochar as a foaming agent. One way to get data from the surface position of slag is to use an electric probe, such as Ito & Fruehan (1989a) have done in their studies. The principle of this method is to use an electric circuit between two steel rods. The end of the first rod is placed at the bottom of the slag, and the end of the second rod is tried to be kept at the surface of the slag. A device connected to the electric probe measures the distance between the ends of the rods, and thus the height of the slag. The foaming phenomenon has also been imaged with X-ray. Kapilashrami et al. (2006) and Chychko et al. (2012) have used X-ray imaging equipment connected to a high-temperature furnace to assess the height of foamy slag. The X-ray imaging has been done through quartz windows at the walls of the furnace, and through the walls of the crucible. The X-ray imaging system has been connected to a CCD camera. The images recorded with this apparatus have been two-dimensional projections, which means that if the surface of the foamy slag is not uniform, the results are not accurate. Based on the results of the previously made studies it is difficult to perform completely exact measurements for the slag height.

7.2 Foaming experiments

The foaming experiments of this thesis were conducted in a Nabertherm HT 08/18 chamber furnace (chamber dimensions 150x150x300 mm, maximum temperature 1800 °C). The temperature of the furnace was measured continuously with a thermocouple during the experiments. Nitrogen gas was used as an inert carrier gas for the injection of the carbonaceous material. The gas was passed through a rotameter and introduced into a screw feeder developed for the injection of fine materials. With the screw feeder carbonaceous powder can be fed to the gas line continuously and adjusting the feed is easy. The feeder was equipped with a 6 mm drill bit and a 40 cm^3 container. A vibrator with an on/off switch was attached to the container to prevent the possible vaulting and blockage problems. In the experiments, the feeder was rotated by hand with a screwdriver. The injection of carbonaceous material into the slag was done via quartz pipe (inner diameter 4 mm). The flow rate of the carrier gas could be adjusted and measured both on a ml/min and a l/min scale.

7.2.1 Crucible

The crucibles used in the foaming experiments were made from MgO-C refractory bricks which are also used in real-life steelmaking processes. Two different versions of the crucible were used in the experiments. The characteristics of those two versions are shown in Table 10. Crucible version 1 was the prototype that was used in the first experiment, and crucible version 2 was a more advanced version that was in use in the rest of the experiments. The main difference between the crucibles was that the inner height of the version 2 was 12 mm higher than the inner height of the version 1, which means a 17.6% increase in the volume of the crucible. The crucibles were tilted at a low angle in the furnace. The purpose of this was to control the possible overflow of the foaming slag and thus prevent the inner parts of the furnace from damage. For this purpose, slag doors were also designed for the crucibles. In the crucible version 1 the slag door was implemented with a separate rim, and in the crucible version 2 the slag door was cut straight to the upper edge of the crucible. Before the experiments the crucibles were treated thermally. The crucible version 1 used in the first experiment was dried at 105 °C. For all of the other experiments, the crucible version 2 was burnt in the chamber furnace overnight at 1000 °C.

Table 10. Crucible versions used in the experiments.

Characteristics	**Version 1**	**Version 2**
Picture		
Inner diameter	58 mm	58 mm
Inner height	68 mm	80 mm
Volume	179.7 cm^3	211.4 cm^3
Outer width	100 mm	100 mm
Outer height	91 mm	100 mm
Slag door	At a height of 40 mm	At a height of 75 mm
Tilt	Done with an additional plate	Done with the shape of the bottom
Drying/burning	Done at 105 °C	Done at 1000 °C

7.2.2 Visualization system

Liquid steel and steelmaking slag emit a large amount of thermal light and are therefore very bright objects. This kind of systems cannot be seen clearly with the naked eye or regular camera-based visualization. By using a suitable light source, such as laser light, and a proper camera with the right accessories, even hot objects like the foaming of liquid slag can be accurately visualized. Short camera exposure time, which means that the camera integrates light only for a short period, is one of the main points in the visualization of highly bright objects. The use of short camera exposure time can be enabled by using laser illumination that can create enough power to illuminate the object properly with already short pulses. Bright light can also be reduced by using a band filter, which allows only a narrow range of wavelengths to pass to the camera. High-temperature processes can be visualized with good image quality by using the compilation of a laser light source, short exposure time, and a proper band filter. (Cavitar Ltd 2018a, p. 1–2)

A complete visualization system was used to image the slag foaming experiments. The system consisted of a CAVILUX HF laser light source system, a Baumer TXG14 CCD camera, and a computer. CAVILUX HF is a pulsed high-power diode laser light source, which is designed especially for the visualization of challenging applications like high-speed or high-temperature industrial processes (Cavitar Ltd 2011). The system can be used for example in the visualization of welding, additive manufacturing, droplets and explosions (Cavitar Ltd 2018b). The pulse output power of the CAVILUX HF version used was 500 W and the wavelength of the operation was 810 nm. The system consists of adjustable laser illumination optics (fiber optic light guide and focusing optics for uniform illumination), a laser unit, a control unit and CAVILUX Control software which can be operated with a regular computer. The software is used for the programming and controlling of the laser control unit. 1.5 mm fiber core and 25 mm focusing optics were used for the visualization. The Baumer TXG14 CCD camera used in sync with the laser was equipped with a Computar TEC-M55 55 mm telecentric lens and a suitable band filter. The camera was operated with CAVITAR Capture software. The settings used in the CAVILUX Control and CAVITAR Capture software during the visualization are presented in Appendix 1. The only adjustment made to the settings between the experiments was the change of preview fps, which means the number of frames the camera captures per second. Preview fps values of 4 and 8 were used in the experiments.

A schematic of the experimental setup can be seen in Figure 17 (not-to-scale), and the actual setup can be seen in Figure 18. For successful visualization and to allow the laser beams to enter the chamber, roughly an 80x150 mm hole was drilled into the roof of the chamber furnace. The hole was kept open only during the visualization, otherwise it was covered with a tight-fitting cover plate.

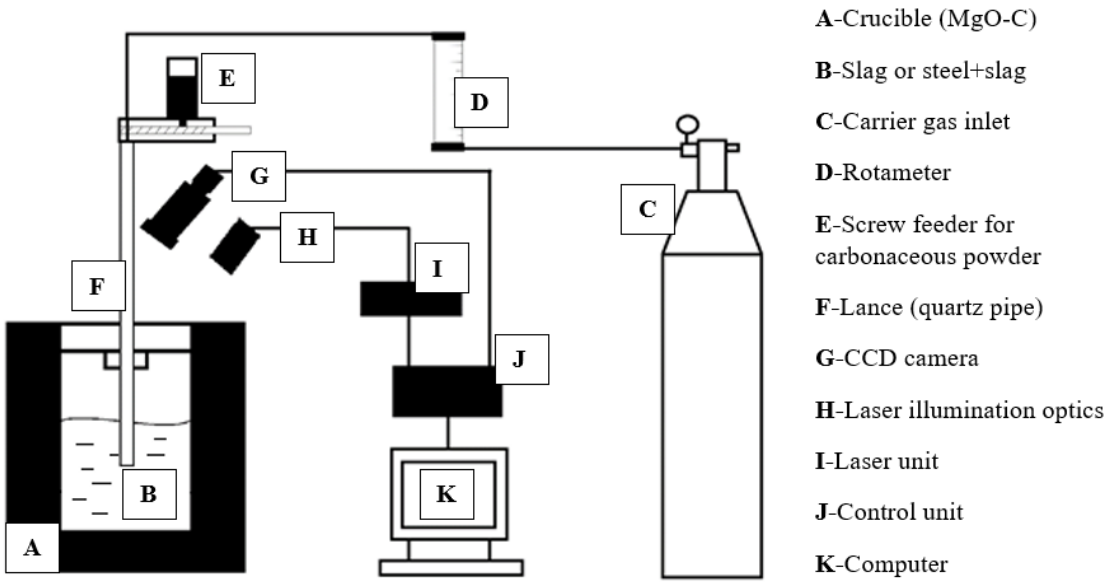

Figure 17. A schematic of the experimental setup.

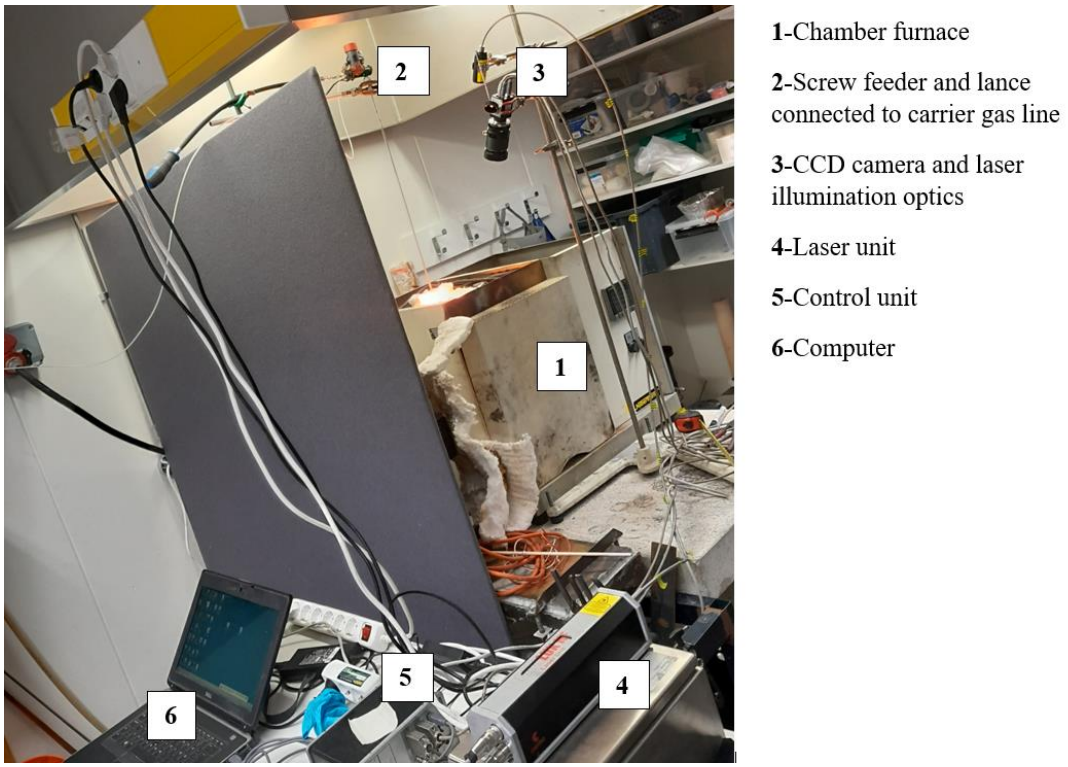

Figure 18. The experimental setup.

7.3 Experimental procedure

A total of 6 foaming experiments were performed as a part of this thesis. Because the experimental setup was never used before and this was the first time the laser illumination-based visualization system was used in experiments like this, a large part of the work was to get the equipment up and running.

The first important step in the experiments was to achieve clear foaming of slag by using the fossil-based coke dust as a foaming agent. The purpose of these reference experiments was to ensure the right parameters for the testing of biochar as a foaming agent. Because the coke dust is widely used in the steel industry as a slag foaming agent and has been proven to work there very well, it was necessary to make the slag foam with the coke dust first. The first experiments were also the ones during which the functionality of the visualization system was verified.

7.3.1 Experiments 1 and 2: steel-slag system, 1600 °C, coke dust

The experiments were made with different parameters. Some of the parameters were changed during the experimental period based on the observations made in the previous experiments, so the experimental design varied during the period, and thus no precise experimental plan could be done prior to the beginning of the experiments. The first two experiments were performed with coke dust with somewhat the same parameters. A steel-slag system was used to simulate the real-life EAF process. In the first experiment, the crucible version 1 was in use. A 180 g steel disc was placed at the bottom of the crucible. 240 g of slag (with 20% CaO addition, the composition of the slag is described in Table 8) was charged on top of the steel. The crucible containing the solid steel and slag was then placed in the furnace. A porous alumina plate was placed in front of the crucible to absorb the possibly overflowing slag and thus to prevent the damage to the furnace. The hole in the roof of the furnace made for the visualization was sealed with a cover plate, and the furnace was heated to 1600 °C. The container of the screw feeder was filled with 15 g of coke dust. Before the injection started and the lance was lowered and introduced into the liquid slag, the nitrogen gas flow was switched on and adjusted to a 150 ml/min flow rate. The tip of the lance was aimed near the slag-metal interface, roughly 15–20 mm above the bottom of the crucible. The cover plate was removed and the hole in the roof of the furnace was opened. The visualization system was switched on, and the recording of the process was started with a preview fps value 4. A total of 10 minutes of

coke dust injection was performed during the first experiment. Both 150 ml/min and 5 l/min flow rates for the carrier gas were tested. The feed rate of the coke dust was tried to be kept as constant as possible by rotating the screw feeder at a steady speed.

For the second experiment, the temperature was also 1600 °C, and again a steel-slag system was used. Based on the results obtained from the first experiment, the crucible version 2 with a larger volume was used in the second experiment. The amount of slag was therefore increased to 360 g. The charged crucible inside the chamber furnace before the experiment 2 is shown in Figure 19.

Figure 19. A crucible charged with steel and slag inside the chamber furnace.

This time, a total of 16 minutes of coke dust injection was performed. The carrier gas flow rate was 150 ml/min for most of the injection time, and the effect of different carrier gas flow rates was studied by doing series of short injections with rates of 2, 4, 6 and 8 l/min. Otherwise, the same parameters were used as in the first experiment.

7.3.2 Experiments 3–6: slag system, 1400 °C, coke dust and biochar

For experiments 3–6, the target temperature was lowered to 1400 °C, and only slag was charged to the crucible. These adjustments were made based on the observations made during the first two experiments. The preview fps value was set to 8 in the experiments 3–6. The purpose of the adjustments was to improve the foaming phenomenon and to make the visualization more clear.

Coke dust was used as the foaming agent in the experiments 3 and 5, and biochar was used as the foaming agent in the experiments 4 and 6. The amount of coke dust charged to the container of the screw feeder was 15 g for all of the experiments, whereas the amount of biochar charged in the experiments 4 and 6 was only 7.5 g. The difference is based on the lower bulk density of the biochar. Preliminary screw feeder trials pointed out that the behavior of coke dust and biochar powder was different in the screw feeder. Especially the flow behavior from the container and through the unloading hole was different, and therefore the weights of the charges needed to be adjusted carefully to ensure the continuous flow of the foaming agent into the slag. With biochar, some disadvantageous vaulting occurred. The vibrator was used continuously in each of the experiments during the injection, and the wall of the container of the feeder was tapped from time to time during the experiments where biochar was used to prevent the vaulting.

Crucible version 2 was used in all the experiments 3–6. Now the position of the crucible was adjusted in a way that the slag door pointed towards the back wall of the furnace, while in the first experiments the slag door pointed towards the door of the furnace. This adjustment was made to improve the visualization angle and to reduce the spreading of the overflowing slag into the furnace. A 30 mm wide MgO-C plate with a cutting was placed between the crucible and the back wall of the furnace to catch the overflowing slag. The arrangement of the crucible to the furnace in the experiments 3–6 can be seen in Figure 20, which is taken from the same angle as the visualization during the experiments was performed. The amount of slag charged to the crucible was 400 g in the experiments 3 and 4, and 300 g in the experiments 5 and 6. 150 ml/min nitrogen gas flow rate was used in all of the experiments 3–6. The total injection time varied between 4 and 9.5 minutes. Because no steel was used in these experiments, the tip of the injection lance was now aimed closer to the surface of the slag (roughly 15–20 mm below the surface). The tip of the quartz pipe used as a lance melted slowly when introduced into the liquid slag, so it had to be lowered several times during the experiments.

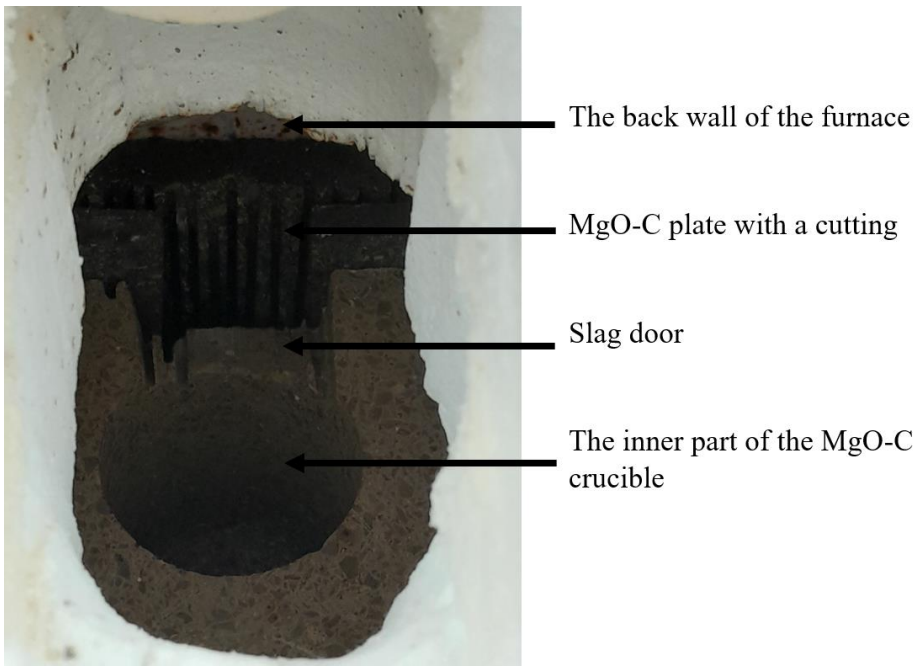

Figure 20. The arrangement of the crucible inside the furnace in the experiments 3–6.

The parameters for all the foaming experiments are listed in Table 11. During the experiments accurate notes were taken down. Because the equipment used for the injection did not collect any data from the test parameters, and because the parameters varied between the experiments, taking these notes was particularly important. After the experiments the crucibles were cooled in air atmosphere inside the furnace. The cooled crucibles were broken up with a sledgehammer or split with a saw for visual and microscope analysis. The amount of foaming agent remained in the container of the screw feeder was weighed. The frames obtained from the visualization were merged into videos, and both the frames and the videos were analyzed and filed. To simplify the test performance, the whole experiment from the lowering of the lance into the slag to the lifting up of the lance after the injection was captured. The total length of the video material obtained from all of the experiments was almost 2 hours.

Table 11. Overview of parameters used in the foaming experiments.

Exp. No.	Foaming agent	T (°C)	W_{steel} (g)	W_{slag} (g)	Crucible	$Q_{carrier\ gas}$ (l/min)	$t_{injection(tot.)}$ (min)
1	Coke dust	1600	180	240	Version 1	0.150 / 5	10
2	Coke dust	1600	180	360	Version 2	0.150 / 2 / 4 / 6 / 8	16
3	Coke dust	1400	–	400	Version 2	0.150	4
4	Biochar	1400	–	400	Version 2	0.150	9.5
5	Coke dust	1400	–	300	Version 2	0.150	4
6	Biochar	1400	–	300	Version 2	0.150	4

7.4 Microscopical study

The slag sections exposed as a result of the splitting of the crucibles from the experiments 3–6 (see Figure 27 and Figure 30) were studied microscopically. From each of the four split crucibles two sections of slag with a diameter of roughly 35–40 mm were cut for microsection sample preparation. The cut sections were placed in molds and epoxy resin was added to the molds under vacuum. Then the molds were left in an oven with a temperature of 40 °C to harden for 24 h. After that the surfaces of the molded microsection samples were polished using Struers LaboPol-6 grinding and polishing machine. The prepared samples are presented in Figure 21. The figure also shows the origin experiments of the samples.

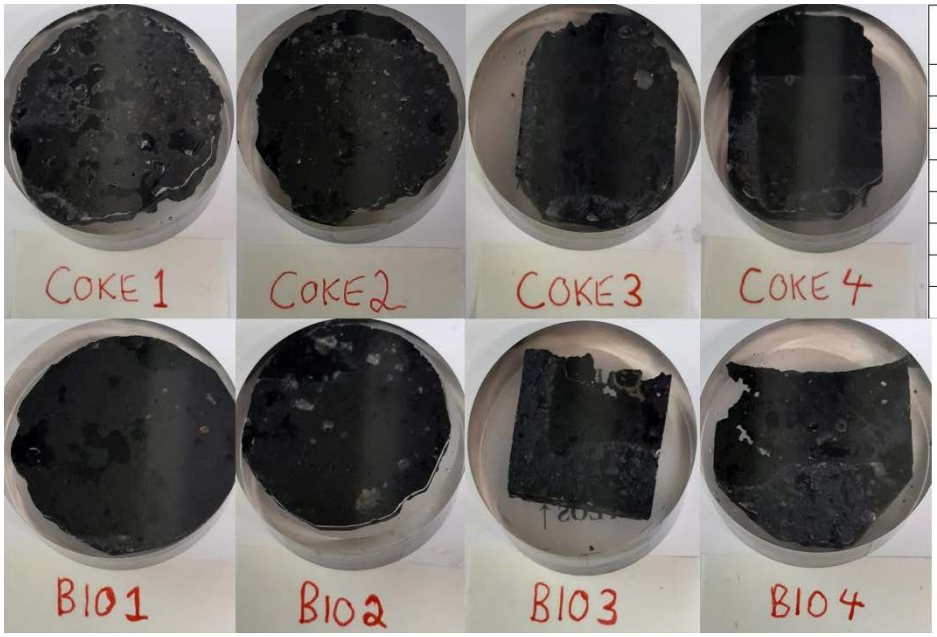

Sample name	From
Coke 1	Exp. 3
Coke 2	Exp. 3
Coke 3	Exp. 5
Coke 4	Exp. 5
Bio 1	Exp. 4
Bio 2	Exp. 4
Bio 3	Exp. 6
Bio 4	Exp. 6

Figure 21. Microsection samples.

The microsection samples prepared as well as the unprepared slag sections exposed as a result of the splitting of the crucibles were studied using Olympus DSX1000 digital microscope. The prepared microsection samples were also examined using Zeiss ULTRA plus field emission scanning electron microscope (FESEM), attached with an energy dispersive spectroscopy (EDS) unit. For the FESEM-EDS-examinations, the samples were coated with a thin layer of carbon using JEOL JEE-420 vacuum evaporator.

8 RESULTS

The results of the foaming experiments are highly based on the images obtained from the visualization of the system during the experiments. The most important part of the results is the foaming phenomenon that was achieved with biochar and which was further compared to the foaming phenomenon achieved with coke dust. In this part of the thesis those results are presented. In addition, the results of visual and microscopic examinations done for the cooled slag after the experiments are given.

8.1 Slag foaming

The results of the 6 foaming experiments vary. Altogether it can be said that the visualization of the foaming experiments succeeded. The movement of the slag surface and the possible change in the surface height of the slag were noticeable from the image obtained with the visualization system. The functionality of the whole experimental setup was verified in the experiments: the screw feeder and the whole injection equipment were suitable for these kind of experiments.

8.1.1 Experiments 1 and 2 (reference)

For both of the reference experiments made with using coke dust as a foaming agent in a steel-slag system at 1600 °C, it can be said that no clear foaming of the slag could be observed from the image. At the beginning of the experiments only nitrogen was injected into the slag for a short period. When injecting nitrogen alone into the slag, the surface of the slag rippled and large bubbles that ruptured rapidly could be observed from the video recording, but the surface of the slag did not rise notably. This was the case for both of the experiments 1 and 2.

When the injection of coke dust started, the first observation was that the movement of the slag surface became more aggressive. Some clouds of smoke could be seen in the image, and some sparkling and smoke was also visible near the hole in the roof of the furnace. However, no clear rise of the surface of the slag could be detected. One reason for this can be the angle of view and the crucible layout in the oven. In both of the first experiments the crucible was tilted towards the camera, and the slag door of the crucible was also pointing towards the camera, mainly outside the picture. In the experiment 1,

the height of the liquid material in the crucible could be inferred to be roughly 30 mm, and the slag door of the crucible was at a height of 40 mm. In the experiment 2, the same heights were 50 mm and 70 mm, respectively. Judging from these, it would be implausible for the slag to overflow unnoticed during the injection. However, after the experiments it was observed that the crucible walls had worn a lot due to the molten slag and steel and the high temperature. As a result of this, the edges of the slag door had also eroded. This may also have affected the maximum height of the liquid and the point of overflow in the crucible.

In Figure 22, the crucible imaged with the visualization system before the experiment 1 can be seen on the left. A measure is placed inside the crucible to visualize the field of view and the height of the crucible. The cut at the back wall of the furnace was made to assist in assessing the height of the liquid slag. However, it was covered with molten slag during the experiment and was therefore not useful. On the right (B), a situation where coke dust is being injected into the molten slag is presented. The estimated edge of the surface of the slag is marked with a red dashed line in the figure. Slightly to the right of the center of the image the injection lance is clearly visible. Some smoke can be seen in the middle of the figure. Also, some solidified slag can be seen at the level of the top right side of the crucible. It is likely to have formed during the melting of the slag when heating the furnace. This solidified slag was in front of the tip of the lance, as can be seen from the image. After the experiment it was noticed that the tip of the lance had melted. The lance was lifted up and lowered a few times during the experiment, but it cannot be verified that the tip of the lance was below the surface of the slag through the whole injection time. This is one possible reason why no clear foaming of the slag could be detected during the experiment 1.

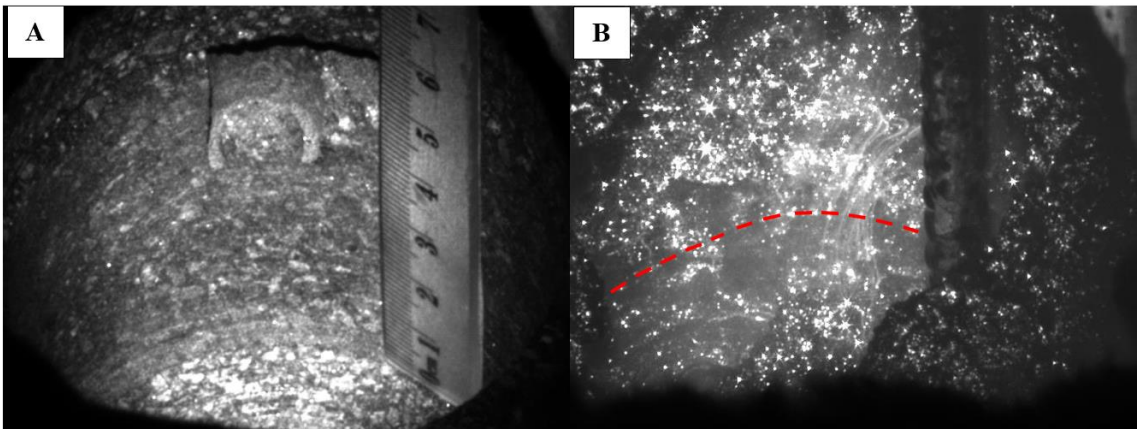

Figure 22. Empty crucible before the first foaming experiment (A) and the slag during the coke dust injection (B).

In the experiment 2, the results were somewhat similar than in the experiment 1. The difference between the experiments was that the higher crucible version 2 was in use in the experiment 2. Efforts were also made to change the angle of view of the visualization so that the slag door would be more visible from the image. This was not successful and the whole visualization of the experiment 2 was somewhat unclear. The image was dark, probably due to the aperture of the CCD camera being set too small, or due to an inaccurate orientation of the laser illumination. The surface of the slag could be seen in the image, but it did not rise noticeably and the foaming of the slag could not be confirmed.

In Figure 23, the crucibles after the foaming experiments 1 and 2 are presented. As can be seen from the figure, the eroding of the crucibles has been considerable. The molten slag had absorbed deep into the walls of the MgO-C crucibles. Some slag is visible in front of the crucibles, which indicates that at some point of the experiment the slag has either overflowed or leaked through the eroded front wall of the crucible. Inside the crucible after the experiment 1 some slag can be seen on top of the steel. The amount of slag left on top of the steel was roughly 50 g, so a large part of the slag either overflowed or absorbed into the refractory material during the experiments. Also, in the experiment 2 the amount of slag left inside the crucible was relatively low. Based on the results of these two experiments, the changes to the parameters were made for the next foaming experiments. It can be concluded from the results of the first two foaming experiments that it is difficult to obtain a clear foaming phenomenon with experiments performed in this way.

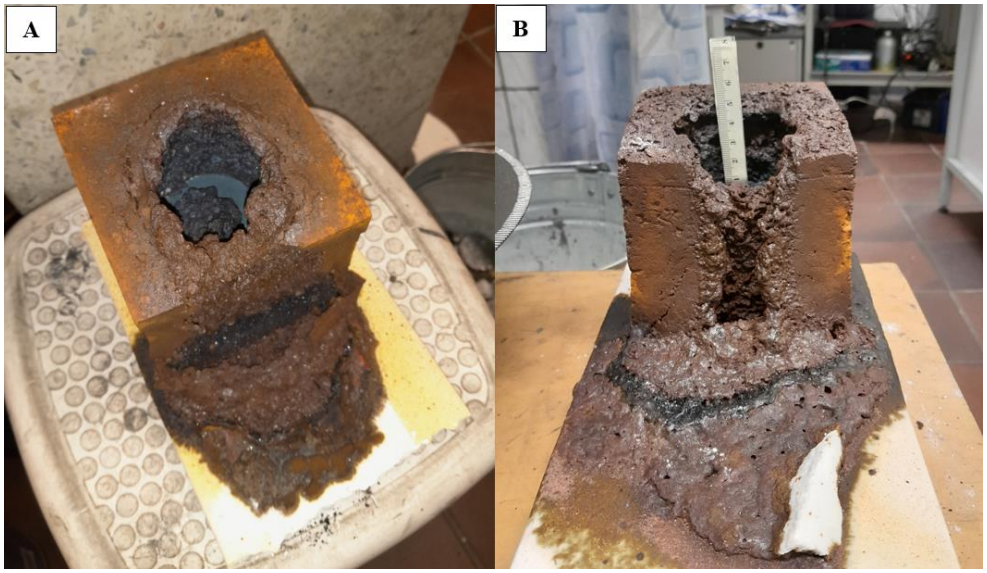

Figure 23. The cooled crucibles after the foaming experiments 1 (A) and 2 (B).

8.1.2 Experiments 3 and 5 (reference)

The reference foaming experiments 3 and 5 were performed at 1400 °C using coke dust as a foaming agent, and the crucible was filled only with slag. The lower temperature of the slag and thus the higher viscosity has been considered to be contributory parameters for good foaming of the slag (see Section 3.3). Foaming of slag was observed in both of these experiments. The rotating of the crucible in a way that the slag door could be seen in the image was a positive change from the experiments 1 and 2, which helped with doing the observations from the images.

In the experiment 3, the crucible was filled with 400 g of slag. The rise of the surface of the slag was observed for the first time during this experiment. When injecting only nitrogen into the slag, the surface of the slag rippled, but it did not rise at all. Almost immediately after the coke dust injection started, the surface of the slag started to rise. The rise of the surface of the slag was mostly constant, but at times the surface came down slightly and then continued to rise again. Two periods of injection were made, and between those, the slag was let settle down for several minutes. The first one of the injection periods was more effective in terms of foaming. In 85 seconds the surface of the slag rose to the top edge of the crucible. The whole slag door was covered up with the slag. Because of the surface tension of the slag, it appeared that the surface of the slag rose even above the edge-level of the crucible. In Figure 24, the starting point (zero-level) and the highest point of the slag surface during the foaming experiment 3 are shown. The height of the slag was assessed based on the preliminary images taken from the empty crucible with a measure. The point where the surface level was observed was the edge of the lance. Immediately after the injection was stopped, the surface of the slag began to go down slowly. The lowering of the surface from the highest point to the zero-level took approximately 80 seconds.

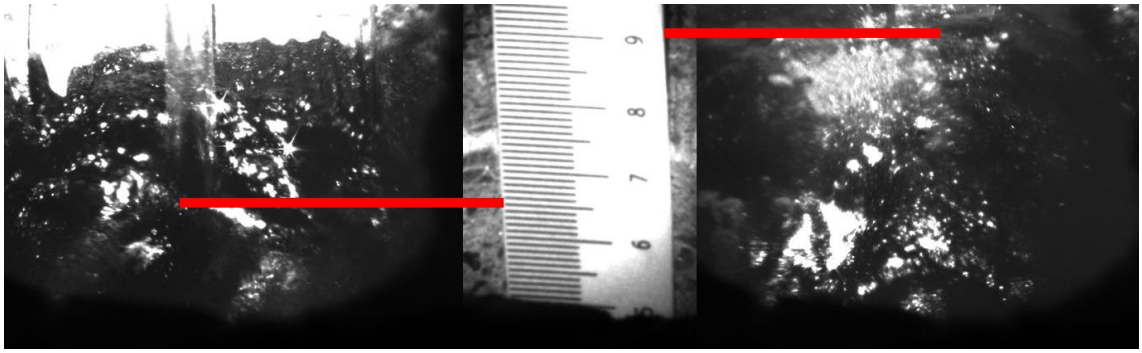

Figure 24. The zero-level and the highest point of the surface of the slag in the foaming experiment 3 (coke dust).

In the experiment 5, the amount of slag was reduced to 300 g. The purpose of this was to lower the zero-level of the surface of the slag and thus make more space for the expansion of the slag during the foaming. Again, two 2-minute periods of injection were made during the experiment. The surface of the slag began to rise when the injection of coke dust started. The phenomenon was quite similar compared to the experiment 3: the first injection period was more effective than the second. In 90 seconds the surface of the slag rose to the top edge of the crucible. In Figure 25, the zero-level and the highest point of the slag surface during the foaming experiment 5 are shown. Compared to the experiment 3, the zero-level of the slag was roughly 17 mm lower. This allowed more space for the slag to expand. However, it must be noted that still the full potential of foaming was not seen. If there had been more empty space in the crucible, the surface of the slag would possibly have risen even more. The lowering of the surface after the injection happened in the same kind of maneuver as in the experiment 3.

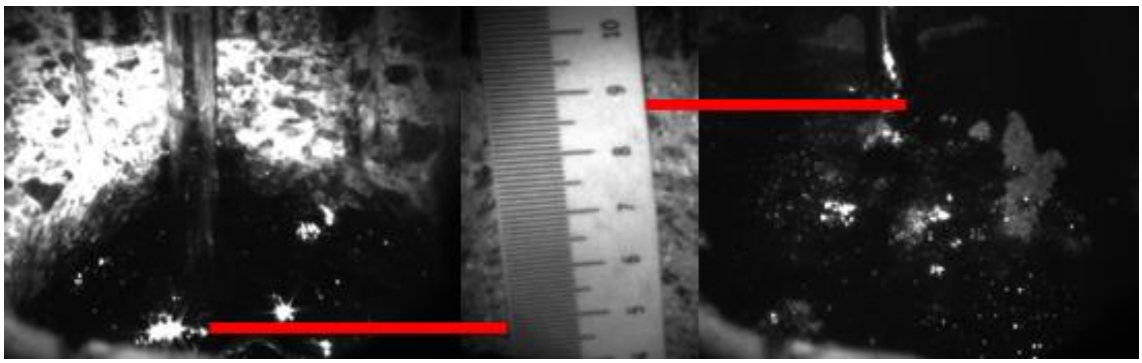

Figure 25. The zero-level and the highest point of the surface of the slag in the foaming experiment 5 (coke dust).

From the image obtained with the visualization system, the size of the bubbles in the foaming slag could also be observed to some extent. Most of the slag in these 2 reference experiments seemed to consist of small (<1 mm) bubbles, but also some large (>10 mm) bubbles could be seen rising to the surface of the slag and rupturing. One observation from the image was that some lighter spots appeared on the surface of the slag, which was otherwise kind of dark in the image. These lighter spots seemed to originate from the bursting of light bubbles that rose to the surface of the slag. In Figure 26, the formation of this kind of lighter spot is being illustrated. It is possible that this lighter material was reduced iron that rose to the surface of the slag with the gas bubbles.

Figure 26. The formation of lighter spots on the surface of the slag during the foaming.

The wear of the crucibles was considerably lower in the experiments 3 and 5 than in the experiments 1 and 2. On the top edges of the crucibles, a few splashes of most-likely reduced iron was noticed after the experiments. The diameter of those splashes was a couple of millimeters. When the crucibles had cooled, they were split from the middle for visual inspection. The splitting was done directly from the center of the slag door to the back wall of the crucible. In Figure 27, the split crucibles can be seen. Among the slag, some reduced iron-like material was observed in both of the crucibles. Related to the experiment 3, a 15x25 mm "cloud" of this iron-like material surrounded by cavities in the slag was clearly visible in the middle of the slag layer. Related to the experiment 5, the iron-like material was similarly distributed in the middle of the slag layer, but not in the same cloud-like form. The amount of those metallic dots was smaller, and the material was more spread horizontally. The crucibles were taken for further microscopic examination, the results of which will be discussed later in this thesis in Section 8.2 and Section 8.3.

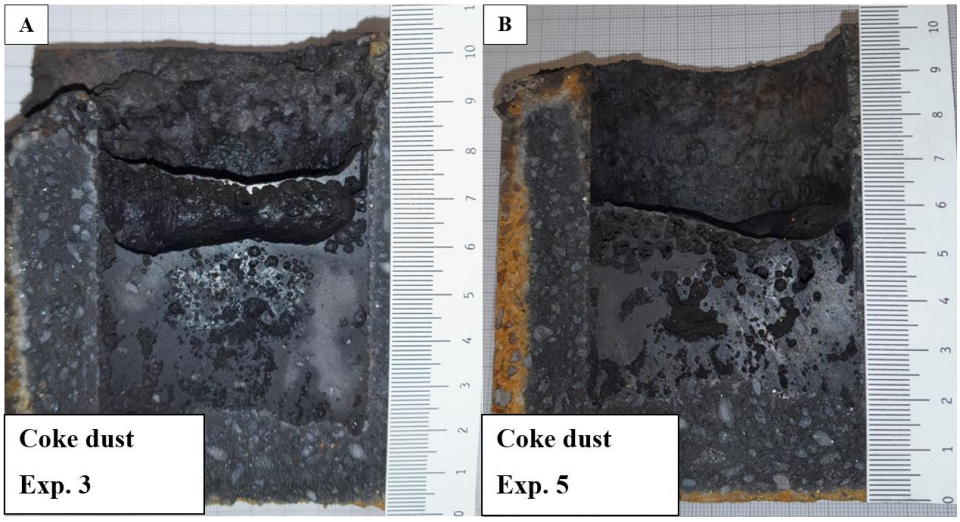

Figure 27. The split crucibles after the experiment 3 (A) and experiment 5 (B).

8.1.3 Experiments 4 and 6 (biochar)

In the experiments 4 and 6, biochar was used as a foaming agent. The parameters used in those experiments were the same as in the reference experiments 3 and 5, respectively: in the experiment 4, 400 g of slag was used and in the experiment 6, 300 g of slag was used.

In the experiment 4, a total of 9.5 minutes of biochar injection was performed. This was made in 4 shorter periods. During the first of the injection periods which was 2 minutes long, the surface of the slag rose notably. The rising of the surface began almost immediately after the injection of the biochar was turned on, just like in the reference experiments 3 and 5. Based on the analysis made from the images obtained from the foaming phenomenon with the visualization system, the surface of the slag did not rise as high as in the reference experiment 3, where the zero-level of the slag was the same. On the other hand, the foaming was a bit more intensive and the surface of the slag rose to the highest point quite fast, only in 25 seconds. In Figure 28, the zero-level and the highest point of the slag surface during the foaming experiment 4 are shown. When the injection was stopped, the surface of the slag lowered back to the zero-level in roughly 30 seconds. Taking into account the smaller change in the height of the slag compared to the reference experiments, the lowering of the surface of the slag was quite similar. The three other injection periods performed after the slag had settled down were not as effective as the first one. The surface of the slag rose during all injection periods, but the phenomenon was not so consistent in second, third and fourth periods, and can be described more in a way that the surface of the slag pulsed and hopped up and down.

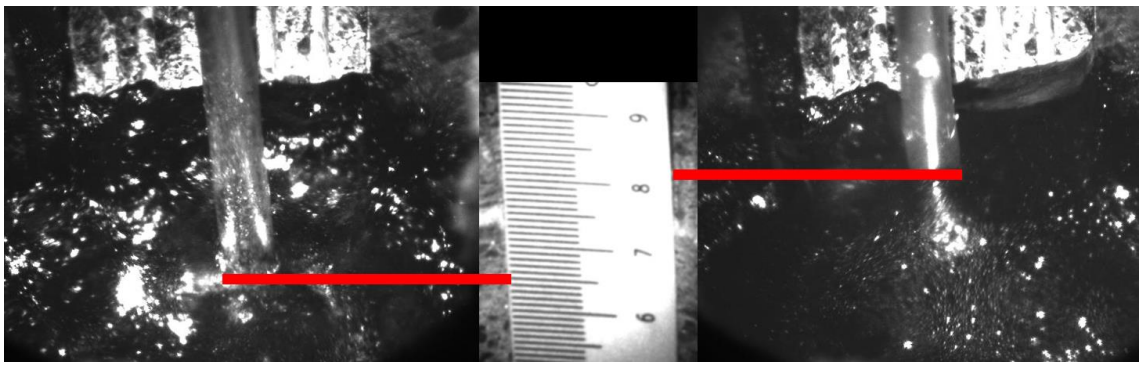

Figure 28. The zero-level and the highest point of the surface of the slag in the foaming experiment 4 (biochar).

In the experiment 6 the amount of slag was 300 g, which allowed a more accurate observation of the slag surface level change than in the experiment 4. The results were promising. Two separate 2 minutes long injection periods were performed, and again the first of the periods was more successful in terms of foaming. The surface of the slag rose in the same way as in the experiments with coke dust. Actually, the highest point of the slag surface was measured to be 10 mm higher than in the corresponding reference experiment 5. It must be noted that the slag surface level measurements are only estimates made from the images, and it is one reason why the highest point of the height is above the top edge of the crucible. Now some slag clearly overflowed and spread to the top surface of the crucible. This was the only one of the experiments where the overflow happened, so the slag foaming can be said to have been the most effective in terms of the surface height of the slag. In 42 seconds the surface of the slag rose to the highest point observed, which was 44% faster than the rise time in the reference experiment 5. In Figure 29, the zero-level and the highest point of the slag surface during the foaming experiment 6 are shown. The slag was quite dark in the image as can be seen from the figure, but from the video the highest point could still be clearly determined.

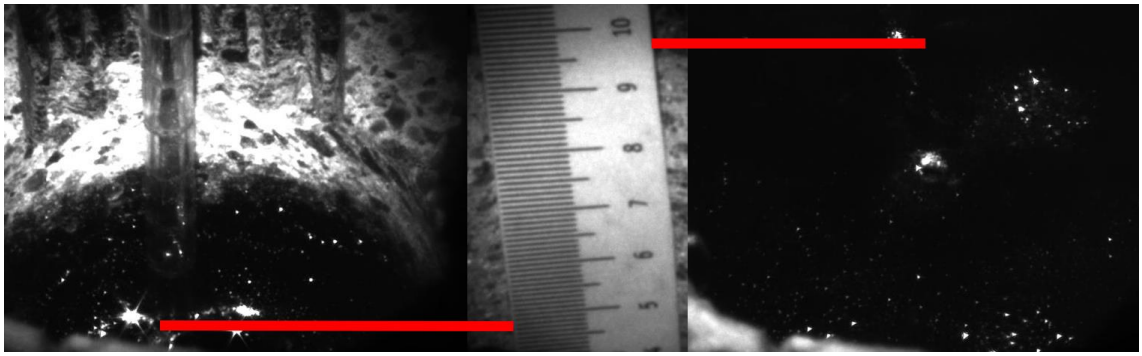

Figure 29. The zero-level and the highest point of the surface of the slag in the foaming experiment 6 (biochar).

The bubble structure of the foamy slag could be determined to some extent from the image obtained from the experiments. The main part of the foamy slag seemed to consist of small, <1 mm bubbles, but also some larger bubbles could be spotted, similar to the reference experiments made with the coke dust. The same kind of lighter spots among the otherwise dark slag could be seen. It can be concluded that the slag behaved quite similarly in the experiments made with the biochar than in the reference experiments.

The crucibles were visually analyzed after they had cooled to room temperature. The crucibles had not been greatly damaged during the experiments. The slag had overflown through the slag door in both of the experiments. In the experiment 4, the amount of leakage was small, but in the experiment 6 a larger volume of the slag had overflown, which could also be inferred from the fact that the amount of slag left in the crucible after the experiment was noticeably lower than in the reference experiment 5, where the original amount of slag was the same. Some splashes of most-likely reduced iron could be noticed from the edges of the crucible used in the experiment 6, but not in the crucible used in the experiment 4. Some reduction of iron probably happened also in the experiment 4 based on the clearly visible foaming phenomenon, but the reduced iron did not end up to the edge of the crucible because the slag did not overflow or because the bursts of bubbles happened at a lower level in the crucible in that experiment.

The crucibles were split in the same way as in the case of previous experiments. In Figure 30, the split crucibles can be seen. Some iron-like material could be observed from the middle of the slag bed inside the crucible used in the experiment 6, but these kinds of marks were not visible inside the slag of the experiment 4. One thing to be noticed is also that a major proportion of the cavities inside the slag seem to be larger in the crucible after the experiment 4 than in the other split crucibles. This supports the observation that the foaming of the slag was not so effective in the experiment 4 as in the experiments 3, 5 and 6; large cavities indicate large bubbles, which are not the most optimal ones for the formation of a stable foam.

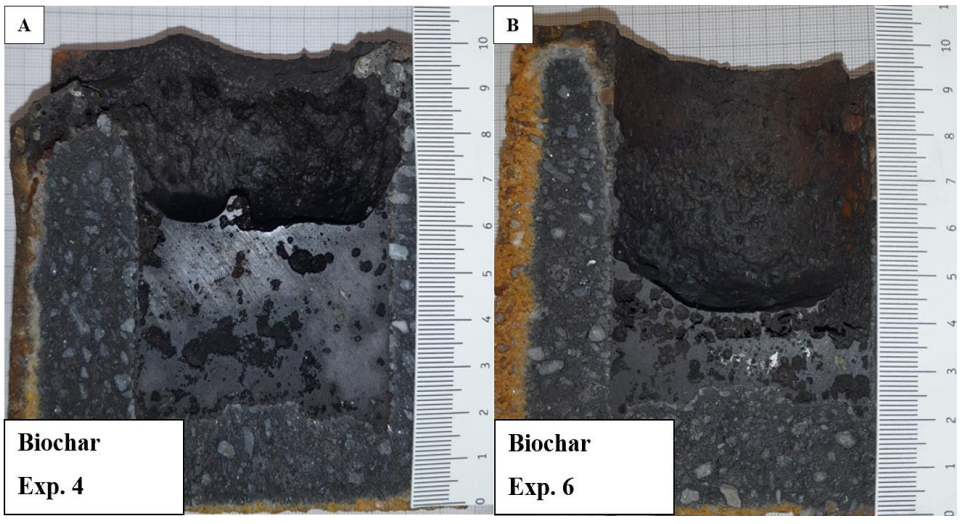

Figure 30. The split crucibles after the experiment 4 (A) and experiment 6 (B).

The results considering the height of the slag during the foaming experiments are gathered in Table 12. In addition, the amounts of injected foaming agents and the average injection rates can be found in the table.

Table 12. The results of the foaming experiments.

Exp. No.	Foaming agent	T (°C)	Slag					Injection	
			h_0 (mm)	Δh (mm)*	t_{rise} (s)*	t_{fall} (s)*	ΔV (%)*	W_{agent} (g)	Avg. rate (g/min)
1	Coke dust	1600	20	–	–	–	–	6.23	0.62
2	Coke dust	1600	40	–	–	–	–	5.78	0.36
3	Coke dust	1400	65	25**	85	80	38.5	1.54	0.39
4	Biochar	1400	65	16	25	30	24.6	6.66	0.70
5	Coke dust	1400	48	40**	75	90	83.3	3.00	0.75
6	Biochar	1400	48	50**	42	110	104.1	5.85	1.46

*results based on the injection period where the highest point of the slag surface was obtained
**the highest point was roughly the top edge of the crucible

The angle of view was a bit different in the experiment 4 than in the corresponding reference experiment, which makes the results of the experiment 4 partly questionable in terms of the height of the slag surface. Based on the results of the experiment 6, the foaming effectiveness of the biochar can be said to be at the same level as the foaming effectiveness of the coke dust.

8.1.4 Effect of gas flow rate and injection rate

Different carrier gas flow rates were tested as a part of the experiments 1 and 2. All of the experiments 3–6 were made using the same flow rate (150 ml/min). Because the actual foaming of the slag was observed only in those experiments 3–6, the effect of the gas flow rate on the foaming itself cannot be assessed as a part of the results from the experiments. In the experiments 1 and 2, carrier gas flow rates of 2, 4, 5, 6 and 8 l/min were used besides the flow rate of 150 ml/min. The effect of the higher flow rate was considered to cause more aggressive rippling of the surface of the slag, but the gas flow rate was clearly not the critical factor for the generation of foam. The 150 ml/min flow rate was evaluated to be suitable for this experimental setup and was therefore used for the rest of the experiments. At this flow rate, the surface of the slag was steady-enough for clear visualization and the formation of large bubbles remained at a low level.

Due to the hand-operated screw feeder, the injection rate of the carbonaceous material varied between the experiments, as can be seen from Table 12. The use of the feeder was

studied before the experiments and the rotating of the feeder was done at a steady rate. Nevertheless, keeping the feed rate constant proved to be challenging. In preliminary feeding experiments made with coke dust (5 min feeding period done with 1 round/second rotational speed) the feed rate varied roughly between 0.40 g/min and 0.60 g/min. With biochar, the feed rate was clearly different. The average feed rate of the biochar was higher than the feed rate of the coke dust and thus the feed rates of the experiments where biochar was used differed from the reference experiments, even though the intention was to keep the feed rate at the same level. The feed rate was not measured during the injection and could not be observed in any way during the experiments, which made accurate controlling of the feed rate impossible.

In the foaming experiments the feed rate of coke dust varied from 0.36 to 0.75 g/min, and the feed rate of biochar varied from 0.70 to 1.46 g/min. The average feed rate for coke dust was 0.53 g/min and for biochar 1.08 g/min. The difference is noticeable, but the total amounts of carbonaceous materials injected during the experiments do not exceed the stoichiometric amount of carbon needed to reduce all of the iron oxide in the slag. In all of the experiments stoichiometrically well over 10 g of carbonaceous material was needed to reduce all of the iron oxide, and the highest amount of carbonaceous material injected during the experiments was 6.66 g in the experiment 4. In this sense, the different injection rates do not affect the results. However, it should be noted that the injection rate of carbonaceous material affects the carbon gasification rate and thus the foaming phenomenon. Ji et al. (2005) have studied the effect of injection rate on the foaming phenomenon. In their studies they used injection rates of 3.5–12.8 g/min per 1 kg of slag. They found that the maximum gasification rate of carbon in slag was 7.9 g/min per 1 kg of slag and that the saturation injection rate of carbon into slag was 10.1 g/min per 1 kg of slag, which means that above this value an excess of carbon particles will be observed in the system. If the injection rates of carbonaceous materials used in the foaming experiments conducted as a part of this thesis are converted to correspond to those pure-carbon values, they are 0.8–4.5 g/min per 1 kg of slag. The injection rates were therefore low compared to the studies of Ji et al. Based on that, the injection rates were at least not too high in any of the experiments. As a summary for the injection rates, it can be said that the rates were relatively low in all of the foaming experiments. The rates varied between the experiments, and the rates for the injection of biochar were higher than for the injection of coke dust. Still, the effect of the injection rate to the foaming phenomenon cannot be estimated based on the results of the experiments. If the effect of the injection

rate is to be assessed more accurately, more precise injection equipment and a wider series of experiments will be needed.

8.1.5 Effect of injection depth

In the real EAF process, the injection lances are targeted to the slag-metal interface. If the tip of the lance penetrates into the metal phase and melts, the lance is being adjusted. In the laboratory-scale foaming experiments quartz pipe was used as a lance. In the experiments 1 and 2, where steel-slag system was used, the injection was aimed near the slag-metal interface. In the experiments 3–6, where the crucible was filled with only slag, the tip of the lance was tried to be kept approximately 10–20 mm below the surface level of the slag. One thing that was found problematic during the experiments was that the tip of the quartz pipe melted and eroded slowly when it was in contact with the liquid slag. During the experiments, roughly 5–10 cm from the end of the quartz pipe eroded. Not much attention was paid to this in the first two experiments, and this may have had an effect on the continuity of the injection. In the experiments 3–6 the injection depth was adjusted actively. Each time the image of the visualization system revealed that the end of the tube was no longer below the surface of the slag, the pipe was lowered. The foaming of the slag occurred at those experiments as long as the end of the pipe was completely below the surface. The depth of 10–20 mm seemed to be appropriate. Naturally, when the surface of the slag rose due to the foaming, the depth of the tip of the quartz pipe increased. However, this was not seen to have an effect on the foaming phenomenon.

8.2 Optical microscopy

One reason why the samples were prepared for microscopical examination was to study the suspected areas of reduced iron among the slag. These areas were successfully included in the microsections based on visual inspection. For example, a large, roughly 10 mm long strip of this metallic material can be seen in the up-right corner of the sample “Bio 3” in Figure 21. These shiny, metallic areas could be seen with the naked eye in all of the samples except “Bio 1” and “Bio 2”, which were from the foaming experiment 4. The shiny areas were not observed at all when the slag was cut into pieces for the microsection samples. However, it must be noted that the prepared samples are only a small cross-section of the entire slag, and it is possible that such areas still were left hidden somewhere inside the slag of the experiment 4.

This supposedly reduced iron was seen as light droplets when studied with optical microscopy. These droplets were observed inside the bulk slag in all of the microsection samples except the “Bio 1” and “Bio 2” samples. In Figure 31, optical microscopy images of the samples “Coke 1” and “Coke 4” can be seen. The presence of shiny light droplets in these images was the most typical way of presence in all of the samples; most of the droplets were roughly 10–100 µm in size, gathered together in either “cloudy”-type (image B in Figure 31) or long and thin (image A in Figure 31) formations. Also, some larger droplets or combined groups of smaller droplets could be observed from the images up to a millimeter-scale. These droplets were located in the middle or top parts of the slag bed and appeared to be partly supported by air bubbles.

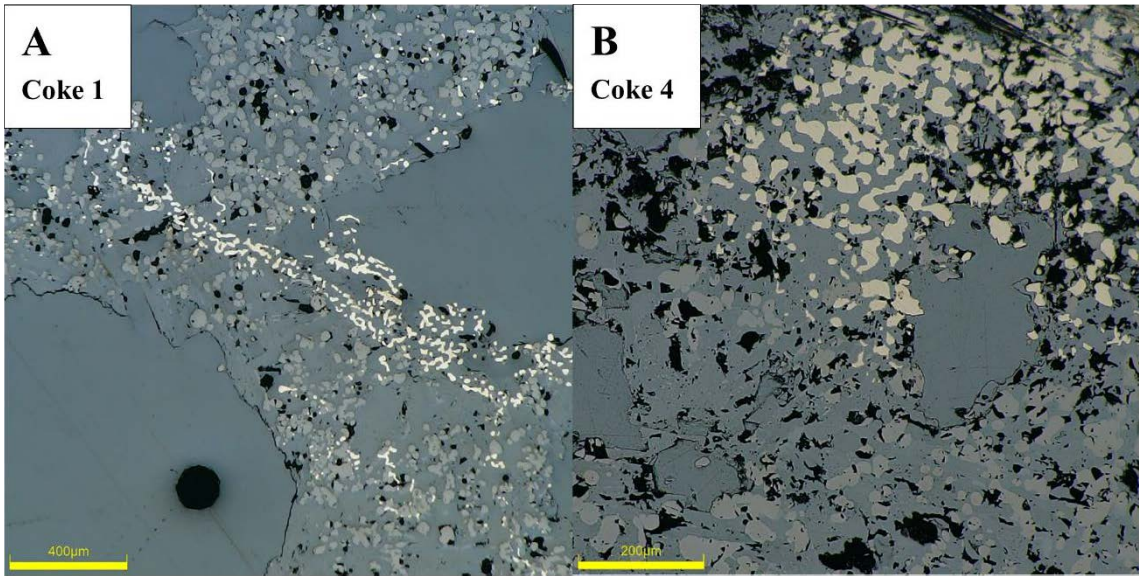

Figure 31. Digital microscope images from slag after the reference foaming experiments 3 and 5 performed with using coke dust as a foaming agent.

In Figure 32, optical microscopy images of the slag samples taken from the foaming experiments made with biochar can be seen. The presence of the light droplets was found to be similar with the samples taken from the slag of the reference experiments. The droplets were found to be in in small “clouds” of 10–100 µm spots, but also in larger areas. The image A in Figure 32 presents one end of the roughly 10 mm long strip of this shiny metallic material in “Bio 3” sample. Now those droplets were found also from the bottom of the slag, against the crucible material, which can be seen in image B in Figure 32. The larger particles below the light droplets in the image are parts of the MgO-C crucible. The reduced iron has settled as a denser material to the bottom of the crucible because now the bubbles have not supported it in the upper parts of the bulk slag. After

every foaming experiment the slag was cooled slowly in air atmosphere inside the furnace, and the number of bubbles left trapped inside the slag was therefore somewhat coincidental. Therefore, the places where these light droplets were found inside the slag varied.

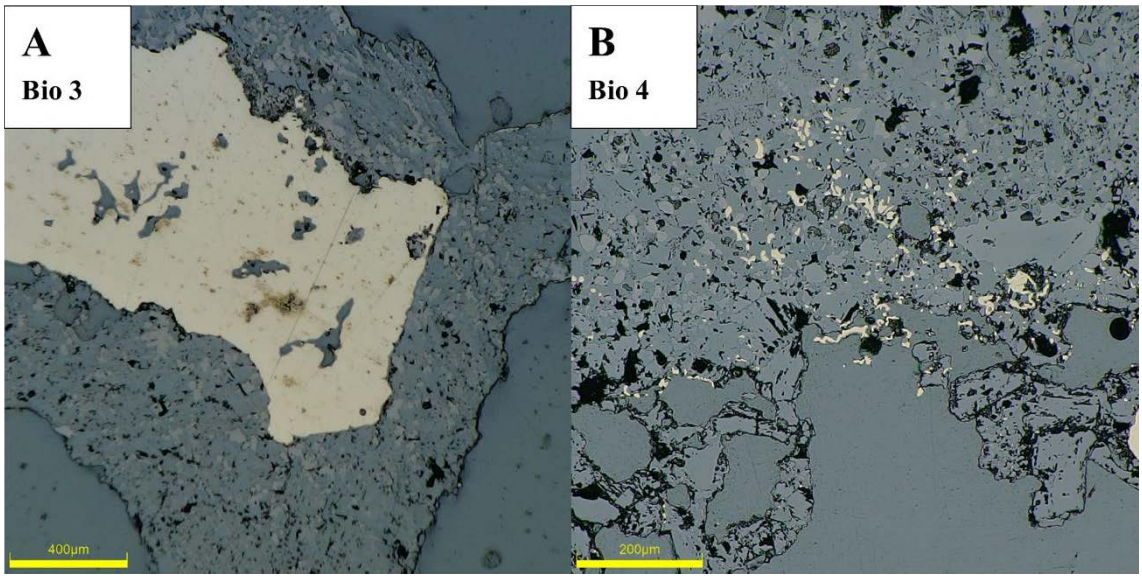

Figure 32. Digital microscope images taken from slag after the foaming experiment 6 performed with using biochar as a foaming agent.

From optical microscopy images, the bubble size in the slag could also be studied. The size of the bubbles in the foaming slag has been considered to be a critical factor to the stability of the foam. As stated earlier in this thesis in Section 3.3.4, the size of the bubbles in the foam is generally divided into two categories: large and small bubbles. In previously made studies both the size of the bubbles generated by injection of gas and by the reactions between fossil-based carbon and FeO in the slag has been studied. Based on the results from those previously made studies, the largest bubbles are generated mainly by the injection of gas, and their size is affected by the inner diameter of the injection lance and by the carrier gas flow rate. The smallest bubbles are generated by the reactions where CO gas is generated. Hara et al. (1983) investigated the size of the bubbles generated by argon injection into molten slags containing iron oxide. They used lance with an inner diameter of 6 mm, and low, <100 ml/min gas flow rates in their studies. The average size of the bubbles they obtained in the slag varied between 4 mm and 8 mm. Kitamura & Okohira (1992) stated as a part of their slag foaming studies that the size of the bubbles, generated by the reaction between FeO containing slag and carbon, was about 0.1 to 0.5 mm. Similar bubble sizes have been reported in studies made by Kim et al.

(2001); they mentioned that the bubble size, in their studies where argon gas and fine cokes were injected into slag, varied between <1 mm and 15 mm.

The slag sections, exposed as a result of the splitting of the crucibles (see Figure 27 and Figure 30), were studied with optical microscopy to determine the size of the bubbles generated by the injection of carbonaceous materials into the slag. Naturally, this solidified slag inside the crucible do not correspond to the actual foam layer during the foaming experiments, but at least indicative bubble size could be studied from the cavities left inside the slag bed. The largest cavities could be seen with the naked eye from the slag, and the smallest ones were detectable under a microscope. In Appendix 2, two example images obtained with digital microscope can be seen. The images are taken from the solidified slag of the experiment 3 (coke dust used as a foaming agent) and the experiment 4 (biochar used as a foaming agent). The measurement of bubble diameter was made with the computer software of the microscope.

The shape of the smallest cavities inside the solidified slag bed was mainly round. Also, some larger cavities with more unregular shapes could be observed, especially from the slag of the experiment 4. This supports the observation that the foaming of the slag was weaker in this particular experiment than in the experiments 3, 5 and 6; large bubbles are not the most optimal for stable and effective foaming. The larger cavities could also be bubbles combined during the solidification of the slag. In the slag of the experiment 4 the number of cavities in relation to the amount of slag was also the smallest. The size of the round bubbles varied mainly from 0.1 to 4 mm in all of the slag sections from the experiments 3–6, which can be also seen in the images in Appendix 2. The light metallic droplets inside the slag were partly supported by bubbles of different sizes. The images in Appendix 2 are taken from areas where these lighter metallic spots can also be seen. Bubbles could also be detected from the prepared microsections, filled with the epoxy resin. The sizes of those bubbles correspond to the sizes of bubbles in the unprepared slag sections in the split crucibles. Based on the bubble size examination, both the coke dust and the biochar produced similar bubbles, both in terms of shape and size. However, the bubble structure in the slag after the experiment 4 differed from the others, which may be a result of, for example, a partly failed injection.

8.3 FESEM-EDS

FESEM-EDS analysis were performed for the microsection samples. With EDS point analysis the light droplets discovered with optical microscopy, and the shiny, metallic material that could be seen with the naked eye amongst the slag could be confirmed to be reduced iron. In Figure 33, one of the point analysis images taken from the “Coke 3” microsection sample can be seen, and in Table 13, the chemical analysis of the spectrums found with the point analysis are presented. The image is a typical example of the phases found with the analysis. The white areas seen in the image represent reduced iron. Both small, roughly 10–50 µm areas, and larger, even several millimeters long areas of reduced iron could be detected from all of the microsection samples, except the samples “Bio 1” and “Bio 2” which were from the foaming experiment 4. There did not appear to be any reduced iron in those two samples. The main phase appears to have a composition similar to gehlenite, which can be seen as black areas in the image. The light-grey phase has a composition similar to magnesiowüstite, MgO·FeO, which has been considered to be an important second-phase particle for the foaming process. The somewhat high FeO content of the slag and the MgO-C-based crucible used in the experiments have caused a large amount of this phase to form. In addition, some dark-grey phase areas with a composition that could be identified close to that of titanite can be seen in the image.

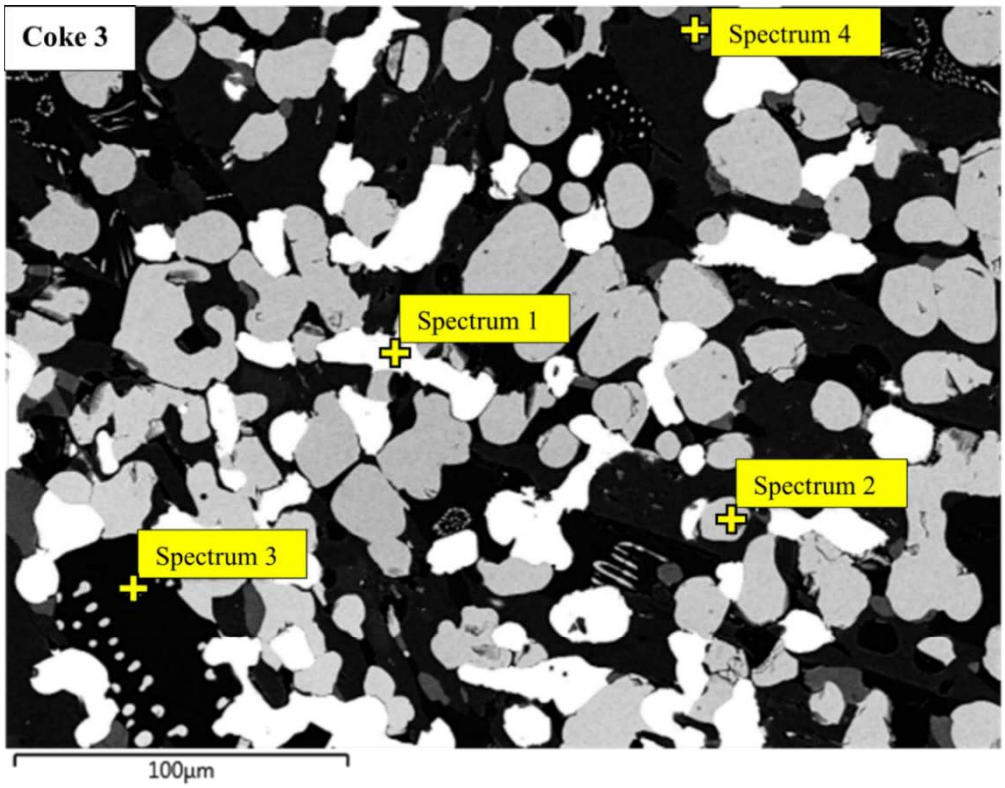

Figure 33. FESEM image and EDS point analysis locations for sample “Coke 3”.

Table 13. Chemical compositions of spectrums in Figure 33.

Spectr.	O	Na	Mg	Al	Si	Ca	Sc	Ti	V	Cr	Mn	Fe
1						0.23						99.65
2	22.48		11.73			0.29			1.05	0.29	1.48	62.68
3	40.23	1.29	1.13	14.81	11.58	28.52	0.25					1.68
4	32.79	0.38	1.98	1.07	6.28	33.71		17.90	2.33			3.57

In Figure 34, point analysis taken from the edge area of a large spot of reduced iron in "Bio 3" sample can be seen, and the elemental analysis of the spectrums are gathered in Table 14. In Appendix 3, elemental mapping analysis done for the same area is presented. A large area of reduced iron can be seen on the left side of the image. In the middle of the image a phase with a composition similar to magnesiowüstite is solidified in a dendritic kind of form. A phase having a composition similar to that of dicalcium silicate, $2CaO{\cdot}SiO_2$, seems to be the most dominant phase outside those areas. It occurs in the structure as long and thin areas. In addition, a phase with a composition similar to gehlenite could be identified from the image.

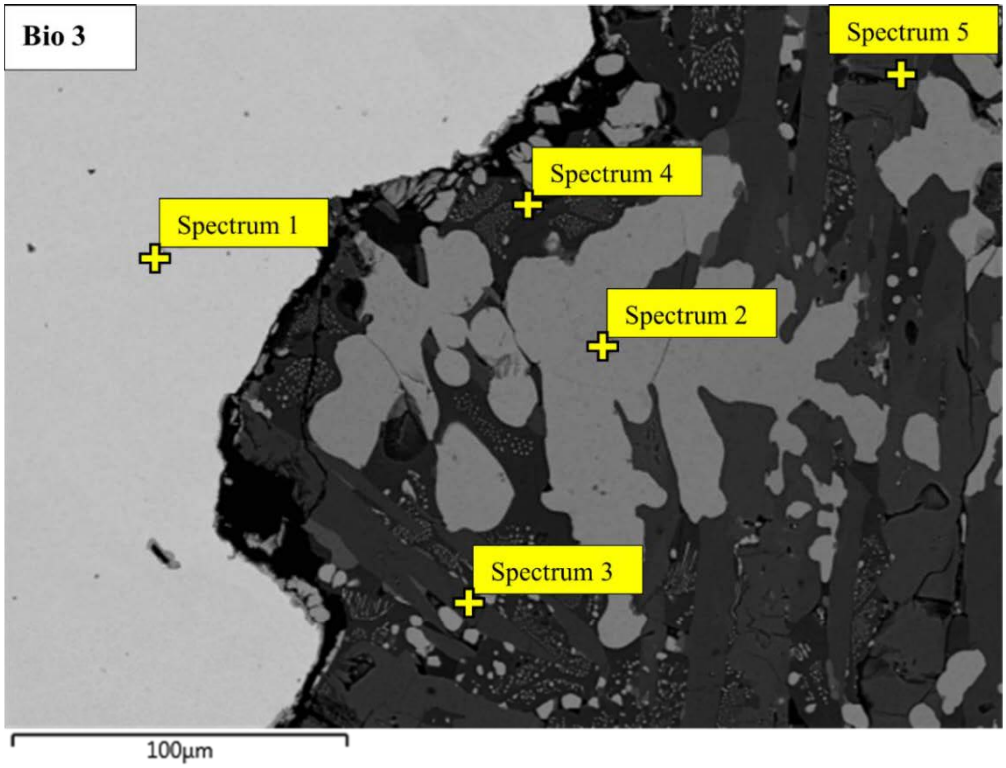

Figure 34. FESEM image and EDS point analysis locations for microsection sample "Bio 3".

Table 14. Chemical compositions of spectrums in Figure 34.

Spectr.	O	Na	Mg	Al	Si	P	Ca	V	Cr	Mn	Fe	W
1					0.13						99.87	
2	21.80		7.21					0.59	0.24	1.50	68.32	0.33
3	36.47	0.25	5.78		16.57	0.30	37.12	0.27			3.23	
4	39.36		0.77	16.41	11.00		29.93				2.53	
5	36.00		2.93		16.43		42.52	0.26			1.87	

The FESEM-EDS analysis conducted for the slags after the foaming experiments supported the findings that the foaming behavior was strong, especially in the experiments 3, 5 and 6. The results of the analysis showed that the iron oxide in the slag was clearly reduced with both of the foaming agents used, fossil coke and biochar. The slag in the samples was cooled slowly in air atmosphere, and this has naturally affected the composition and the form of the phases in the solidified slag. Therefore, it cannot be said exactly whether these solid second phase particles such as magnesiowüstite or dicalcium silicate have been among the liquid slag during the foaming experiments, or have these phases formed during the cooling of the slag after the experiments.

9 CONCLUSIONS AND PROPOSITIONS FOR FURTHER WORK

The conclusions that can be drawn from the results of the laboratory-scale studies are mostly clear, and they encourage further research on this topic. This section of the thesis provides these conclusions and presents some recommendations and guidelines for the future studies.

9.1 Conclusions

The aim of this thesis was to study the use of biochar as a slag foaming agent in a laboratory-scale. The development of a new kind of laboratory equipment, successful experiments made with a commonly used fossil carbon-based foaming agent, and two experiments made with biochar made up the experimental part of this thesis.

9.1.1 The suitability of the laboratory equipment for this kind of studies

The laboratory equipment assembled for the foaming experiments consisted of several parts. The chamber furnace and the crucible, the injection system including the carrier gas line, the screw feeder and the lance, and the visualization system were the parts of the equipment. All of these parts were important for the experiments, and they functioned well together. The usability of the equipment proved to be good, and a series of experiments can be performed with the equipment in a relatively short amount of time. The cooling of the furnace and the crucible inside it takes the most time (if air-cooling is used). Both the feeding of the carbonaceous material to the carrier gas line and the injection of this material into the liquid slag functioned well with the equipment, and the desired simulation of industrial scale injection was achieved.

This was the first time the visualization system used in the experiments was used to visualize the foaming of the slag. By positioning the laser light source and the camera carefully, the visualization of the foaming could be performed accurately and repeatably. The size of the crucibles used in the experiments was suitable in terms of the visualization, and the roughly 80x150 mm hole drilled into the roof of the furnace provided a proper field of view for the visualization. The image obtained with the visualization system was accurate and sharp, and the foaming of the slag could be clearly observed from the image.

9.1.2 Conclusions drawn from the reference experiments

Total of 4 reference experiments in which coke dust was used as a foaming agent were done as a part of the thesis. The first two experiments were performed at 1600 °C with a steel-slag system. In those experiments no foaming of the slag was observed. The reason for this remained unclear. Ji et al. (2003; 2005), King et al. (2009) and Zhu et al. (2012) have used same kind of experimental setup in their slag foaming experiments, and in all of those experiments a clear foaming effect and rise of the surface of the slag has been detected. Common to all previously made studies has been a temperature near 1600 °C, a steel-slag system, high MgO crucibles, and injection of fine, fossil-based carbonaceous material using nitrogen as a carrier gas. Zhu et al. (2012) reported the chemical composition of the slag used in their foaming experiments, and the basicity (CaO/SiO_2 1.94) and the FeO content (23.4 wt-%) of the slag they used were close to those of the slag used in the experiments of this thesis. Based on those parameters, the foaming of the slag should therefore have been possible. Since the experiments were the first two to be performed with the equipment, it may be possible that some mistakes were made, which affected either the foaming of the slag itself or the visualization and the observation of the foaming. Due to the holding of the high-temperature steel-slag system inside the crucible for several hours before doing the experiments, the crucibles were badly worn before performing the injection. This may have resulted in a situation where the slag has leaked out of the crucible from a worn point. Therefore, the surface of the slag may not have risen when the foaming has happened, and thus it may have been impossible to detect the foaming of the slag. During the first experiments, the melting of the quartz pipe injection lance may also not have been sufficiently taken into account. Therefore, continuous injection of coke dust into the slag may have been disrupted in the first two reference experiments.

The latter two reference experiments were performed at 1400 °C with a slag system. In these experiments the rise of the surface of the slag was clear, and its association with the injection of coke dust could be detected. Injection of nitrogen into the slag alone did not cause the surface of the slag to rise. When the coke dust was injected into the slag, the surface of the slag rose to the top edge-level of the crucible in both experiments, and if the crucible had been higher, the rise of the surface would probably have been greater. The lower temperature of the slag significantly reduced the wear of the crucible material, and the higher viscosity of the slag may have contributed to the foaming. As a conclusion, it can be said that the 1400 °C slag seemed to be appropriate for this kind of experiments,

as the foaming of the slag into which coke dust was injected could be clearly detected. The cooled slag of these two experiments was studied with digital microscope and FESEM-EDS, and the results showed that a large amount of FeO was reduced as a result of the coke dust injection. In addition, the size and the shape of the bubbles generated during the foaming was analyzed from the cooled slag bed. The bubble characteristics corresponded well to the results obtained in previously made studies.

9.1.3 Conclusions drawn from the use of biochar as a foaming agent

Two foaming experiments were done with biochar. In both of those experiments temperature of 1400 °C and a slag system were used. The biochar was pretreated before the experiments in a way that its properties corresponded closely to those of coke dust. Grinding the coal with a centrifugal mill and drying it before the experiments were suitable pretreatments. In terms of chemical composition, the biochar that was used was high-grade; the fixed carbon concentration was high, and the ash and volatile matter concentrations were low.

In the first of the foaming experiments made using biochar as a foaming agent the slag did not foam in the same way as in the reference experiments. The surface of the slag did rise, but not as high as in the reference experiments. The angle of view was a bit different in this experiment than in the others, which might be one of the reasons why the foaming of the slag did not seem so efficient. In the second experiment made with biochar the foaming of the slag corresponded to the reference experiments. The surface of the slag rose to the top edge-level of the crucible, and some slag also overflowed during the foaming. On this basis, there does not appear to be a difference between the biochar used and coke dust in terms of the foaming effectiveness. The surface of the slag rose a bit faster with biochar than with coke dust, which may be due to unwanted differences in injection rates.

The injection behavior of the biochar differed from the injection behavior of coke dust. The average injection rate for coke dust was 0.53 g/min, and for biochar 1.08 g/min. The flow properties of the carbonaceous materials used were not under particular investigation in this thesis. The bulk density for coke dust and for ground and dried biochar were 1.01 g/cm^3 and 0.47 g/cm^3, respectively. This could be seen as a difference in the storage behavior of these materials, especially when filling the container of the screw feeder. The true densities for the carbonaceous materials were 2.13 g/cm^3 for coke dust, and

2.56 g/cm^3 for biochar. The results for the density measurements indicate that there are differences in particle shapes of the carbonaceous materials, and thus the amount of void space between the particles can differ a lot between coke dust and biochar. With the equipment used, the injection of biochar was trickier than the injection of coke dust; some additional tapping needed to be done to the container of the screw feeder when biochar was injected to ensure the continuous flow of the material. The injection of both of the materials was successful with the equipment used, but the injection rates did not match. Thus, the differences in injection behaviors of the materials should definitely be taken into account if biochar is to be used more widely as a foaming agent.

All in all, based on the results of the foaming experiments, a conclusion that this particular biochar worked well as a foaming agent can be drawn. However, it must be noted that only a few experiments were performed quantitatively, with only one kind of slag and only one kind of biochar. Some further studies will be needed before biochar can be widely deployed as a foaming agent in industrial scale.

9.2 Propositions for further work

Based on the results of this thesis, it is recommended that more research and laboratory-scale slag foaming experiments are done. Some things that could be considered in further work are presented in Table 15. Because the laboratory equipment worked well in the foaming experiments performed as a part of this thesis, the same equipment can be used in the further studies, also. Possibly some modifications could be done to the equipment. The screw feeder could be developed in a way that the feeding rate could be controlled more accurately. Automating the use of the feeder, e.g. with a cordless drill, could be favorable. The use of another type of feeder could also be considered. A method for taking slag samples during the foaming experiments should be developed; e.g. by utilizing some kind of suction pipe, slag sampling could be possible through a hole in the roof of the furnace.

In the experiments of this thesis, only one type of slag composition and one type of biochar were tested. In the future studies larger variations of slag compositions and biochar grades should be used in order to gain more practical experience and information on how different properties of slag and biochar affect the foaming phenomenon.

Table 15. Propositions for further studies.

Suggestions and issues to consider in future laboratory-scale studies	
Slag	**Details**
Temperature	The temperature of slag affects the foaming behavior; doing foaming experiments with different temperatures would be desirable
Composition	The properties of the slag depend on its composition; e.g. experiments with different basicity or FeO concentrations could be done
Biochar	**Details**
Composition	Doing foaming experiments with different kinds of biochars would be desirable (e.g. biochar with a high VM content)
Flow and storage properties	The flow and storage properties of ground biochar could be studied (e.g. with a rheometer)
Raw materials	What kind of biomasses are suitable for the production of biochars used as a foaming agent? Availability, price?
Experimental procedure	**Details**
Steel-slag system	A steel-slag system should be further used in the foaming experiments
Sampling	By sampling the liquid slag during the experiments the amounts of iron oxides in the slag and the amount of reduced iron could be determined
Crucible dimensions/slag amount	With a taller/narrower crucible and/or less slag the maximum increase in the slag volume during the foaming could be observed
Feed device	The feeder should be developed in a way that accurate injection rates could be used; automation? Other feeder types?

10 SUMMARY

The foaming of slag is a necessary part of modern EAF steelmaking. The benefits it brings to the process, such as energy and refractory material savings, are great. The foaming of slag is nowadays created by fossil foaming agents, which will need to be replaced by fossil-free agents when moving towards fossil-free steel production. The aim of this thesis was to study how biochar acts as a slag foaming agent. In the literature review part of this thesis the foaming of slag in general, the properties of slag that affect the foaming phenomenon, and the previously made studies on the topic are reviewed. In the experimental part, foaming experiments were performed in a laboratory-scale. Both reference experiments with coke dust and foaming experiments with biochar were done.

The properties of the EAF slag affect the foaming phenomenon a lot. The chemical composition of the slag has a connection to properties such as basicity, surface tension and viscosity of the slag. It is not possible to determine one right composition for the EAF slag in terms of foaming. In general, the lower basicity of the slag leads to higher viscosity, lower surface tension and better foaming of the slag. However, with higher values of basicity the potential for the presence of suspended second phases increases. The suspended second phase particles in the slag have been considered to be one of the most important factors affecting the foaming phenomenon. These solid particles among the liquid slag, such as magnesiowüstite or dicalcium silicate, act as gas nucleation sites and increase the effective viscosity of the slag, which improves the foaming potential of the slag. The amount of these particles is greatly affected by the temperature of the slag. FeO is also a necessary component for the foaming of the slag, which can be related to the CO gas forming reactions. Therefore, there must be suitable amount of FeO in the slag so that the foaming can happen. The amount cannot be too high so that the viscosity of the slag stays at a proper level. Based on previously made studies on the topic, it can be said that the foamability of the slag is a sum of several different factors. Slags with different kinds of composition variations are proven to foam, but still some limits and suggestions can be given related to the suitability of the slag for foaming.

The use of biochar as a slag foaming agent has been previously studied to some extent. The reactions between biochar and EAF slag have been studied with sessile drop method, and some laboratory-scale foaming experiments have been done in a way that the biochar has been loaded to a crucible at one time. Some industrial scale foaming experiments have

also been done. The results from the previously made studies have varied a lot, and no clear indications that the biochars used in the experiments could actually act as a full-time foaming agent in the industry have been obtained in the studies discussed in this thesis. Some of the biochars have shown a clear tendency to produce foaming, but with some of the biochars no foaming at all has occurred. The foaming efficiency of the biochars has varied, and some biochars have reacted too aggressively with the slag. No injection experiments have been previously performed with biochar in a laboratory-scale, and all of the measurement methods for the foaming have not been accurate.

The main tasks of the experimental part of the thesis were: 1) Designing and building suitable laboratory-scale foaming equipment with a real-time visualization system 2) Performing successful reference foaming experiments with coke dust 3) Performing foaming experiments with biochar and analyzing the results and the suitability of the biochar to act as a foaming agent. The suitability of the foaming equipment for this kind of experiments proved to be good. With the laser light source-based visualization system real-time image from the foaming of the slag could be obtained. The change in the surface height of the slag could be estimated from the image. A total of 6 foaming experiments were performed as a part of the thesis, of which 2 were performed with biochar. EAF slag including 29.02 wt-% of FeO with basicity (CaO/SiO_2) of 2.0 was used in the experiments. These were evaluated to be suitable values for slag foaming experiments based on the results of earlier work in this field. Based on the images obtained with the visualization system, the biochar seemed to work similarly as a foaming agent as coke dust. The biochar was able to foam the EAF slag and injecting it into the slag lead to a volume increase. From the results of the microscopical analysis done to the slag after the experiments, it can be stated that the reduction behavior of the biochar and the coke dust seemed to be similar, and both of the materials caused similar bubbling when injected into the slag.

Because only a limited number of foaming experiments were performed as a part of this thesis, it is highly recommended that some further work is focused on the topic. This thesis provides some tools for this future work related to the use of biochar as a slag foaming agent in EAF steelmaking.

REFERENCES

Abdullah, H. & Wu, H., 2009. Biochar as a fuel: 1. Properties and grindability of biochars produced from the pyrolysis of mallee wood under slow-heating conditions. Energy and Fuels, 23 (8), P. 4174–4181.

Baracchini, G., Bianco, L., Cirilli, F., Echterhof, T., Griessacher, T., Marcos, M., Mirabile, D., Reichel, T., Rekersdrees, T. & Sommerauer, H., 2018. Biochar for a Sustainable EAF Steel Production (GREENEAF2). Luxembourg: Publications Office of the European Union, 110 p. ISBN 978-92-79-98291-0

Barella, S., Gruttadauria, A., Mapelli, C. & Mombelli, D., 2012. Critical evaluation of role of viscosity and gas flowrate on slag foaming. Ironmaking and Steelmaking, 39 (6), P. 463–469.

Battle, T., Srivastava, U. & McClelland, J., 2014. The Direct Reduction of Iron. In: Treatise on Process Metallurgy. Elsevier Ltd., P. 89–176. ISBN 978-0-08-096988-6

Bhoi, B., Jouhari, A. K., Ray, H. S. & Misra, V. N., 2006. Smelting reduction reactions by solid carbon using induction furnace: Foaming behaviour and kinetics of FeO reduction in CaO-SiO2-FeO slag. Ironmaking and Steelmaking, 33 (3), P. 245–252.

Bianco, L., Baracchini, G., Cirilli, F., Di Sante, L., Moriconi, A., Moriconi, E., Millan Agorio, M. M., Pfeifer, H., Echterhof, T., Demus, T., Jung, H. P., Beiler, C. & Krassnig, H-J., 2013. Sustainable Electric Arc Furnace Steel Production: GREENEAF. Berg- und Hüttenmännische Monatshefte, 158 (1), P. 17–23.

Cavitar Ltd, 2011. CAVILUX HF Operating Manual, Version 4.4 [Operating manual].

Cavitar Ltd, 2018a. Effective and versatile laser illumination [Web document]. Tampere: Cavitar Ltd. Available: https://www.cavitar.com/library/effective-and-versatile-high-power-laser-illumination/ [referred 16.4.2022]. 5 p.

Cavitar Ltd, 2018b. CAVILUX HF [Brochure].

Chang, W. T., Lin, C. M., Su, Y. L., Li, C. C., Chang, Y. E., Shen, J. M. & Wu, W., 2021. Effect of FeO Content on Foaming and Viscosity Properties in FeO-CaO-SiO2-MgO-Al2O3 Slag System. Metals, 11 (2), P. 1–10.

Chychko, A., Teng, L. & Seetharaman, S., 2012. Foaming in electric arc furnace-Part II: Foaming visualization and comparison with plant trials. Metallurgical and Materials Transactions B: Process Metallurgy and Materials Processing Science, 43 (5), P. 1078–1085.

Corbari, R., Matsuura, H., Halder, S., Walker, M. & Fruehan, R. J., 2009. Foaming and the rate of the carbon-iron oxide reaction in slag. Metallurgical and Materials Transactions B: Process Metallurgy and Materials Processing Science, 40 (6), P. 940–948.

Curay, Ma. G., Ching, A. J., Duran, K., Talingting, R. M. & Balladares, S., 2020. Characterization of charcoal produced by different Pyrolyzing techniques. Annals of Tropical Research, 42 (2), P. 131–148.

De Almeida, R. A. M., Vieira, D., Bielefeldt, V. & Vilela, A. C. F., 2017. Slag foaming fundamentals - A critical assessment. Materials Research, 20 (2), P. 474–480.

Dutta, S. K. & Sah, R., 2016. Direct Reduced Iron: Production. In: Encyclopedia of Iron, Steel, and Their Alloys. CRC Press, P. 1082–1108. ISBN 978-146-651-104-0

Echterhof, T. & Pfeifer, H., 2011. Potential of biomass usage in electric steelmaking. Proceedings of 1st international conference on energy efficiency and CO2 reduction in steel industry.

Emrich, W., 1985. Handbook of Charcoal Making. Springer Netherlands, 278 p. ISBN 978-90-481-8411-8

Fidalgo, B., Berrueco, C. & Millan, M., 2015. Chars From Agricultural Wastes as Greener Fuels for Electric Arc Furnaces. Journal of Analytical and Applied Pyrolysis, 113 (12), P. 274–280.

Gaskell, D. R., 2007. The Determination of Phase Diagrams for Slag Systems. In: Chao J. C. Methods for Phase Diagram Determination. Elsevier Ltd., P. 442–458. ISBN 978-0-08-044629-5

Hannula, S-P., Haimi, E. & Lindroos, V., 2020. Uudistettu Miekk-ojan metallioppi Osa 2. Helsinki: Teknologiateollisuus ry, 272 p. ISBN 978-952-238-244-3

Hara, S., Ikuta, M., Kitamura, M. & Ogino, K., 1983. Foaming of molten slags containing iron oxide. Tetsu-To-Hagane/Journal of the Iron and Steel Institute of Japan, 69 (9), P. 1152–1159.

Hara, S. & Ogino, K., 1992. Slag-foaming Phenomenon in Pyrometallurgical Processes. ISIJ International, 32 (1), P. 81–86.

He, H., Guan, H. & Lee, H., 2017. Assessment on the energy flow and carbon emissions of integrated steelmaking plants. Energy Reports, 3, P. 29–36.

Hong, L., Hirasawa, M. & Sano, M., 1998. Behavior of Slag Foaming with Reduction of Iron Oxide in Molten Slags by Graphite. ISIJ International, 38 (12), P. 1339–1345.

Hosseini, S., Soltani, S. M., Fennell, P., Choong, T. & Aroua, M. K., 2016. Production and applications of electric-arc-furnace slag as solid waste in environmental technologies: a review. Environmental Technology Reviews.

Huang, X. A., Ng, K. W., Giroux, L., Duchesne, M., Li, D. & Todoschuk, T., 2021. Interaction Behavior of Biogenic Material with Electric Arc Furnace Slag. Fuels, 2 (4), P. 420–436.

Huang, X. A., Ng, K. W., Giroux, L. & Duchesne, M., 2019. Carbonaceous Material Properties and Their Interactions with Slag During Electric Arc Furnace Steelmaking. Metallurgical and Materials Transactions B: Process Metallurgy and Materials Processing Science, 50 (3), P. 1387–1398.

Husslage, W., 2004. Dynamic distributions: Sulphur transfer and flow in a high temperature packed coke bed [Doctoral thesis]. 228 p.

Ireland, P. M., 2009. Coalescence in a steady-state rising foam. Chemical Engineering Science, 64 (23), P. 4866–4874.

Ito, K. & Fruehan, R. J., 1989a. Study on the foaming of CaO-SiO2-FeO slags: Part I. Foaming parameters and experimental results. Metallurgical Transactions B, 20 (4), P. 509–514.

Ito, K. & Fruehan, R. J., 1989b. Study on the foaming of CaO-SiO2-FeO slags: Part II. Dimensional analysis and foaming in iron and steelmaking processes. Metallurgical Transactions B, 20 (4), P. 159–521.

Ji, F. Z., Barati, M., Coley, K. & Irons, G. A., 2003. Overall reaction kinetics of coal injection into slags. Yazawa International Symposium: Metallurgical and Materials Processing: Principles and Technologies; Materials Processing Fundamentals and New Technologies, P. 787–800.

Ji, F. Z., Barati, M., Coley, K. & Irons, G. A., 2005. Kinetics of coal injection into iron oxide containing slags. Canadian Metallurgical Quarterly, 44 (1), P. 85–94.

Jiang, R. & Fruehan, R. J., 1991. Slag foaming in bath smelting. Metallurgical Transactions B, 22 (4), P. 481–489.

Jones, J. A. T., Bowman, B. & Lefrank, P. A., 1998. Chapter 10: Electric Furnace Steelmaking. In: The Making, Shaping and Treating of Steel. 11th Edition. Pittsburgh: The AISE Steel Foundation, P. 525–660. ISBN 978-0-930767-02-0

Jung, S. M. & Fruehan, R. J., 2000. Foaming characteristics of BOF slags. ISIJ International, 40 (4), P. 348–355.

Kapilashrami, A., Görnerup, M., Lahiri, A. K. & Seetharaman, S., 2006. Foaming of slags under dynamic conditions. Metallurgical and Materials Transactions B: Process Metallurgy and Materials Processing Science, 37 (1), P. 109–117.

Kekkonen, M., Oghbasilasie, H. & Louhenkilpi, S., 2012. Viscosity models for molten slags. Aalto University publication series, SCIENCE + TECHNOLOGY. 38 p. ISBN 978-952-60-4602-0

Kim, H. S., Min, D. J. & Park, J. H., 2001. Foaming behavior of CaO-SiO2-FeO-MgOsatd-X (X=Al2O3, MnO, P2O5, and CaF2) slags at high temperatures. ISIJ International, 41 (4), P. 317–324.

King, M. P., Ji, F. Z., Irons, G. A. & Coley, K. S., 2009. Kinetics of carbon reaction with electric Arc furnace slags during slag foaming. AISTech - Iron and Steel Technology Conference Proceedings, P. 617–626.

Kipepe, T. M, & Pan, X., 2015. Energy improvement in induction furnace using foaming slag with variation of carbon injection. Journal of Energy in Southern Africa, 26 (3), P. 64–73.

Kitamura, S. & Okohira, K., 1992. Influence of Slag Composition and Temperature on Slag Foaming. ISIJ International, 32 (6), P. 741–746.

Lahiri, A. K. & Pal, S., 2004. Foaminess of slag: cause and control. VII International Conference on Molten Slags Fluxes and Salts, P. 473–478.

Lahiri, A. K., Yogambha, R., Dayal, P. & Seetharaman, S., 2003. Foam in Iron and Steelmaking. High Temperature Materials and Processes, 22 (5–6), P. 345–352.

Lee, J., Hoai, L. T., Choe, J. & Park, J. H., 2012. Density measurements of CaO-MnO-SiO2 slags. ISIJ International, 52 (12), P. 2145–2148.

Lehmann, J. & Joseph, S., 2009. Biochar for Environmental Management: Science and Technology. London: Earthscan, 416 p. ISBN 978-1-84407-658-1

Liukkonen, M., Penttilä, K. & Koukkari, P. S., 2012. A Compilation of Slag Foaming Phenomenon Research: Theoretical Studies, Industrial Experiments and Modelling. Espoo: VTT Technical Research Centre of Finland, 128 p. ISBN 978-951-38-7897-9

Luz, A. P., Tomba Martinez, A. G. & Pandolfelli, V. C., 2018. Slag foaming practice in the steelmaking process. Ceramics International, 44, P. 8727–8741.

Luz, A. P., Ávila, T. A., Bonadia, P. & Pandolfelli, V. C., 2011. Slag Foaming: Fundamentals, Experimental Evaluation and Application in the Steelmaking Industry. Refractories WorldForum, 3 (2), P. 91–98.

Maayas, M., Nekouei, R. K. & Sahajwalla, V., 2019. Valorization of lignin biomass as a carbon feedstock in steel industry: Iron oxide reduction, steel carburizing and slag foaming. Journal of Cleaner Production, 219, P. 971–980.

Madias, J., 2014. Electric Furnace Steelmaking. In: Treatise on Process Metallurgy. Elsevier Ltd., P. 271–300. ISBN 978-0-08-096988-6

Meier, T., Echterhof, T. & Pfeifer, H., 2017. Investigating the Use of Biomass and Oxygen in Electric Steelmaking by Simulations Based on a Dynamic Process Model. 2nd ISIJ-VDEh-Jernkontoret Joint Symposium, 12.-13. June 2017, Stockholm, Sweden. P. 81–93.

Memoli, F., Mapelli, C., Ravanelli, P. & Corbella, M., 2004. Evaluation of the energy developed by a multipoint side-wall burner-injection system during the refining period in a EAF. ISIJ International, 44 (9), P. 1511–1516.

Micromeritics. Accupyc II 1345 Gas Diplacement Pycnometry System [Brochure].

Miller, K., 2013. Coal analysis. In: The Coal Handbook: Towards Cleaner Production. Elsevier Inc., P. 151–189. ISBN 978-0-85709-730-9

Mills, K. C., Yuan, L. & Jones, R. T., 2011. Estimating the physical properties of slags. Journal of the Southern African Institute of Mining and Metallurgy, 11 (10), P. 649–658.

Morales, R. D., Romero, J. A. & Camacho, J., 1995. The Slag Foaming Practice in EAF and Its Influence on the Steelmaking Shop Productivity. ISIJ International, 35 (9), P. 1054–1062.

Nachenius, R. W., Ronsse, F., Venderbosch, R. H. & Prins, W., 2013. Chapter 2: Biomass Pyrolysis. In: Murzin, D. Y. Advances in Chemical Engineering. 42nd Edition. San Diego: Academic Press, P. 75–139. ISBN 978-0-12- 386505-2

Nakashima, K. & Mori, K., 1992. Interfacial Properties of Liquid Iron Alloys and Liquid Slags Relating to Iron- and Steel-making Processes. ISIJ International, 32 (1), P. 11–18.

Nexhip, C., Sun, S. & Jahanshahi, S., 2004. Physicochemical properties of foaming slags. International Materials Reviews, 49 (5), P. 286–298.

Ozturk, B. & Fruehan, R. J., 1995. Effect of temperature on slag foaming. Metallurgical and Materials Transactions B, 26 (5), P. 1086–1088.

Pfeifer, H., Kirschen, M. & Simoes, J-P., 2002. Thermodynamic analysis of EAF electrical energy demand. 8th European Electric Steelmaking Conference.

Pretorius, E. B. & Carlisle, R. C., 1998. Foamy Slag Fundamentals and their Practical Application to Electric Furnace Steelmaking. Iron and Steelmaker, 26 (10), P. 79–88.

Rafiei, R., Kermanpur, A. & Ashrafizadeh, F., 2008. Numerical thermal simulation of graphite electrode in EAF during normal operation. Ironmaking & Steelmaking, 35 (6), P. 465–472.

Rodriguez, H. H., Conejo, A. N. & Morales, R. D., 2001. Theoretical analysis of the interfacial phenomenon during the injection of carbon particles into EAF slags. Steel Research, 72 (8), P. 298–303.

Sahajwalla, V., Rahman, M., Hong, L., Saha-Chaudhury, N. & Spencer, D., 2006. Influence of Carbonaceous Materials on Slag Foaming Behavior During EAF Steelmaking. Iron and Steel Technology, 3 (2), P. 639–650.

Seetharaman, S., Mukai, K. & Sichen, D., 2005. Viscosities of slags - An overview. Steel Research International, 76 (4), P. 267–278.

Shu, Q. F. & Chou, K. C., 2013. Calculation for density of molten slags using optical basicity. Ironmaking and Steelmaking, 40 (8), P. 571–577.

Singh, R., 2020. Production of steel. In: Applied Welding Engineering. Elsevier Ltd., P. 35–52.

Skaf, M., Manso, J., Aragón, Á., Fuente, J. & Ortega-López, V., 2017. EAF Slag in Asphalt Mixes: A Brief Review of its Possible Re-use. Resources, Conservation and Recycling, 120 (10), P. 176–185.

Skupien, D. & Gaskell, D. R., 2000. The surface tensions and foaming behavior of melts in the system CaO-FeO-SiO2. Metallurgical and Materials Transactions B: Process Metallurgy and Materials Processing Science, 31 (5), P. 921–925.

Slag Atlas (1995). 2nd Edition. Düsseldorf: Verlag Stahleisin GmbH. Verein Deutscher Eisenhüttenleute. 616 p. ISBN 3-514-00457-9

Son, K., Lee, J., Hwang, H., Jeon, W., Yang, H., Sohn, I., Kim, Y. & Um, H., 2021. Slag foaming estimation in the electric arc furnace using machine learning based long short-term memory networks. Journal of Materials Research and Technology, 12, P. 555–568.

Suopajärvi, H., 2013. Biomaterian prosessointitavat: esikäsittelyt, termokemiallinen konversio ja käyttö masuunissa. Bioreducer: Biomateriapohjaisen pelkistysaineen mahdollisuudet 2013, University of Oulu, Laboratory of Process Metallurgy.

Suopajärvi, H., Dahl, E., Kemppainen, A., Gornostayev, S., Koskela, A. & Fabritius, T., 2017. Effect of charcoal and Kraft-lignin addition on coke compression strength and reactivity. Energies, 10 (11), 1850.

Suopajärvi, H. & Fabritius, T., 2013. Towards more sustainable ironmaking-an analysis of energy wood availability in Finland and the economics of charcoal production. Sustainability (Switzerland), 5 (3), P. 1188–1207.

Teo, P. T., Zakaria, S. K., Salleh, S. Z., Taib, M. A. A., Mohd Sharif, N., Abu Seman, A., Mohamed, J. J., Yusoff, M., Yusoff, A. H., Mohamad, M., Masri, M. N. & Mamat, S., 2020. Assessment of Electric Arc Furnace (EAF) Steel Slag Waste's Recycling Options into Value Added Green Products: A Review. Metals, 10 (10), 1347.

Teräskirja, 2014. 9th Edition. Porvoo: Metallinjalostajat ry, Bookwell Oy, 112 p. ISBN 978-952-238-120-0

Toloue Farrokh, N., Suopajärvi, H., Mattila, O., Umeki, K., Phounglamcheik, A., Romar, H., Sulasalmi, P. & Fabritius, T., 2018. Slow pyrolysis of by-product lignin from wood-based ethanol production – A detailed analysis of the produced chars. Energy, 164, P. 112–123.

Toloue Farrokh, N., Suopajärvi, H., Mattila, O., Sulasalmi, P. & Fabritius, T., 2020. Characteristics of wood-based biochars for pulverized coal injection. Fuel, 265.

Turkdogan, E. T., 1996. Fundamentals of Steelmaking. London: Institute of Materials, 352 p. ISBN 978-1-906540-97-5

Vaiana, R., Balzano, F., Iuele, T. & Gallelli, V., 2019. Microtexture performance of EAF slags used as aggregate in asphalt mixes: A comparative study with surface properties of natural stones. Applied Sciences (Switzerland), 9 (15).

Vogl, V., Åhman, M. & Nilsson, L. J., 2018. Assessment of hydrogen direct reduction for fossil-free steelmaking. Journal of Cleaner Production, 203, P. 736–745.

Wang, G. C., 2016. Ferrous metal production and ferrous slags. In: The Utilization of Slag in Civil Infrastructure Construction. Elsevier Ltd., P. 9–33. ISBN 978-0-08-100994-9

Wang, R. R., Zhao, Y. Q., Babich, A., Senk, D. & Fan, X. Y., 2021. Hydrogen direct reduction (H-DR) in steel industry—An overview of challenges and opportunities. Journal of Cleaner Production, 329.

Weber, K. & Quicker, P., 2018. Properties of biochar. Fuel, 217, P. 240–261.

Wu, K., Qian, W., Chu, S., Niu, Q. & Luo, H., 2000. Behavior of slag foaming caused by blowing gas in molten slags. ISIJ International, 40 (10), P. 954–957.

Wu, L. S., Albertsson, G. J. & Sichen, D., 2010. Modelling of slag foaming. Ironmaking and Steelmaking, 37 (8), P. 612–619.

Xin, J., Gan, L., Jiao, L & Lai, C., 2017. Accurate density calculation for molten slags in SiO2-Al2O3-CaO-MgO systems. ISIJ International, 57 (8), P. 1340–1349.

Yaman, S., 2004. Pyrolysis of biomass to produce fuels and chemical feedstocks. Energy Conversion and Management, 45 (5), P. 651–671.

Ye, L., Peng, Z., Wang, L., Anzulevich, A., Bychkov, I., Kalganov, D., Tang, H., Rao, M., Li, G. & Jiang, T., 2019. Use of Biochar for Sustainable Ferrous Metallurgy. JOM, 71 (11), P. 3931–3940.

Zhang, B., Wang, R., Hu, C., Liu, C. & Jiang, M., 2021. Effect of viscosity on dynamic evolution of metallurgy slag foaming. ISIJ International, 61 (5), P. 1348–1356.

Zhang, Y. & Fruehan, R. J., 1995. Effect of the bubble size and chemical reactions on slag foaming. Metallurgical and Materials Transactions B, 26 (4), P. 803–812.

Zhu, T. X., Coley, K. S. & Irons, G. A., 2012. Progress in Slag Foaming in Metallurgical Processes. Metallurgical and Materials Transactions B, 43 (4), P. 751–757.

Screenshots where the software settings for the visualization system are presented APPENDIX 1

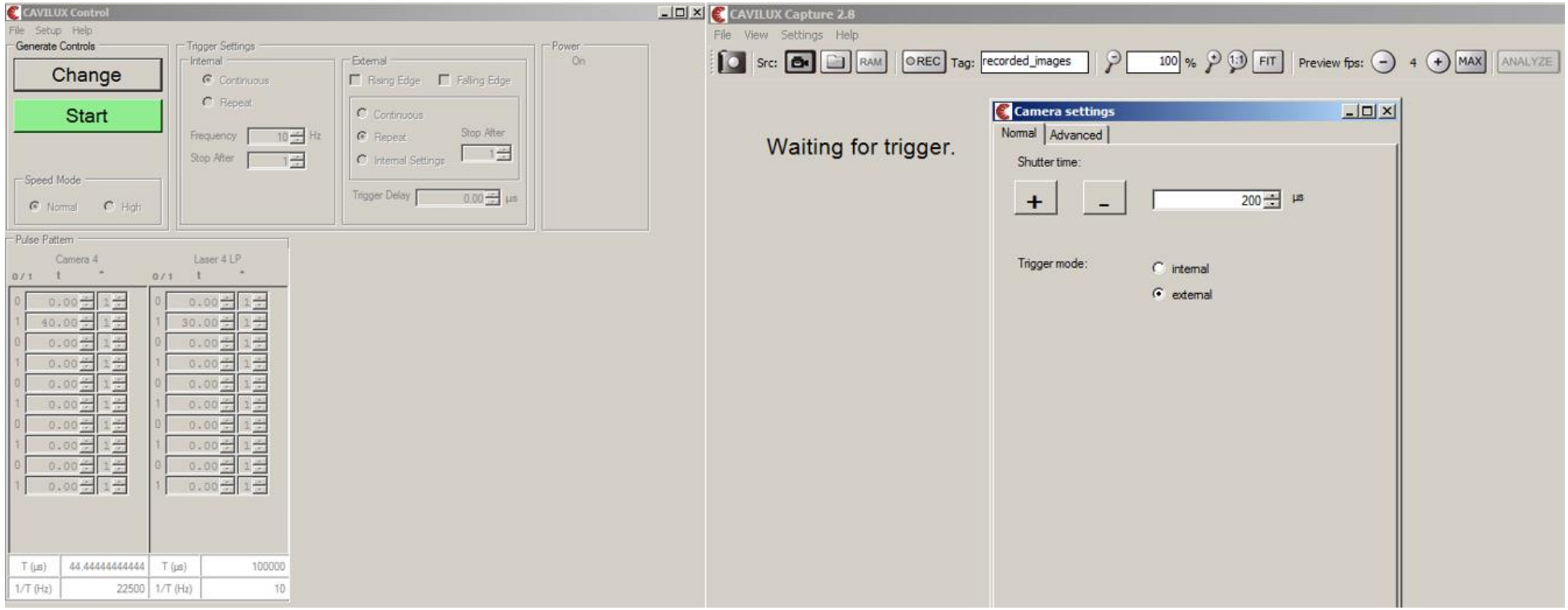

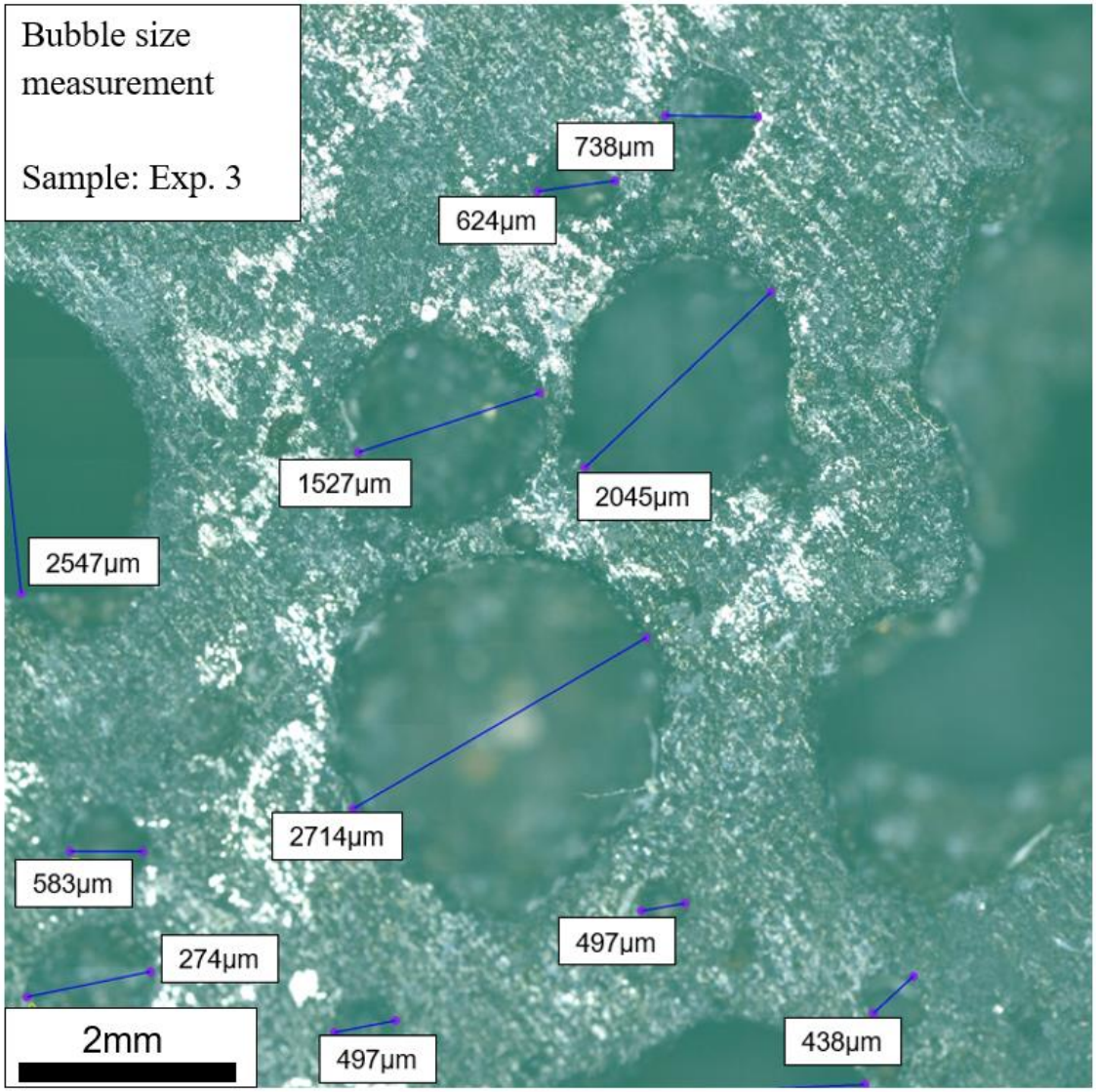
Bubble size measurement
Sample: Exp. 3
738µm
624µm
1527µm
2045µm
2547µm
2714µm
583µm
497µm
274µm
2mm
497µm
438µm

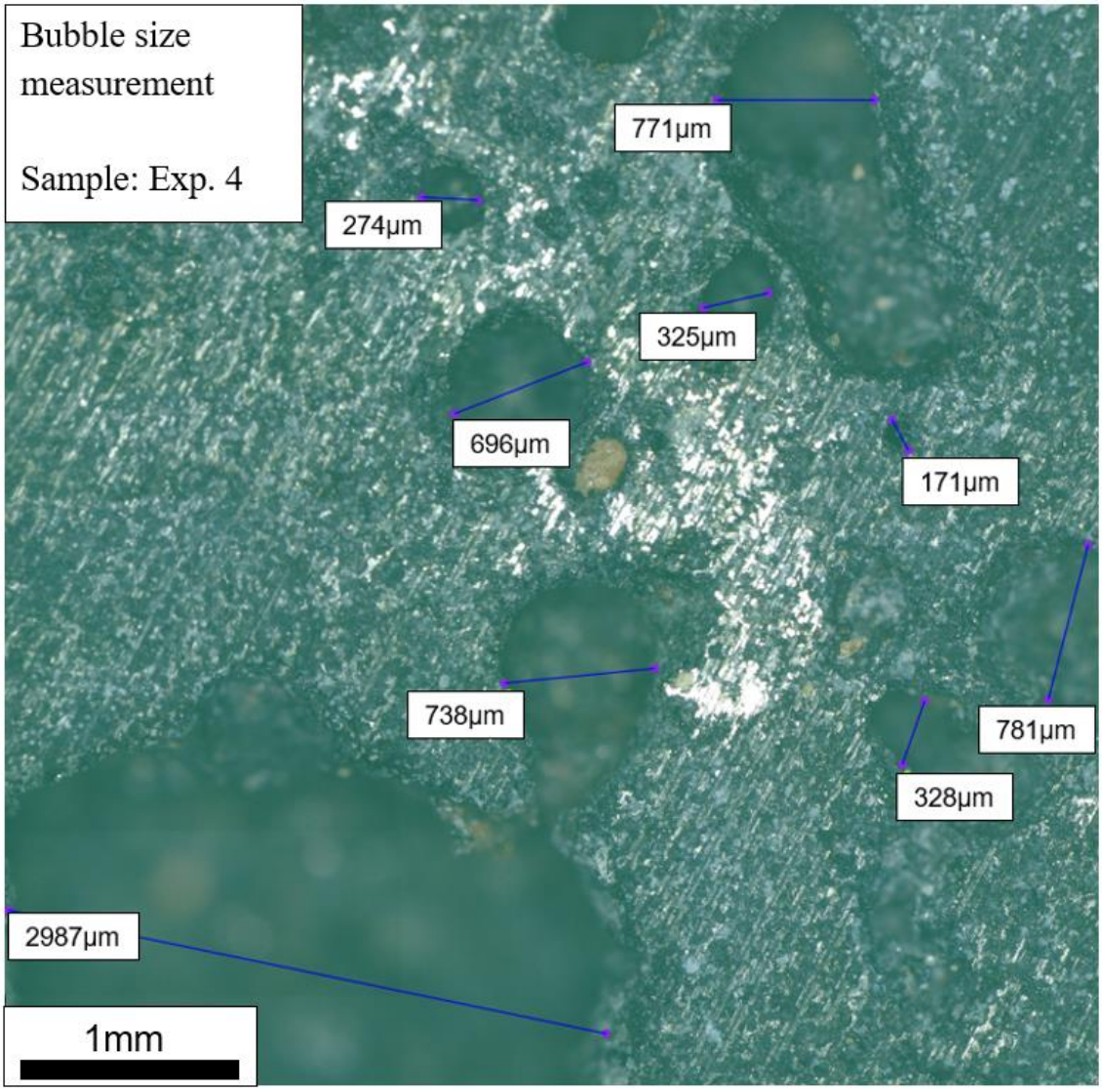
Bubble size measurement
Sample: Exp. 4
771µm
274µm
325µm
696µm
171µm
738µm
781µm
328µm
2987µm
1mm

FESEM-EDS elements map for a slag sample APPENDIX 3